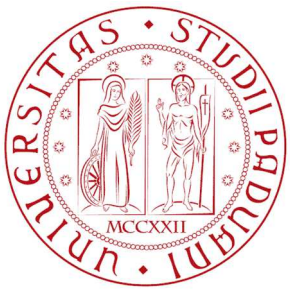

Università Degli Studi di Padova

Department of Biomedical Sciences

PhD Program in Biomedical Sciences CICLO XXXII

OPA1 ORCHESTRATES PRECOCIOUS SENESCENCE, DEGENERATION OF MULTIPLE ORGANS AND PREMATURE DEATH THOUGHT INFLAMMATION AND METABOLIC CHANGES

Coordinator: Prof. Paolo Bernardi

Supervisor: Prof. Marco Sandri

PhD Candidate: Caterina Tezze

Index

List of abbreviations

ADP	Adenosine diphosphate
Akt/Pkb	Protein kinese B
AMPk	AMP-activated protein kinase
Atg7	Autophagy related 7
Atg8	Autophagy related 8
ATP	Adenosine triphosphate
Atrogin 1/Mafbx	E3 ubiquitin ligase muscle-specific F-box
Bnip3	BCL2/adenovirus E1B 19 kDa protein-interacting protein 3
Cre/LoxP	Recombinase system
CSA	Cross sectional area
Drp1	Dynamin related protein 1
ER	Estrogen receptor or Endoplasmic Reticulum
f/f	double floxed alleles
FGF21	Fibroblast growth factor 21
Fis1	Mitochondrial fission 1
$Foxo_3$	Forkhead box O3
GABARAP	Gamma-aminobutyric acid receptor associated protein
GH	growth hormone
GTPasi	Enzimes hydrolyze guanosine triphosphate (GTP) to guanosine diphosphate (GDP)
GTT	Glucose tollerance test
HSA	Human Skeletal Actin
IGF-1	Insulin growth factor 1
IL1α	Interleukine-1α
IL1β	Interleukine-1β
IL6	Interleukine-6
IMF	Intermyofibrillar mitochondria
IMM	Inner mitochondrial membrane
Ko	Knock out
LC3	Microtubule-associated protein 1A/1B-light chain 3
Mff	Fission factor of mitochondria
Mfn1	Mitofusin 1
Mfn2	Mitofusin 2
miRNA	microRNA
MIS	Mitochondrial import sequence
MLC	Myosin light chain promoter

mtDNA	Mitochondrial DNA
mTOR	Mechanistic target of rapamycin kinase
Murf-1	Muscle ring finger-1 E3 ubiquitin ligase
NCAM	Neural Cell Adhesion Molecules
NF-kB	Nuclear Factor kappa B
OMM	Outer mitochondrial membranes
OPA1	Optic Atrophy Protein 1
p62	Protein 62
PGC-1β	Proliferator-Activated Receptor-Gamma Coactivator-1b
PGC-1α	Proliferator-Activated Receptor-Gamma Coactivator-1a
Pink3	PTEN-induced putative kinase 1
PPARy	Peroxisome Proliferator-Activated Receptor y
RCC	Mitochondrial respiratory chain complex
RCS	assembly of respiratory complexes
ROS	Reactive oxygen species
rRNA	Ribosomal RNA
SDH	Succinate deidrogenate
shRNA	Short hairpin RNA
SS	Subsarcollemal mitochondria
TLR9	Toll-like receptor 9
TNFα	Tumor necrosis factor-alpha
tRNA	Transport RNA
WAT	White adipose tissue
Wt	Wild type

SOMMARIO

Un network funzionale di mitocondri è essenziale per un tessuto post-mitotico come il muscolo. Il macchinario delle dinamiche mitocondriali è downregolato nella sarcopenia e preservato nei soggetti che fanno attvità fisica costante.
La proteina OPA1, coinvolta nel processo di fusione mitocondriale, gioca un ruolo essenziale nelle dinamiche mitocondriali. I livelli di espressione di questa proteina correlano significativamente con la disfunzione muscolare associata all'invecchiamento, in umani e topi.
Per caratterizzare il ruolo della proteina OPA1 nel muscolo scheletrico, e soprattutto il suo coinvolgimento nell'invecchiamento, abbiamo generato 2 modelli di delezione del gene nel tessuto muscolare. Il primo modello (costitutivo) presenta la delezione del gene a partire dallo stadio embrionale e il secondo (condizionale) permette di effettuare la delezione in seguito a somministrazione farmacologica, in età adulta.
Il modello costitutivo ha un fenotipo molto grave che porta alla morte dopo otto giorni post-nascita. Per questa ragione ci siamo concentati su quello condizionale. I topi adulti con delezione di OPA1 mostrano un fenotipo di invecchiamento precoce.
Il blocco della fusione è sufficiente a indurre cambiamenti metabolici e infiammazione sistemica. Il fattore chiave in questo processo è la miochina FGF21. La delezione simultanea di OPA1 e FGF21 non presenta le principali caratteristiche patologiche del fenotipo, ma pensiamo che altri fattori siano coinvolti nel processo di invecchiamento precoce. Dal confronto tra i diversi modelli a nostra disposizione (Opa1 ko, Opa1/fgf21 ko, Drp1 ko e Opa1/Drp1 ko), che a differenza degli OPA1 ko non muoiono ma hanno livello di FGF21 elevati, abbiamo capito che la differenza principale è l'infiammazione sistemica, presente solo negli Opa1 ko. In particolare, l'unica citochina di origine muscolare espressa per un periodo prolungato e secreta è l'interleuchina 6 (IL6). Vista la mancanza di dati in letteratura sui segnali molecolari che portano all'induzione di IL6, nel muscolo scheletrico, ci siamo concentrati su questo aspetto.

RIASSUNTO

L'invecchiamento è un processo naturale che può essere fisiologico o patologico (Sarcopenia). La sarcopenia è caratterizzata da una profonda perdita di massa muscolare, associata a fragilità, perdita di indipendenza, sviluppo di co-morbidità e mortalità precoce. La principale differenza tra i soggetti sarcopenici e quelli in salute è, infatti, una maggiore riduzione di muscolatura. In generale, la perdità di massa muscolare è un normale processo che si associa a tutti i tipi di invecchiamento, ma è molto più severo nei soggetti sarcopenici. E' importante sapere che questo processo è irreversibile e patologico una volta perso almeno il 60% della massa muscolare iniziale. Attualmente, l'unico modo per rallentare il catabolismo muscolare è praticare esercizio costante durante l'intera vita, perché non esistono ancora farmaci per il trattamento della sarcopenia.

Il tessuto muscolare scheletrico costituisce quasi il 50% della massa totale del corpo umano ed è uno dei maggiori siti di attività metabolica. Consuma quotidianamente un'elevatissima quantità di ATP, adenosina trifosfato, per garantire la contrazione muscolare. La quantità di mitocondri in questo tessuto è elevata, in quanto sono il centro metabolico della cellula, garantendo la conversione del cibo assunto con la dieta in ATP, la molecola energetica utilizzabile e richiesta dalla maggior parte dei processi endoergonici. E' importante sapere che i tessuti con alto turnover cellulare possono eliminare i mitocondri disfunzionanti sia diluendoli nelle cellule figlie durante la divisione cellulare, sia tramite mitofagia in seguito al rimodellamento conseguente alle dinamiche mitocondriali (fissione e fusione). I tessuti post-mitotici, come il muscolo scheletrico, possono utilizzare solamente il secondo meccanismo per preservare la funzione mitocondriale. La fissione consente alla cellula di eliminare porzioni di mitocondri danneggiati dal *network* mitocondriale, mentre la fusione permette la formazione di una rete di mitocondri interconnessi per mantenere il potenziale di membrana.

Nei mammiferi, il processo di fusione mitocondriale della membrana esterna è mediato dalle mitofusine (Mfn1 e 2) e Opa1 media la fusione della membrana interna. Il processo di fissione è mediato dalle proteine Drp1 e Fis1. Una volta frammentate, le porzioni alterate vengono rimosse tramite mitofagia. Ormai è

chiaro dalla letteratura che alterazioni in questi processi sono associati con disfunzioni del muscolo scheletrico e ripercussioni nell'intero organismo. Il nostro laboratorio ha partecipato in modo molto significativo ad incrementare le conoscenze in questo ambito con le suguenti pubblicazioni:

- Masiero E. et al, Autophagy is required to mantian muscle mass, Cell Metabolism 2009

-Romanello V. et al, Mitochondrial fission and remodelling contributes to muscle atrophy, EMBO J. 2010

- Carnio S. et al, Autophagy impairment in muscle induces neuromuscular junction degeneration and precocious aging. Cell rep. 2014

- Tezze C. et al, Age-Associated Loss of OPA1 in Muscle Impacts Muscle Mass, Metabolic Homeostasis, Systemic Inflammation, and Epithelial Senescence, Cell Metabolism 2017

- Favaro G. et al, DRP1-mediated mitochondrial shape controls calcium homeostasis and muscle mass, Nature Comunication 2019

- Romanello V. et al, Inhibition of the Fission Machinery Mitigates OPA1 Impairment in Adult Skeletal Muscles, Cells 2019

SCOPO DELLO STUDIO

Inizialmente, lo scopo dello studio corrente è stato di capire approfonditamente il ruolo delle dinamiche mitocondriali in vivo di cui poco era conosciuto. Il muscolo scheletrico è di grande interesse in questo contesto, in quanto, metabolicamente molto attivo e severamente colpito in patologie caratterizzate da disordini mitocondriali. Non era stato ancora studiato il ruolo di questa proteina, in vivo, in un tessuto metabolicamente attivo attraverso un approccio *loss of function nonostante la presenza di una malattia genetica (ADOA, autosomal dominant optic atrophy), caratterizzata dalla delezione in eterozigosi di OPA1*. La difficoltà di questo eventuale studio, era legata al fatto che i topi knock out per OPA1 muoiano a livello embrionale (Romanello and Sandri, 2013). A tale scopo sono stati generati modelli di topo deleti per la proteina Opa1 solamente nel muscolo scheletrico. Nel corso dello studio si sono aperte nuove strade di ricerca e il focus finale del lavoro è stato caratterizzare il

secretoma di questi muscoli e in che modo fosse in grado di modificare l'intero metabolismo dell'organismo, tanto da procurare un fenotipo di invecchiamento precoce cosi severo.

RISULTATI

Il modello costitutivo è caratterizzato da una letalità del 100% entro i primi 9 giorni post-natali. Questi topi mostrano un severo difetto di crescita, associato a ipoglicemia, nonostante il buono stato di nutrizione. Considerando la severità di questo fenotipo si è passati allo studio della delezione sul muscolo adulto. L'efficacia dei modelli genetici è stata validata sia con analisi trascrizionale sia con analisi dei livelli di espressione proteica , dai quali risulta che in entrambi i modelli, il trascritto è ridotto significativamente del 60%, mentre l'espressione della proteina è ridotta del 70%. I topi sono stati monitorati nel corso del trattamento e dopo il 40° giorno, gli Opa1 *knock-out* perdono peso spontaneamente. Questa riduzione è dovuta a una diminuzione della massa muscolare e allo stesso tempo a una riduzione del tessuto adiposo.
Nei muscoli adulti deleti non vi è segno di infiammazione né di degenerazione; dalla colorazione per l'enzima mitocondriale succinato deidrogenasi (SDH), invece, i muscoli dei topi con il gene OPA1 deleto risultano più chiari, questo è dovuto a una significativa riduzione della massa mitocondriale.
Sono state condotte analisi sulla morfologia, la distribuzione e la funzionalità dei mitocondri che hanno evidenziato un'importante riduzione delle massa mitocondriale e organelli altamente frammentati.
Considerando che durante la frammentazione mitocondriale è noto esserci un aumento dello stress ossidativo, è stato misurato attraverso la carbonilazione delle proteine. L'aumento dei ROS è noto indurre anche lo stress del reticolo, che è stato confermato, trovando un aumento della fosforilazione del fattore eif2alfa (noto marker di stress del reticolo) e dell'aumento della trascrizione dei geni target come ATF4, XBP1s, CHOP e GADD34. Inoltre, FGF21, una mitochina di grande interesse per la comunità scientifica, che si sa essere indotta sia dallo stress del reticolo sia dalla disfunzione mitocondriale è fortemente indotta nel

muscolo ed è aumentata progressivamnete in circolo, in linea col peggiorare del fenotipo.

Successivamente è apparso evidente che i topi sviluppassero un invecchiamento precoce, tanto che entro due mesi dalla delezione del gene sviluppano cifosi, pelo bianco, senescenza dei tessuti mitotici, estrema debolezza, intolleranza all'esercizio e infiammazione sistemica. Nella pubblicazione del 2017 della prima parte di questo lavoro è stata dimostrata la centralità della mitochina FGF21. Questo fattore, rilasciato effettivamente soltanto dal muscolo, in risposta allo stress mitocondriale, del reticolo e ai ROS è in grado di essere secreto e di promuovere la maggior parte del fenotipo. La dimostrazione è avvenuta grazie alla generazione dei topi doppi ko muscolari per FGF21 e OPA1 che mostrano un fenotipo molto più modesto.

Nella seconda parte dello studio abbiamo concentrato la nostra attenzione su fattori in grado di sinergizzare con FGF21 per promuovere l'invecchiamento. Dal confronto con altri due modelli del nostro laboratorio, Drp1 (fissione bloccata) e Opa1/Drp1 (fissione e fusione bloccata) ko, abbiamo capito che FGF21 da solo non è in grado di promuovere per intero tutto il fenotipo. Entrambi i modelli infatti, nonostante un aumento di FGF21 muscolare e circolante, non presentano invecchiamento precoce. E' emerso che a differenza dei singoli Opa1 ko gli altri due modelli non presentino infiammazione sistemica nè la liberazione dei ROS dai mitocondri. Dopo aver dimostrato che l'unica citochina che aumentata in circolo per lungo tempo fosse IL6, e che l'unica fonte della stessa fosse il muscolo, abbiamo confermato che fosse attiva sui tessuti periferici (analisi del midollo osseo, sangue, fegato). In seguito, attraverso trattamenti farmacologici e utilizzando la tecnica di trasfezione dei muscoli abbiamo dimostrato la cascata del segnale che dai mitocondri, con la delezione di Opa1, porta all'aumento della trascrizione e della secrezione della citochina.

CONCLUSIONI

Innanzitutto, la mancanza di Opa1 nel muscolo scheletrico sia durante lo sviluppo che in età adulta risulta così importante da provocare un impatto a livello sistemico. E' rilevante evidenziare che il fenotipo sia più compromesso

rispetto agli altri knock-out delle proteine coinvolte nelle dinamiche mitocondriali e ciò evidenzia che per l'omeostasi muscolare e metabolica è più importante la morfologia mitocondriale che non la singola funzione delle proteine. A livello muscolare la delezione di OPA1 durante lo sviluppo porta velocemente alla morte e nell'adulto è sufficiente per indurre atrofia muscolare e debolezza, e allo stesso tempo per avere un effetto sistemico.

I mitocondri risultano altamente frammentati e di conseguenza troviamo un eccesso di stress ossidativo, che è noto aumentare durante la fissione mitocondriale. Allo stesso tempo questo è causa di alterazione nel *folding* delle proteine portando ad un aumento dello stress del reticolo.

L'atrofia è dovuta ad un eccesso di degradazione proteica attraverso attivazione sia del sistema ubiquitina proteasoma, sia dell'autofagia. Questo è possibile in seguito a una diminuzione dell'attività di Akt che permette a FoXO3 di attivare le vie di segnale cataboliche.

La mancanza di Opa1 risulta chiave nell'omeostasi muscolare, tanto che la sua riduzione correla, negli anziani, con l'inattività e la riduzione della massa e della forza. Nei topi la sua assenza è sufficiente a indurre forti alterazioni nel metabolismo e causare invecchiamento precoce. Nel nostro lavoro per la prima volta si è provata una diretta funzione patologica per la mitochina FGF21. Inoltre è stata dimostrata dettagliatamente la capacità delle cellule muscolari di indurre la citochina IL6, che è un fattore pleiotropico di cui non si sa ancora molto nell'ambito della fisiopatologia muscolare. La sua induzione negli OPA1 ko è subordinata alla frammentazione/produzione di ROS che aumenta in modo importante lo stress del retocolo, inducendo l'aumento di FGF21. FGF21 è in grado di promuovere mitofagia nel muscolo. L'eccesso di mitofagia causa un eccesso di carico del lavoro degli autofagolisosomi e di conseguenza un recettore che fa parte dell'immunità innata, TLR9, trasloca dall'ER all'autofagolisosoma e interagisce col DNA mitocondriale che non riesce ad essere compeltamente digerito. Il TLR9 attiva cosi NF-kB, importante fattore nucleare nella risposta infiammatoria, che in questo modo attiva la trascrizione dell'IL6. Questo lavoro pone in rilievo l'importanza del secretoma del muscolo scheletrico nelle patologie infiammatorie e metaboliche.

SUMMARY

A healthy mitochondrial network is essential for post-mitotic tissues like muscles. During aging sarcopenia, mitochondria-shaping machinery declines. On the contrary, lifelong exercise preserves it.

OPA1 is a profusion protein that plays an essential role in mitochondrial dynamics. Interesting, OPA1 protein decreases in sedentary seniors and in 18 months-old mice. Exercise in aged mice is sufficient to increase OPA1 levels in old muscles. To address the OPA1 role in skeletal muscle and further investigate its involvement in aging, we generated muscle-specific ko mice. Indeed, Opa1 mice show severe precocious senescence, degeneration of multiple organs, and premature death. Surprisingly, mitochondrial dysfunction in muscle tissue is sufficient to directly drive metabolic changes and systemic inflammation by increasing the expression and secretion of the mitokine FGF21. Although the simultaneous deletion of OPA1 and FGF21 almost reverted the phenotype, we have new evidence that connects aging with mitochondrial dysfunction, autophagy alteration, and inflammation. Our findings underscore the central role of muscle mitochondria in the regulation of signaling pathways and the maintenance of total body metabolism, underlying the importance of a functional mitochondrial population for healthy aging.

BACKGROUND

Aging is a natural process characterized by a phase of growth and a phase of decline. There are two ways of becoming old, one is healthy, and the other one is unhealthy aging. The pathological way is called Aging Sarcopenia and is typically associated with a considerable reduction in the mass of the skeletal muscle. Based on this, the subjects became frail; they lose independence, increased their probability to have co-morbidity and precocious mortality. The muscle loss is a natural part of the aging process, but more than 60% of skeletal muscle wasting leads to the loss of independence. There are no drugs available for treating aging sarcopenia. The only way to counteract this catabolic process is by performing a lifelong exercise.

The skeletal muscle tissue constitutes almost 50% of the total mass of the human body, and it is one of the major sites of metabolic activity.

This tissue consumes daily a high amount of ATP to ensure muscle contraction. The amount of mitochondria in this tissue is high, ensuring the conversion of food taken with the diet into ATP, the usable energetic molecule and required by most of the energetic processes. Usually, tissues with high cell turnover can eliminate dysfunctional mitochondria through their dilution among cell division, or by mitophagy after fusion and fission processes. Post-mitotic tissue, such as skeletal muscle cells, do not divide and can use only the second mechanism to preserve or recover mitochondrial function. The events of fusion and fission regulate mitochondrial morphology and their subcellular localization, allowing the cells to maintain mitochondrial network dynamics. In mammals, mitochondrial fusion proteins required in the process are the mitofusin (Mfn1 and 2) and OPA1 and in the fission process, mainly Drp1.

AIM OF THE STUDY

Initially, the study aimed to understand the role of the mitochondrial dynamics in a post-mitotic tissue, such as skeletal muscle. This tissue is metabolically active and needs a functional network of mitochondria. Moreover, it is known to be affected by human mitochondrial disorders.

Before our work, the role of OPA1 protein in skeletal muscle was unknown because of the lethality of the total ko. For this reason, we generated muscle-specific OPA1-null mice. During the study of the model, we further focus our attention on the role of OPA1 in the aging process and on the muscle secretome that can promote unhealthy aging.

RESULTS

The constitutive model OPA1 knock out muscle-specific dies after 9 days of post-natal life. Thus, we generated an inducible muscle-specific Opa1 knock out mice, using the Cre-LoxP system activable by food tamoxifen. OPA1-/- showed a spontaneous decrease in weight due to both, muscular atrophy and white adipose tissue reduction. We found a reduction in absolute muscle force as a consequence of atrophy. Muscle morphology was normal, but we found a decrease in SDH staining, and further analysis suggested alterations in mitochondrial morphology and function.

Indeed, we measured an increase in ROS production during mitochondrial fission that caused an increased in unfolding proteins leading to UPR activation. FGF21, a known downstream target of UPR and a marker of mitochondrial dysfunction was increased as mRNA levels in muscle and as a circulating factor. Extending the deletion mice developed a premature aging phenotype, characterized by kyphosis, white hairs, profound weakness, exercise intolerance, and systemic inflammation.

In Tezze et al., 2017, we demonstrated that FGF21 is a crucial factor in Opa1 KO phenotype. In our model, the circulating FGF21 is produced and released exclusively by the skeletal muscle tissue. We generated mice with the simultaneous deletion of fgf21 and opa1, and they do not display a precocious aging phenotype. However, from the comparison between OPA1 ko and the other mitochondrial models in our laboratory, it was clear that FGF21 cannot be per se the cause of the all pathological features that we observed. We published two papers in which we studied the consequences of a block of fission (Favaro et al., 2019) and a simultaneous block of fusion and fission (Romanello et al., 2019) in skeletal muscle. Although mitochondrial dysfunction, alteration in

mitochondrial morphology and FGF21 induction were present in these models, as in Opa1 deleted mice, they do not display premature aging and mortality. Only the Opa1 model presented systemic inflammation which, from our data, raised from the skeletal muscle compartment. Thus, in the second part of this work, we focus our attention on inflammaging. In particular, IL6 is the only pro-inflammatory cytokines induces over time in the skeletal muscle of OPA1 ko, and that is released. Finally, we demonstrated step by step the signaling pathways from altered mitochondria induced IL6 release from muscle. For that purpose, we performed two pharmacological treatment and in vivo muscle transfection.

DISCUSSION

First, the specific deletion of Opa1 only in skeletal muscle leads to a striking systemic phenotype in both models generated.

Moreover, the phenotypes of the muscle-specific Mfn1/Mfn2 double knockout or Opa1/Drp1 ko are different from Opa1 ko suggest that cristae shape and bioenergetics more than fusion plays an essential role in muscle secretome.

The absence of OPA1 protein appears critical for muscular homeostasis both in mice and humans. In sedentary persons, OPA1 reduction correlates with the reduction of force and mass. In mice, its reduction results in metabolic alteration and premature aging.

In our paper, for the first time, is assessed that FGF21 can have a pathological function in skeletal muscle.

Moreover, we demonstrated that muscle cells can directly induce and secrete IL6. IL6 induction in OPA1 ko mice is dependent on the excess of mitochondrial fragmentation and ROS production that promotes Fgf21 induction. FGF21 is known to promote mitophagy in skeletal muscle cells. The excess of mitophagy causes an overload of mitochondria in autophagolysosomes. The receptor TLR9, involved in innate immunity, can translocate from ER to autophagolysosomes, and it senses mitochondrial DNA incompleted digested.

Then, TLR9 activates NF-kB which then activates IL6. Altogether, this work underlines the importance of skeletal muscle secretome in the whole body health.

1. INTRODUCTION

1.1. SKELETAL MUSCLE: Structure and function

Skeletal muscle is the most abundant tissue in the whole organism, it represents almost 40% of the body weight and it is responsible for the body posture and movement. Skeletal muscle is composed of multinucleated and elongated cells called muscle fibers. Muscles fibers are organized in bundles and separated by a specific membrane system. Each muscle is surrounded by a connective tissue membrane called epimysium; the muscle itself is formed by well-organized bundles of muscle fibers that are grouped in fascicular and are surrounded by another layer of connective tissue, called perimysium. Within the fasciculus, each individual muscle fiber is surrounded by connective tissue called the endomysium (Figure 1.1).

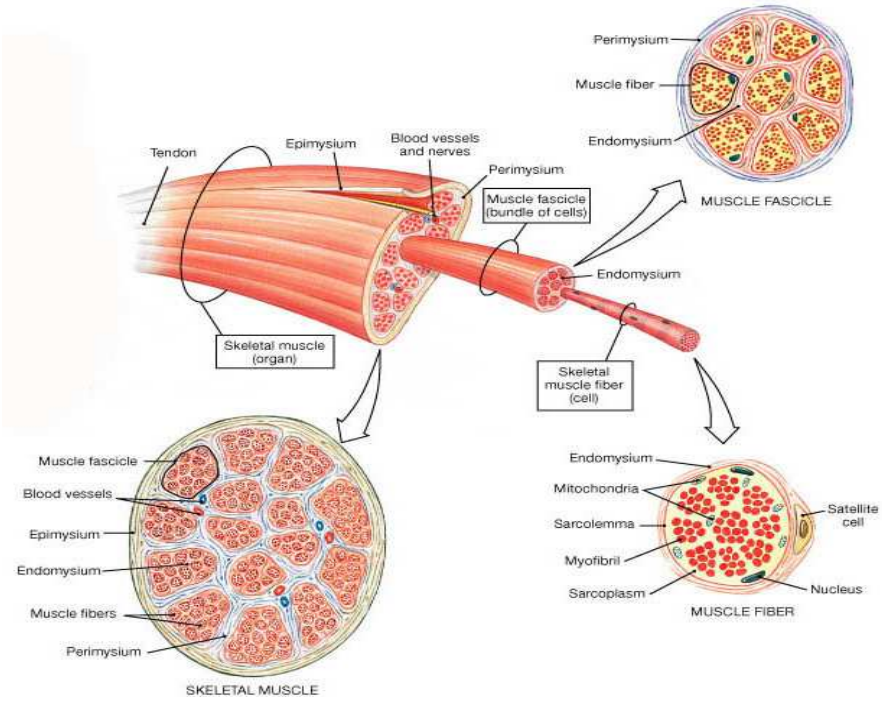

Figure.1.1: Schematic representation of skeletal muscle structure.

The plasma membrane surrounding muscle fibers is called sarcolemma. Each muscle fiber is formed by thousands of myofibrils, contains contractile proteins responsible for muscle contraction. The unit of muscle contraction is called sarcomere. Its structure was described first thank microscopy techniques that individuated isotropic (light band) and anisotropic (dark band) zones, forming the specific striated aspect of the skeletal muscle. For this reason, the sarcomere is usually defined as the segment between two neighbors Z-lines, that appears as a series of dark lines. Surrounding the Z-line, there is the region of the I-band (the light band). Following the I-band there is the A-band (the dark band). Within the A-band, there is a paler region called the H-band. Finally, inside the H-band there is a thin M-line, the middle of the sarcomere. These bands are not only morphological unit but also functional, because are characterized by the presence of different contractile proteins required for muscle contraction. Actin filaments (thin filaments) are the major component of the I-band and extend into the A band. Myosin filaments (thick filaments) extend throughout the A-band and are thought to overlap in the M-band. A huge protein, called titin, extends from the Z-line of the sarcomere, where it binds to the thin filament system, to the M-band, where it is thought to interact with the thick filaments. Several proteins important for the stability of the sarcomeric structure are found in the Z-line as well as in the M band of the sarcomere (Figure 1.2). Actin filaments and titin molecules are cross-linked in the Z-disc via the Z-line protein alpha-actinin. The M-band myosin, as well as the M proteins, bridge the thick filament system to the M-band part of titin (the elastic filaments). Moreover, several regulatory proteins, such as tropomyosin and troponin bind myosin molecules, modulating its capacity of contraction.

Muscle contraction is due to the excitation-contraction coupling, by which an electrical stimulus is converted into mechanical contraction. The general scheme is that an action potential arrives to depolarize the cell membrane. By mechanisms specific to the muscle type, this depolarization results in an increase in cytosolic calcium that is called a calcium transient. This increase in calcium activates calcium-sensitive contractile proteins that then use ATP to cause cell shortening. Concerning skeletal muscle, upon contraction, the A-bands do not change their length, whereas the I bands and the H-zone shorten.

This is called the sliding filament hypothesis, which is now widely accepted. There are projections from the thick filaments, called cross-bridges which contain the part (head) of myosin linked to actin. Myosin head can hydrolyze ATP and converting chemical energy into mechanical energy. The cross-bridges are mostly oriented transverse to the fiber axis in relaxed fibers, while angled at around 45 degrees in rigor.

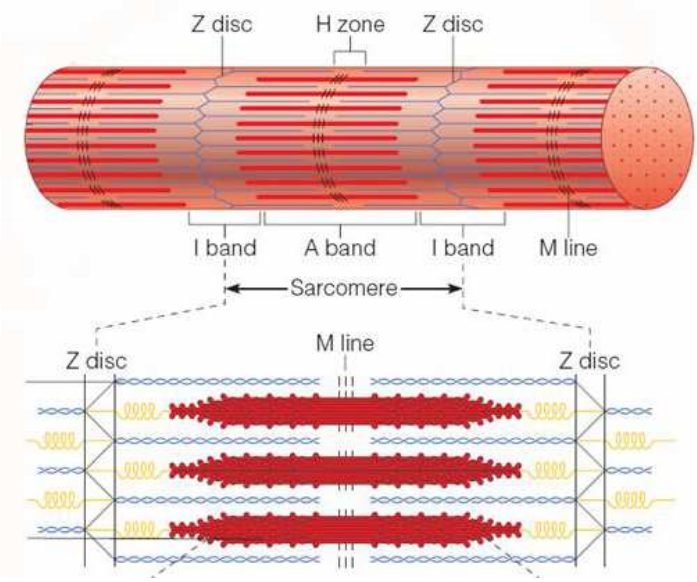

Figure.1.2: Schematic representation of skeletal muscle sarcomere.

To allow the simultaneous contraction of all sarcomeres, the sarcolemma penetrates the cytoplasm of the muscle cell between myofibrils, forming membranous tubules called transverse tubules (T-tubules) (Figure 3). The T-tubules are electrically coupled with the terminal cisternae which continue into the sarcoplasmic reticulum. Thus the Sarcoplasmic Reticulum, which is the enlargement of smooth Endoplasmic Reticulum (ER) and which contains the majority of calcium ions required for contraction, extends from both sides of T-tubules into the myofibrils. Anatomically, the structure formed by T-tubules surrounded by two smooth ER cisternae is called the triad and it allows the transmission of membrane depolarization from the sarcolemma to the ER. The contraction starts when an action potential diffuses from the motor neuron to the sarcolemma and then it travels along T-tubules until it reaches the sarcoplasmic reticulum. Here the action potential changes the permeability of

the sarcoplasmic reticulum, allowing the flow of calcium ions into the cytosol between the myofibrils. The release of calcium ions induces the myosin heads to interact with the actin, allowing the muscle contraction. The contraction process is ATP dependent. The energy is provided by mitochondria which are located close to the Z line.

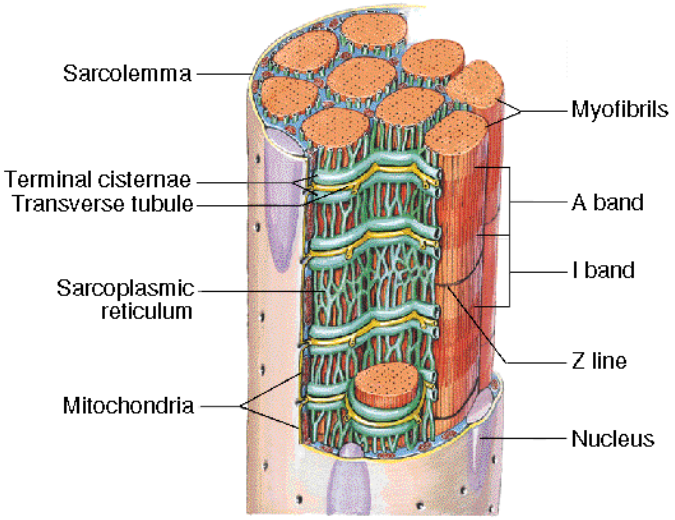

Figure.1.3: Schematic representation of the organization of T-tubules in skeletal muscle.

The contraction properties of a muscle depending on the fiber type composition. Mammalian muscle fibers are divided into two distinct classes: type I, also called slow fibers, and type II, called fast fibers. This classification considers only the mechanical properties. However, the different fiber types also show peculiar features such as myosin ATPase enzymes, metabolism (oxidative or glycolytic), mitochondrial content revealed by succinate dehydrogenase (SDH) staining, and resistance to fatigue (Pette and Heilmann, 1979; Schiaffino et al., 2007). Each muscle is composed by a combination of fiber types, whose abundance affects the type of contraction the muscle undergoes (slow or fast); regarding that, a muscle is defined as slow, if it containing more type I fibers, or fast, if type II fibers are more abundant. The different fiber types are also characterized by peculiar Myosin Heavy Chain (MHC) proteins expression. The fiber type I expresses the slow isoform of MHC (MHCβ or MHC1) and shows a great content of mitochondria, high levels of myoglobin, high capillary densities and high oxidative capacity. Muscles containing many types I fibers display red color for

the great vascularisation and the high myoglobin content. The type II, fast, myofibers are divided into three groups depending on which myosin is expressed. Distinct genes encode for MHC IIa, IIx (also called IId) and IIb. Type IIa myofibers are faster than type I, but they are still relatively fatigue-resistant. IIa fibers are relatively slower than IIx and IIb and have an oxidative metabolism due to the rich content of mitochondria (Schiaffino and Reggiani, 1996). Given all these characteristics, IIa fibers are also termed fast oxidative fibers. They exhibit fast contraction, high oxidative capacity, and relative fatigue resistance. The IIx and IIb fiber types are called fast-glycolytic fibers and show a prominent glycolytic metabolism containing few mitochondria of small size, high myosin ATPase activity, expression of MHC IIb and MHC IIx proteins, the fastest rate of contraction and the highest level of fatigability.

The fiber-type profile of different muscles is initially established during development independently of neural influence, but nerve activity has a major role in the maintenance and modulation of its properties in adult muscle. Indeed during postnatal development and regeneration, a default nerve activity-independent pathway of muscle fiber differentiation, which is controlled by thyroid hormone, leads to the activation of a fast gene program. On the contrary, the postnatal induction and maintenance of the slow gene program are dependent on slow motoneuron activity. The muscle fiber-type then undergoes further changes during postnatal life, for example, fiber-type switching could be induced in adult skeletal muscles by changes in nerve activity (Murgia et al., 2000).

1.2. MUSCLE HYPERTROPHY AND ATROPHY

Skeletal muscle mass is orchestrated by several complex mechanisms that regulate the rate of muscle growth and muscle loss. Muscle growth is mainly due to protein synthesis, that, when exceeds, leads to muscle hypertrophy. On the contrary, excessive protein degradation, loss of organelles and cytoplasm are major causes of muscle atrophy.

1.2.1. MUSCLE HYPERTROPHY

Skeletal muscle hypertrophy is defined as an increase in muscle mass, which in the adult animal comes as a result of an increase in the size of pre-existing skeletal muscle fibers. This growth, as stated above, is mainly due to increased protein synthesis and concomitantly decreased protein degradation. The Insulin-like growth factor (IGF-1)-AKT signaling is the major pathway that controls muscle growth. Muscle-specific IGF-1 overexpression in transgenic mice results in muscle hypertrophy and, importantly, the growth of muscle mass matches with a physiological increase of muscle strength. Furthermore, the over-expression of a constitutively active form of AKT, a downstream target of IGF-1, in adult skeletal muscle induced muscle hypertrophy. Moreover, AKT transgenic mice display muscle hypertrophy and protection from denervation-induced atrophy, showing that the AKT pathway promotes muscle growth and simultaneously blocks protein degradation (Schiaffino et al., 2013). AKT pathway, in fact, controls in an opposite manner two important downstream targets: mammalian target of rapamycin (mTOR) and glycogen synthase kinase 3 betas (GSK3β). In the first case, AKT activates mTOR, that is a key regulator of cell growth, promoting the activation of S6 kinase (S6K) and blocking the inhibition of eif4e binding protein 1 (4EBP1) on eukaryotic translation initiation factor 4E (eif4e), thus leading to protein synthesis. In the other case, the inhibition of GSK3β from AKT stimulates proteins synthesis, since GSK3β normally blocks protein translation initiated by eIF2B protein (Glass, 2005). Taken together with other observations, these results suggest that IGF-1- AKT axis is a major mediator of skeletal muscle hypertrophy. Recently, it has been reported that also the TGF-β pathway contributes to the regulation of muscle mass in adulthood (Sartori et al., 2013). Sartori et al. showed that when the BMP pathway is blocked or myostatin expression is increased, more Smad4 is available for phosphorylated Smad2/3, leading to an atrophy response. Therefore, under nor¬mal circumstance, a balance between these competing pathways is required to maintain muscle mass. Moreover, they identify a newly characterized ubiquitin-ligase, named MUSA1, as the molecular mechanism underlying the anti-atrophic action of the BMP pathway that has a negative

effect on its expression. This work provided shreds of evidence that also BMP signaling is involved in the regulation of adult muscle mass in normal and pathological situations (Sartori et al., 2013).

1.2.2. MUSCLE ATROPHY

Atrophy is defined as a decrease in cell size mainly due to protein degradation and then to the loss of organelles and cytoplasm as well. This is because protein turnover is dominant over cellular one during acute phases of muscle wasting.
Recent studies have highlighted a complex scenario whereby these catabolic signalings modulate one another at different levels and are also connected at various levels to biosynthetic pathways (Bonaldo and Sandri, 2013). The result is a coordinated balance between protein degradation and synthesis that reflects the physiological state of the muscle fiber.
Muscle loss is mediated by two highly conserved pathways: the ubiquitin-proteasomal system (UPS) and the autophagy-lysosomal pathway (ALP).
In all of these catabolic conditions, protein breakdown is enhanced and exceeds protein synthesis resulting in myofiber atrophy. The activation of the major proteolytic systems requires a transcription-dependent program. Comparing gene expression in different models of muscle atrophy leads to the identification of a subset of genes that are commonly up- or down-regulated in atrophying muscle (Bodine et al., 2001; Lecker et al., 2004; Sacheck et al., 2007). These common genes are thought to regulate the loss of muscle components and were thus designated atrophy-related genes or atrogenes.

1.2.3. THE UBIQUITIN-PROTEASOME SYSTEM

Degradation of a protein via the Ubiquitin-Proteasome Pathway (UPP) involves two discrete and successive steps: tagging of the substrate protein by the covalent attachment of multiple ubiquitin molecules (Conjugation); and the

subsequent degradation of the tagged protein by the 26S proteasome, composed of the catalytic 20S core and the 19S regulator (Degradation). This classical function of ubiquitin is associated with housekeeping functions, regulation of protein turnover and antigen-peptide generation. Ubiquitin (Ub) is covalently attached to substrate proteins via a three-step mechanism involving the sequential actions of E1 (ubiquitin-activating enzyme), E2 (ubiquitin-conjugating enzyme) and E3 (ubiquitin ligase) enzymes. The rate-limiting enzyme of UPS is the E3 which catalyzes the transfer of ubiquitin from the E2 to the lysine in the substrate. This reaction is highly specific and the proteins, committed to ubiquitination and proteasomal degradation, are recognized by the E3. Thus the amount and the type of proteins degraded by the proteasome is largely determined by which E3 ligases are activated in the cell (Gomes et al., 2001) (Figure 1.4).

FoxO3 transcription is the key regulator of these systems, being it necessary and sufficient for the induction of autophagy in skeletal muscle in vivo(Mammucari et al., 2007; Zhao et al., 2007). Moreover, it induces the transcription of two fundamental muscles ubiquitin-ligases: Atrogin-1 and MuRF-1(Bodine et al., 2001; Gomes et al., 2001; Sandri et al., 2004). These ubiquitin-ligases were identified through gene expression profile analysis performed on different atrophic models, as part of a set of genes, called 'atrogenes', that triggered or were involved in the atrophic program. These genes encode for proteins involved in different cellular processes like energy production, transcription factors, regulators or protein synthesis and enzymes of metabolic pathways. Among the upregulated atrophy-related genes there is a subset of transcripts related to protein degradation pathways.

Together these findings indicate that muscle atrophy is a process that requires the activation of a specific transcriptional program.

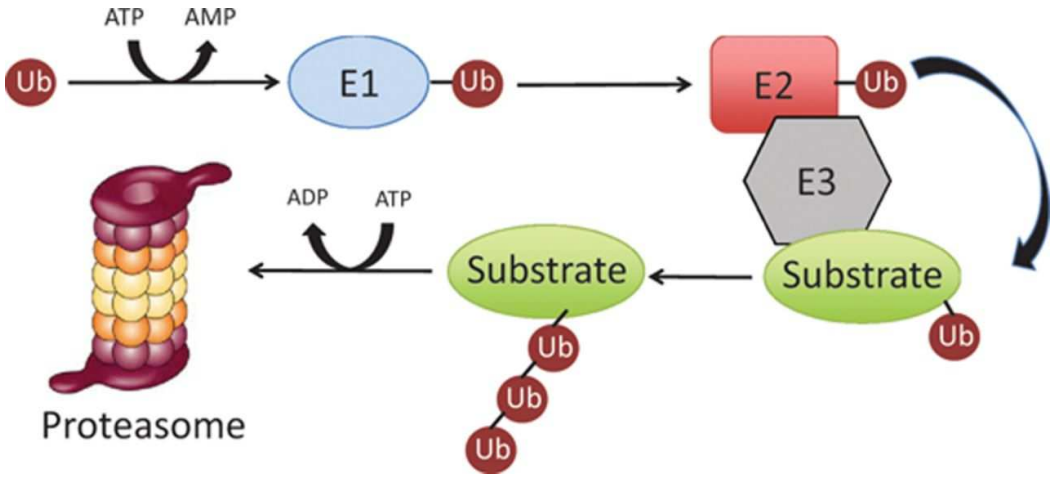

Figure.1.4: The proteasome degradation of specific substrates and misfolded proteins occurs through an enzymatic cascade of ubiquitination.

1.2.4. THE AUTOPHAGY-LYSOSOMAL SYSTEM

The autophagy-lysosomal pathway is an evolutionarily conserved catabolic process essential for metabolic homeostasis maintenance, depending on nutrient availability. This process is responsible for the degradation of cytosolic component, long-lived proteins, damaged organelles, protein aggregates, and intracellular pathogens. Autophagy, in fact, takes place at basal levels in all eukaryotic cells to maintain or rejuvenate function of proteins and organelles, but can also be induced by limitation of various types of nutrients, such as amino acids, growth factors, oxygen and energy as an adaptive mechanism essential for cell survival (Mizushima and Komatsu, 2011). During the autophagy process, the cargo that needs to be degraded is engulfed by double membranes layer called autophagosomes. This role in recycling is complementary to that of the ubiquitin-proteasome system, which degrades proteins to generate oligopeptides that are subsequently degraded into amino acids (Lecker et al., 2004).

The autophagy system is highly regulated through the action of various kinases, phosphatases, and guanosine triphosphatases (GTPases).

There are mainly three classes of autophagy: macroautophagy, microautophagy, and chaperone-mediated autophagy (Figure 5).

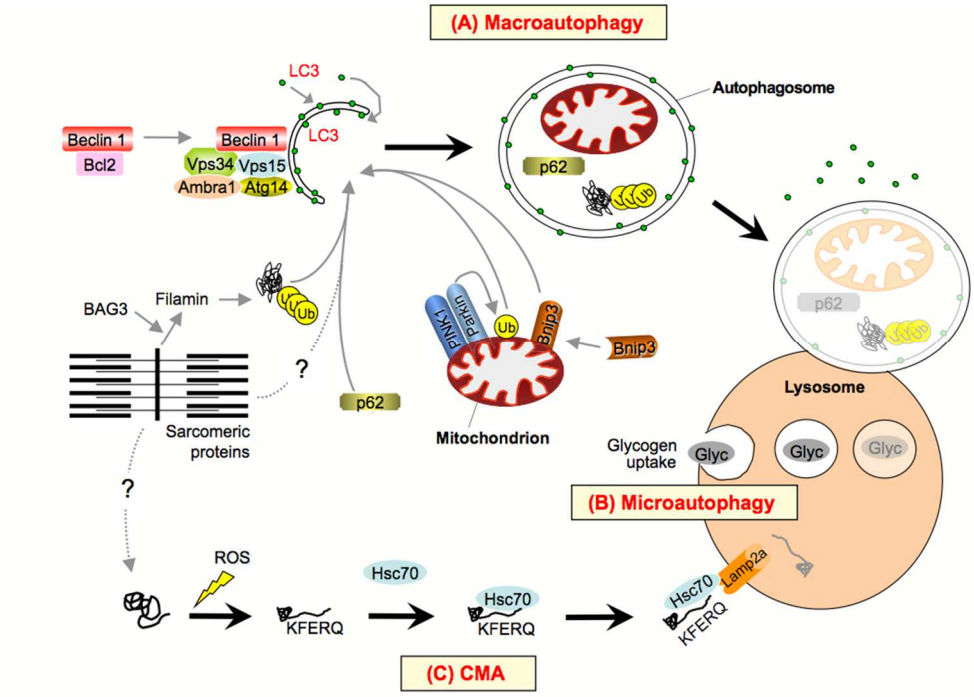

Figure.1.5: Scheme of the different type of autophagy: macroautophagy (a), microautophagy (b), chaperone-mediated autophagy (c) (Bonaldo and Sandri, 2013).

1.3. THE ROLE OF MITOCHONDRIA IN SKELETAL MUSCLE

Mitochondria are double-membrane organelles, they are characterized by two membranes that have different properties. The composition of the outer mitochondrial membrane (OMM) is similar to the eukaryotic one instead the inner mitochondrial membrane (IMM) resembles prokaryotic membranes in its physical properties and composition (Scorrano, 2013). Skeletal muscle is a major site of metabolic activity and the most abundant tissue in the human body, accounting for almost 40% of the total body mass. Healthy, trained muscles have an important role in the prevention of metabolic disorders such as obesity, diabetes, and hypertension. Muscle is a plastic tissue that responds and adapts

to changes in exercise, loading, nutrition, and hormones (Sandri, 2008). The major modifications that take place in skeletal muscle involve alteration of contractile properties and metabolic capacities. Different signaling pathways regulate protein content and energy transfer in adult myofibers. Skeletal muscle requires adenosine triphosphate (ATP), and muscle energy level is one of the cellular checkpoints between growth and hypertrophy or protein breakdown, which can provide alternative energy substrates for ATP production during energy stress (Sandri, 2008). Mitochondria are organelles depurate to produce energy, they are key organelles in intermediate cellular metabolism, energy conversion. Energy conversion occurs at the inner mitochondrial membrane (IMM) that can be further divided into two subcompartments: the so-called "boundary membrane" and the cristae, separated from the former by narrow tubular junctions (Cogliati et al., 2013).

The importance of mitochondria in skeletal muscle is underlined by the presence of two distinct population of these organelles in these tissues. They are classified in intermyofibrillar (IMF) and subsarcolemmal (SS) population and it's known they have different properties and localization. SS mitochondria represent 20% of mitochondria within skeletal muscle and IMF mitochondria account for the remaining 80% [10]. These two distinct mitochondrial populations have precise functional and biochemical properties. It has been suggested that SS mitochondria provide energy for membrane-related events including signaling and transport of ions and substrates, whereas IMF mitochondria supply ATP for the interaction of myosin with actin and therefore for muscle contraction. The two populations show different biochemical properties of mitochondrial enzymes (Sandri et al., 2013). In the last years, different papers underline that a decline in mitochondrial quality and activity has been associated with normal aging and correlated with the development of a wide range of age-related diseases (Ibebunjo et al., 2013; Sun et al., 2016).

1.3.1. MITOCHONDRIA-SHAPING MACHINERY

In the skeletal muscle, because is a post-mitotic tissue, the only way to preserve or restore the mitochondrial function is based on the balances on the fusion and fission events (Romanello and Sandri, 2015). Mitochondria are dynamic organelles and their number and morphology depend on the balance between two processes: fusion and fission. A fusion of isolated mitochondria generates and extend the mitochondrial network and is useful for mitochondrial membrane potential maintenance. Fission prevents the accumulation of abnormalities and defects into the network. Fragmented mitochondria can be removed by mitophagy. The machinery involved in mitochondria dynamics have been deeply investigated and its well-known both mechanisms are conserved from yeast to human. The key players in mammals are, mitofusin 1 (Mfn1), mitofusin 2 (Mfn2), and optic atrophy protein 1 (OPA1) require for the fusion of the outer mitochondrial membrane (OMM) and inner mitochondrial membrane (IMM). Mouse knockouts for each of these genes (Mfn1, Mfn2, and OPA1) are lethal to embryos because of mitochondrial dysfunction. Importantly, muscle-specific knockout mice for Mfn1 and Mfn2 are viable at birth, although they display profound muscle atrophy characterized by mitochondrial dysfunction, reduction of mtDNA in skeletal muscle, and accumulation of point mutations and deletions in the mitochondrial genome (Chen et al., 2010; Romanello et al., 2010). Mitochondrial fission depends on the GTPase cytosolic dynamin-related protein 1 (DRP1), which translocates to the OMM. DRP1 activity is regulated by phosphorylation in conserved serine residues within the GTPase effector domain, as well as by ubiquitination and processes of sumoylation, involving small ubiquitin-related modifiers (SUMOs). Fis1 is an OMM-anchored protein. It has been proposed to be required for mitochondrial division and to be the receptor for the recruitment of DRP1 on OMM. New potential Drp1 interactors, has been proposed like Mff, MiD49, and MiD51 (Otera et al., 2010; Palmer et al., 2011) (Figure 1.6).

1.1.1. OPA1 PROTEIN: STRUCTURE AND FUNCTION

OPA1, was identified "in silico" as a human homolog of Mgm1p in Saccharomyces cerevisiae and Msp1p in Schizosaccharomyces pombe, and its mutations were found responsible for an optic neuropathy Human OPA1 ORF is built from 30 exons, 3 of which (4, 4b and 5b) are alternatively spliced leading to 8 mRNA. While exon 4 is evolutionarily conserved, both exons 4b and 5b are specific to vertebrates (Delettre et al., 2000).

The OPA1 gene encodes a mitochondrial protein that belongs to the dynamins' family; with which it shares three conserved regions: a GTPase domain, a middle domain, and a GTPase effector domain (GED) containing a coiled-coil domain (CC2). Interestingly,

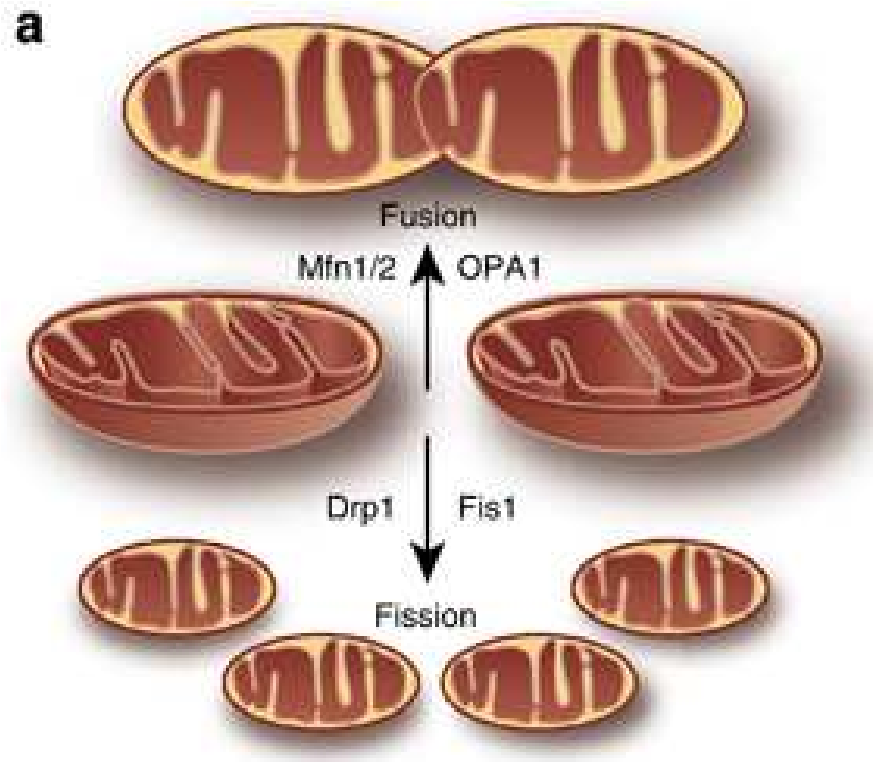

Figure.1.6: mitochondrial dynamics (Zhan, 2013)

the recombinant short isoform of OPA1 (discussed below) assembles into higher-order oligomers on the surface of cardiolipin-containing liposomes. The amino-terminal region of OPA1, preceding the GTPase domain, displays a mitochondrial import sequence (MIS) followed by a predicted transmembrane helix (TM1) that is conserved in all OPA1 homologs. Two additional hydrophobic domains are present, TM2a and TM2b, and they are encoded by alternatively spliced exons 4b and 5b (Delettre et al., 2000). Each l-OPA1 isoform might then be subjected to distinct proteolytic processing that generates short isoforms termed s-OPA1. Both short and long isoforms of OPA1 are localized in the IMS and are associated with mitochondrial membranes. It is proposed that l-OPA1 is anchored to the IMM(inner mitochondrial membrane) whiles-OPA1 is peripherally attached to the IMM, a fraction of it can diffuse in the IMS and to associate, within this compartment, to the OMM

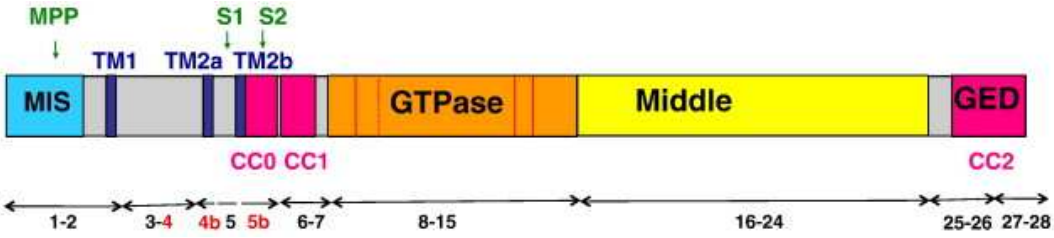

Figure. 1.7. Schematic representation of OPA1 structure

(outer mitochondrial membrane). Numerous and discordant studies on the generation of s-OPA1 have implicated four mitochondrial proteases recognizing two cleavage sites. The rhomboid protease PARL. The mAAA-protease paraplegin is proposed to cleave OPA1 at S1 (Figure. 1.7). However, neither PARL nor paraplegin does wholly explain the processing of OPA1 since their knockdown/out does not affect the ratio of l- to s-isoforms of the dynamic. The i-AAA protease YME1L was shown to be responsible for cleavage at S2 (Figure. 1.7), and other sites in mammals. Inducible OMA1-mediated cleavage of OPA1 on S1 site too.

OPA1 is ubiquitously expressed, with high mRNA expression levels in retina, brain, liver, heart, and pancreas; typically, all the 8 spliced forms of the OPA1

transcripts are expressed, but the abundance of each variant seems to be under tissue-specific control (Belenguer and Pellegrini, 2013).

Besides constitutive processing, cleavage of l-OPA1 was also shown to be induced by the dissipation of mΔψ and apoptosis and correlated with mitochondrial fragmentation.

Opa1 is involved in different important function, first is needed with MFN1 for mitochondrial fusion (Cipolat et al., 2004) moreover is essential for controls apoptotic cristae remodeling (Frezza et al., 2006) for determines respiratory chain supercomplexes assembly and respiratory efficiency (Cogliati et al., 2013)finally is important for mtDNA maintenance (Amati-Bonneau et al., 2008).

1.2. SKELETAL MUSCLE PLASTICITY

Skeletal muscle tissues have generally been considered to be pure locomotor organs, but in the 2000s a secretory function for these muscles was recognized. In 2003 it was proposed that IL6 and other cytokines were induced and secreted by skeletal muscles into their circulation during physical activity. In consideration of these findings, the muscle-secreted molecules were named "myokines" (Pedersen et al., 2003). Increasing evidence underlines that skeletal muscle secretes a wide variety of molecules like cytokines, miRNA, exosomes, mtDNA during exercise but also in different acquired and inherited diseases (Alipoor et al., 2016; Delezie and Handschin, 2018; Hoffmann and Weigert, 2017; Inagaki et al., 2007; Safdar and Tarnopolsky, 2018). Thus, skeletal muscles are a source of myokines, metabolites, and muscle-derived molecules. They mediate the communication between distant organs to adapt the whole-body metabolism to nutritional and environmental pressures (Rai and Demontis, 2016; Whitham and Febbraio, 2016). This systemic regulation helps to explain why physical activity, and thereby muscle contraction, elicits several beneficial effects in a variety of diseases. However, the nature and the function of most of the myokines and muscle-derived molecules are still unclear. In the last years, FGF21 started to be studied as an important myokine, because of its plethora of positive and negative effect.

1.2.1. FGF21: A CONTROVERSIAL MYOKINE

Fibroblast growth factor 21 (FGF21) is a hormone, released by liver, pancreas, white adipose tissue, heart, brain and skeletal muscle as well, that regulates important metabolic pathways. The fibroblast growth factor (FGF) family is a group of multifunctional signaling molecules that have a wide variety of functions. The family comprises of 22 related proteins, each grouped into subfamilies, based on genetic and functional similarity. In 2000 the *Fgf21* gene was identified in mouse embryos by RT-PCR (Nishimura et al., 2000). It was the 21st discovered *Fgf* gene, which was later included into the FGF19 subfamily (also called endocrine FGF), together with *Fgf15* (mouse ortholog of human FGF19) and *Fgf23*. FGF21 function remained completely unknown until 2005 when it was proposed to be a novel metabolic regulator and a potential anti-diabetic drug (Kharitonenkov et al., 2005). Several studies showed that FGF21 stimulates the oxidation of fatty acids, the production of ketone bodies and the inhibition of lipogenesis (Fisher and Maratos-Flier, 2016; Staiger et al., 2017). Therefore, the finding that FGF21 regulates glucose-lipid metabolism has made it a promising therapeutic target for metabolic diseases. However, despite some studies showing that administrating FGF21 prevents diet-induced obesity and insulin resistance (Fisher and Maratos-Flier, 2016; Staiger et al., 2017) in mice and humans, there is a paradoxically positive correlation with elevated serum FGF21 levels and metabolic disorders like obesity, diabetes, mitochondrial diseases, and aging (Staiger et al., 2017; Tezze et al., 2017a). Interestingly, all these conditions have in common muscle loss. In addition, several reports indicate a pathophysiological role for FGF21: a) it promotes muscle atrophy (Oost et al. 2019), bone loss and reduced bone mineral density (Fazeli et al., 2015; Wei et al., 2012); b) it is a stress-induced myokine which is released during starvation, ER stress and mitochondrial dysfunction (Izumiya et al., 2008; Keipert et al., 2013; Pereira et al., 2017; Rodríguez-Nuevo et al., 2018; Tezze et al., 2017a). Thus, FGF21 is a powerful and debated hormone that belongs to the list of factors controlling energy homeostasis and metabolism. Thus, the beneficial or detrimental actions of FGF21 are affected by multiple

variables including the tissue source, serum concentration, animal age, and the presence of synergizing /antagonizing factors (Tezze et al., 2019).

1.3. AGING SARCOPENIA

Sarcopenia is a progressive loss of skeletal muscle mass and function in the elderly people that decrease mobility, reduces the quality of life, and can lead to severe co-morbidities. Loss of muscle mass during aging is largely due to the progressive loss of motoneurons and lead to a reduced muscle fiber number and size. Muscle function progressively and importantly declines because motor neuron loss is not compensated by reinnervation of muscle fibers (Larsson et al., 2018). Qualitative changes in posttranslational modifications of muscle proteins and the loss of contractile, mitochondrial, and sarcoplasmic reticulum protein expression. In experimental models, specific intervention strategies have shown encouraging results on limiting deterioration of motor unit structure and function under conditions of impaired innervation. Translated to the clinic, if these or similar interventions, by saving muscle and improving mobility, could help alleviate sarcopenia in the elderly, there would be both great humanitarian benefits and large cost savings for health care systems (Larsson et al., 2018).

1.3.1.INFLAMM-AGING

In 2000 the Italian gerontologist Claudio Franceschi proposed a new theory on the role of inflammation during aging and he called it inflamm-ging (Franceschi et al., 2000). This new point of view is based on the concept that the aging process is associated with a change in the grade of inflammation and that is, until a certain point, a way for the whole body to adapt itself at the changes that happened during life. Then, this chronic low grade of inflammation during the time induces dramatic and irreversible changes (Fulop et al., 2018). The natural aging process is associated with a chronic inflammatory phenotype characterized by a systemic overabundance of proinflammatory cytokines such

as TNFa, and IL6. This condition is associated with anemia, and hematopoietic stem cells fate alteration (Pietras, 2017).

1.3.2.NFKB pathway in skeletal muscle

Mechanistically, the large array of defense factors and mechanisms linked to the NF-κB system seem to be involved in the aging process (Balistreri et al., 2013). This concept leads in proposing inductors of NF-κB signaling pathway as potential aging biomarkers in the whole-body and in skeletal muscle. NF-kB represents a family of five transcription factors (p65, c-Rel, RelB, p52 and p50)(Figure 1.11) expressed in skeletal muscle (Hunter et al., 2002), which play a key role in activation of immune and inflammatory responses in skeletal muscle cell (Zhang et al., 2007). This NF-kB pathway is activated by phosphorylation, ubiquitination, and proteolysis of the inhibitory protein IkB by IkKB, which otherwise binds and retains the NF-kB heterodimer in the cytosol. After this degradation, NF-kB can go into the nucleus and activate the gene target transcription. It has been demonstrated that NF-kB constitutes activation in vivo induced atrophy (Cai et al., 2004) and that constitutive inhibition of the same pathway protects from atrophy caused by disuse and so is considered particularly important in sarcopenia (Mourkioti et al., 2006). This pathway is not yet elucidated in skeletal muscle but some pieces of evidence suggest that NF-κB might play a pivotal role in the expression of proinflammatory molecules and muscle loss, mainly during sepsis (Li et al., 2008). Since the discovery in 1991 that NF-kappaB may be activated by H(2)O(2), several laboratories have put a considerable effort into dissecting the molecular mechanisms underlying this activation (Gloire et al., 2006).

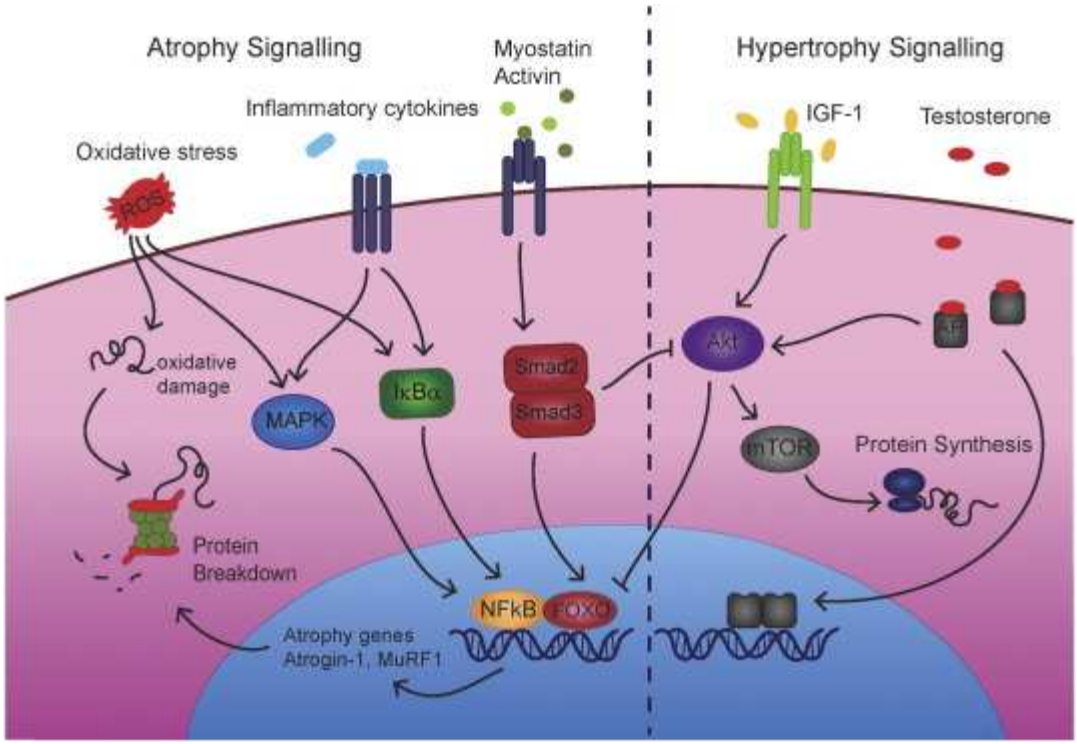

Figure 1.11 NF-kB signaling pathways

2. METHODS

2.1. Human subjects

All participants were healthy volunteers and declared not to have any specific physical/disease issues. The specific exclusion criteria were body mass index ≥40kg/m2; previous knee replacement; recent deep vein thrombosis or any infection; myopathy; neurologic, pulmonary, or symptomatic cardiovascular diseases; vertigo or impaired cognitive function; recent or past cancer; rheumatism; or any other relevant limitations of the musculoskeletal system. All participants were informed about the testing procedures and the possible risks and written informed consent had to be signed prior to inclusion in this study. In addition, ethical approval was obtained from the ethical committee of the municipality of Vienna (EK 07-057-0407) and (EK08-102-0608).

Nutritional status before skeletal muscle biopsy consisted of daily routine. Muscle biopsy collection was performed quite at the same time in the morning between 10.00 and 11.00 from the Vastus Lateralis of three different groups of male subjects as described (Zampieri et al., 2015): Young subjects (23 to 34 years of age) performing moderate training activities; sedentary seniors(53 to 82 years of age), either inactive healthy subjects performing only routine daily activities or seniors with knee arthropathy, and senior sportsmen: (66 to 72 years of age) who routinely practiced (lifelong) sport activities more 3 to 5 times a week (one –to –two hours per session).

Torque measurement and testing

An isometric measurement on a dynamometer (S2P Ltd., Lubljana, Slovenia) with 90° hip flexion and 60° knee flexion (full knee extension = 0°) was performed as described (Šarabon et al., 2013a,b) three times at each leg to assess the maximal isometric torque of the left and right knee extensors. The mean of the best values of each leg was taken for further analyses.

The time up and go test (TUGT) (Podsiadlo and Richardson, 1991) was performed to evaluate mobility and function in activities of daily living. Briefly,

the subjects were asked to stand up from a standard chair, walk a distance of 3 m, turn around, walk back to the chair, and sit down again all as fast as possible. VAS-48h (visual analog scale in rest and during activity) and WOMAC (Western Ontario and McMaster Universities Arthritis Index) questionnaire were performed to evaluate pain in the activities of daily living in the last 48h prior to the assessment.

2.2. Plasma Human samples

The human samples used in this study were obtained from volunteers of different ages, ranging from 19-103 years-old. recruited in the framework of the EU FP6 Project "Geha – Genetics of Healthy Ageing"; the EU FP7 Project "MYOAGE – Understanding and combating age-related muscle weakness"; and the Italian National Project "PRIN2009CB4C9F - Ruolo Della epigenetica e della Genetica del DNA mitocondriale nella longevità: Studi su soggetti con più di 105 anni di età (semi-supercentenari)".

The study protocols were approved by the local Ethical Committees responsible for the Bologna unit, respectively:

- for the Geha study: Sant'Orsola-Malpighi University Hospital (Bologna), ethical clearance n. 118/2004/U/Tess issued on 20/07/2004;
- for the MYOAGE study: Istituto Ortopedico Rizzoli (Bologna) ethical clearance n. 10823 issued on 26/04/2010;
- for the PRIN study: Sant'Orsola-Malpighi University Hospital (Bologna) ethical clearance n. 22/2007/U/Tess issued on 27/02/2007, amendment n. EM 157/2011/U issued on 25/11/2011.

Inclusion/ Exclusion criteria:

MYOAGE samples from 24-96 years-old subjects: Healthy subjects. Exclusion criteria were: to be non-autonomous in the daily living activities, to be unable to walk a distance of 250 m, presence of morbidity (neurologic disorders, metabolic diseases, rheumatic diseases, recent malignancy, heart failure, severe chronic obstructive pulmonary disease (COPD), haemocoagulative syndromes), use of medication (immunosuppressive drugs, insulin), immobilization for 1

week during last 3 months, and orthopedic surgery during the last 2 years or still causing pain or functional limitation.

Hip replacement subjects: Subjects who underwent surgery for hip dysplasia. Age (> 20 years) and the ability to provide informed consent and to cooperate with the study personnel were inclusion criteria, while exclusion criteria were presence of diseases, i.e. chronic kidney and/or liver diseases, bleeding disorders, severe type 2 diabetes, rheumatic diseases, osteoarthritis, neuromuscular disorders, malignancies and systemic infections, other than chronic steroid use, major psychological problems or history of alcohol or drug abuse, evidence of prior surgery in the involved hip.

GEHA samples: Inclusion criteria of participants: i) they should be at least 90 years of age (a nonagenarian); ii) they should have a living sibling who also is a nonagenarian; iii) they should be able to understand the scope of the project.

PRIN2009CB4C9F samples: Inclusion criteria: 100+ years old subjects

For FGF21 detection the HUMAN FGF-21 IMMUNOASSAY CAT NUM DF2100 (R&D SYSTEMS) kit was used.

2.3. Animal handling and generation of muscle-specific OPA1 knockout mice

Animals were handled by specialized personnel under the control of inspectors of the Veterinary Service of the Local Sanitary Service (ASL 16 - Padova), the local officers of the Ministry of Health. All procedures are specified in the projects approved by the Italian Ministero Salute, Ufficio VI (authorization number 1060/2015 PR). Muscles were removed at various time periods and frozen in liquid nitrogen for subsequent analyses.

To generate constitutive muscle-specific OPA1 knockout animals, mice bearing *Opa1* floxed alleles *(Opa1$^{f/f}$)* (Cogliati et al. 2013) were crossed with transgenic mice expressing Cre under the control of a Myosin Light Chain 1 fast promoter (MLC1f-Cre) and kept in a homozygous mating system. Experiments were performed on newborns at post-natal day 7 or 8. Cre-negative littermates were used as controls.

A second knockout model with inducible muscle-specific deletion of OPA1 was obtained by crossing the *Opa1*$^{f/f}$ line with mice carrying Cre-ER driven by human skeletal actin promoter (HSA). Tamoxifen-induced Cre LoxP recombination was activated by oral administration of tamoxifen-containing chow (Tam400/Cre ER Harlan) which was provided ad libitum for 5 weeks. A third knockout model was obtained by crossing HSA- *Opa1*$^{f/f}$ line with *Fgf21*$^{f/f}$. Tamoxifen-induced CreLoxP recombination was activated by oral administration of tamoxifen-containing chow (Tam400/Cre ER Harlan) which was given ad libitum for 5 weeks. Animals with food intake received

indicatively, 1 mg of tamoxifen per day. Muscles were collected at different times: 30, 50 or 120 days after the beginning of the tamoxifen diet. Cre-negative littermates, also receiving tamoxifen treatment were used as controls. Adult mice (3 to 5 months old) of the same sex and age were used for each individual experiment. *Fgf21* floxed (*Fgf21*$^{f/f}$) were purchased by The Jackson Laboratory and crossed with HSA- *Opa1*$^{f/f}$ Cre positive.

PCR genotyping was performed with the following primers:

OPA1 Fw: CAGTGTTGATGACAGCTCAG

OPA1 Rv: CATCACACACTAGCTTACATTTGC

FGF21 Fw: AGGAGGCTAGGGCTTGACTCT

FGF21 Rw: TGACAGGGTCTCAGGTTCAA

Cre Fw: CACCAGCCAGCTATCAACTCG

Cre Rv: TTACATTGGTCCAGCCACCAG

2.4. EXPERIMENTAL TIME-LINE

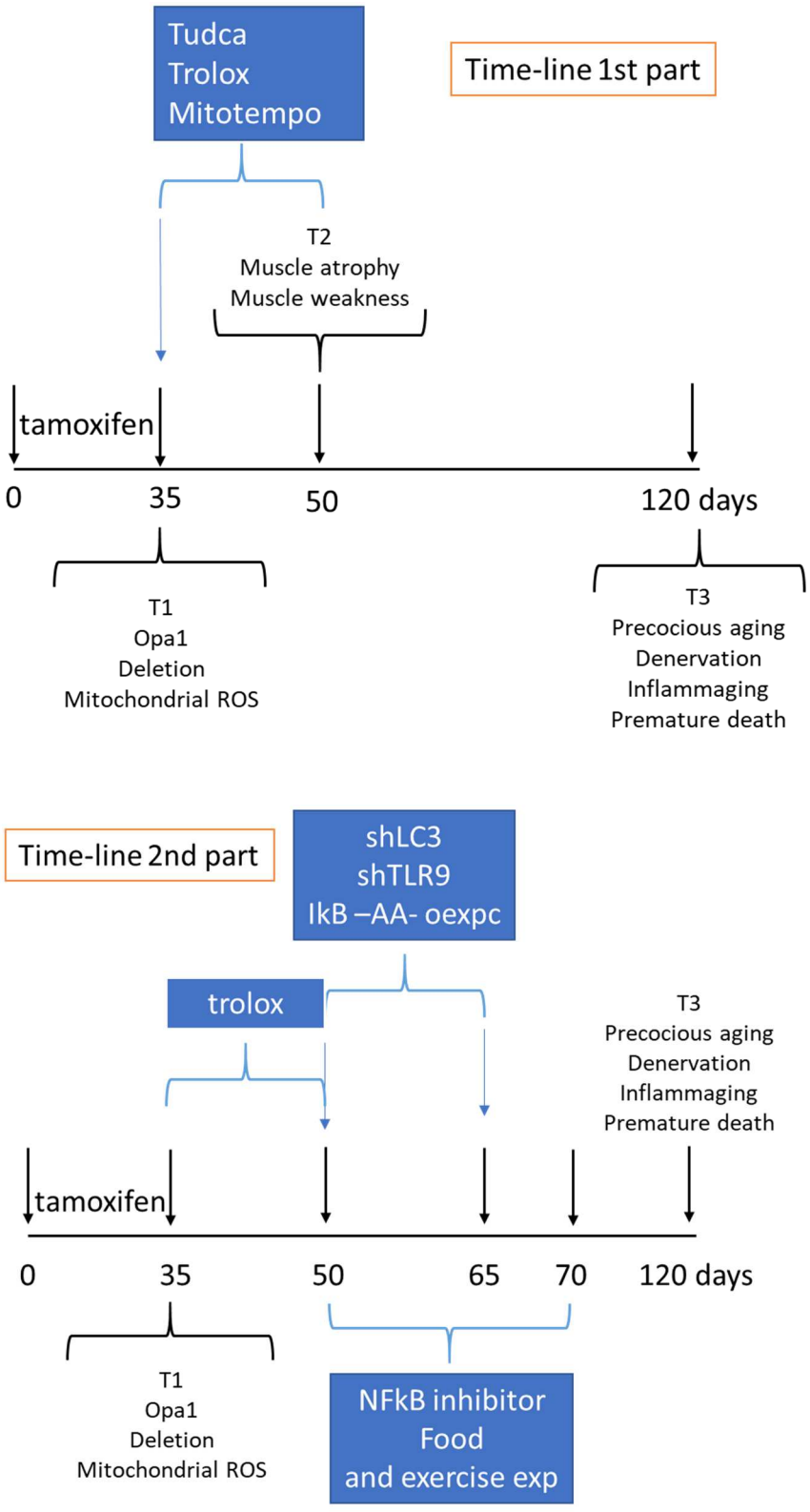

2.5. Gene expression analyses

Total RNA was prepared from muscles using TRIzol (Invitrogen). Complementary DNA was generated from 0.4 μg of RNA reverse-transcribed with SuperScript III Reverse Transcriptase(Invitrogen). Duplicates of cDNA samples were then amplified on the 7900HT Fast Real-Time PCR System (Applied Biosystems) using the Power SYBR Green RT-PCR kit (Applied Biosystems). All data were normalized to GAPDH and to actin expression and plotted in arbitrary units as mean±SEM. The oligonucleotide primers used are shown in the following table.

2.6. Immunoblotting

Muscles were lysed and immunoblotted as previously described (Mammucari et al., 2007). Blots were stripped using Restore western blotting stripping buffer (Pierce) according to the manufacturer's instructions and probed again when necessary. List of antibodies is depicted in the key resources table

2.7. ß-galactosidase assay

In vitro ß-galactosidase measurement was performed on different tissues (liver, skin, and gut). Lysates were prepared using T-PER™ Tissue Protein Extraction Reagent (cat n78510, Thermofisher) then Pierce™β-Galactosidase Assay Reagent (Product No. 75705) and β-Galactosidase Assay Stop Solution (Product No. 75706) to develop the reaction.

2.8. Imaging and Transmission Electron Microscopy

Cryosections of both P8 newborns hindlimb cross-sections and adult TA were stained for H&E and SDH. Total myofiber number was calculated from entire hindlimb cross-section based on an assembled mosaic image. (20X magnification). CSA was performed on adult TA as described (Mammucari et al, 2007). ATPase staining: Serial cryosections (8 μm) from human muscle biopsies were mounted on polylysine glass slides, air dried, and stained either with

hematoxylin and eosin (H&E) or conventional techniques for myofibrillar ATPases to evaluate muscle fiber type. For ATPase stains, slow-type fibers are dark, whereas fast-type fibers are lightly stained following preincubation at pH 4.35. Fiber type grouping is identified on the basis that one myofiber is completely surrounded by fibers of the same phenotype. Morphometric analyses were performed on stained cryosections using Scion Image for Windows version Beta 4.0.2 (2000 Scion Corporation) (Zampieri et al., 2015). For immunostaining, we used antibodies specific for Pax7 (1:20, Hybridoma Bank), BrdU (1:40, Roche) and TOM20 (1:100, Santa Cruz). The secondary antibodies, goat anti-mouse Cy3 were obtained from Jackson lab. Hoechst co-staining, allowed to identify the subsarcolemmal position of myonuclei.
For electron microscopy, we used conventional fixation-embedding procedures based on glutaraldehyde-osmium fixation and Epon embedding.

2.9. Measurement of Mitochondrial DNA Copy Number

Total gastrocnemius DNA was isolated using the Puregene Cell and Tissue Kit(Qiagen) and was amplified using specific primers for mtCOXII and 18S by real-time PCR using the Power SYBR Green RT-PCR kit (Applied Biosystems). The mtDNA copy number was calculated using 18S amplification as a reference for nuclear DNA content.

2.10. Mitochondrial Assays

Muscle mitochondria from the indicated genotype were isolated as described (Frezza et al., 2007). To detect RCS, Blue Native PAGE was performed by resuspending mitochondrial pellets in Native Buffer (Invitrogen) plus 4% Digitonin (SIGMA) to a final concentration of 10µg/µl and incubated for 1 hour on ice. After 20 min of centrifugation at 16,000 g, the supernatant was collected and one-third of digitonin percentage of Sample Buffer 5% G250 (Invitrogen) was added. Then 50µg of mitochondrial membrane proteins were applied and run on a 3-12% Bis-Tris gel (Invitrogen) as described in the NativePAGE™ Novex® Bis-Tris Gel System manual. Western blot was performed using a

Trans-Blot transfer cell (Bio-Rad) at 4°C ON. List of antibodies is depicted in Supplementary Table 2.

To measure respiration, mitochondria (1 mg/ml) were incubated in Experimental Buffer (EB: 150 mM KCl, 10 mM Tris Mops,10 mM EGTA-Tris, 10mM ATP). When indicated, mitochondria were transferred into Clark's type oxygen electrode chamber and 5mM glutamate/2.5 mM malate or 2 mM rotenone/10 mM succinate were added. Basal O2 consumption was recorded (state 2) and after 2 min 100 mMADP was added (state 3), followed by 2.5 mg/ml oligomycin (state 4) and 200 mMFCCP (state 3u). Assessment of mitochondrial respiratory chain enzymatic activities on muscles was determined as described (Spinazzi et al., 2012). Results were normalized to citrate synthase enzymatic activity.

2.11. Protein Carbonyls Detection

Carbonylation of muscle proteins was detected by using the OxyBlot Protein Oxidation Detection Kit (Millipore, s7150). (Masiero et al., 2009) Quantification analysis was performed with ImageJ Software and all values were normalized for the housekeeping GAPDH.

2.12. Mitochondrial oxidative stress measurement

Mt-roGFP1, which measures the thiol/disulfide equilibrium in the mitochondrial matrix, was used as an indicator of mitochondrial redox status, as previously described (Lo Verso et al,2014). Briefly, Adult FDB muscles were transfected by electroporation with mt-roGFP1 plasmid. After 7 d of transfection single muscle fibers were isolated from control and knock-out mice. Mt-roGFP1 fluorescence (excitation: 405 and 480 nm, emission: 535 nm, 20× objective) was measured for 5 min every 10 s and upon H_2O_2. The ratio of fluorescence intensities (exc 405/480) was determined by ImageJ software.

2.13. In vivo protein synthesis measurements

In vivo protein synthesis was measured by using the SUnSET technique(Goodman et al., 2011; Schmidt et al., 2009). Mice were anesthetized and then given an intraperitoneal injection of 0.040
μmol/g puromycin dissolved in 100 μl of PBS. At exactly 30 min after injection, muscles were collected and frozen in liquid N2 for WB analysis using a mouse IgG2a monoclonal anti-puromycin antibody (clone 12D10, 1:5000).

2.14. In vivo drug treatments

Knockout and control mice received TUDCA (Tokyo Tanabe, Tokyo, Japan) at a dose of 500 mg/kg twice a day (8:00 AM and 8:00 PM) by oral administration for 5 days or 2 weeks.
Mice were intraperitoneally injected daily for 5 days or 2 weeks with 30 mg/kg of TROLOX (6-hydroxy-2,5,7,8-tetramethylchroman-2-carboxylic acid).
Mito-TEMPO (Enzo Life Science, ALX-430-150-M005) at a dose of 1.4 mg/kg was administered through an intraperitoneal injection every day for 5 days or 2 weeks. In vivo NF-kB inhibitor was administered by food, between 50 and 70 days, specific references can't communicate because this is confidential.

2.15. In vivo Glucose uptake

Glucose uptake was measured using a non-radioactive colorimetric method (Saito K and Minokoshi Y et al. Analytical Biochem 412: 9-17, 2011), by means of the 2-deoxyglucose uptake measurement kit (Cosmo Bio Co., LTD, Tokio, Japan). Mice fasted 5 h before the beginning of the experiment. Mice were then injected intraperitoneally with a solution containing D-glucose (1 g/Kg) and 2-deoxy-D-glucose (0.027 g/Kg). One hour after injection, mice were killed by cervical dislocation, and tissues (soleus, tibialis anterior, liver, epididymal white adipose tissue) were rapidly removed, weighed and placed in ice-cold Tris-HCl (10mM, pH8) buffer. Muscles from the left and right legs were separately processed. Entire soleus and tibialis anterior muscles, 50-100 mg of the liver and

100-200 mg of adipose tissue were used for the assay. Tissues were subsequently homogenized in 1ml of Tris-HCl (10mM, pH8) with TissueLyser II (Qiagen), by shaking at maximum speed for 3 minutes, and heated at 95°C for 15 minutes. Samples were then centrifuged at 16000g for 15 minutes at 4°C to remove tissue debris. Supernatants were finally collected, and a portion was diluted in 20µl (final volume; 2µl for soleus, 5µl for tibialis anterior, 1µl for liver and 10µl for WAT) with the sample dilution buffer provided with the kit. The assay was then performed following the manufacturer's instructions.

2.16. In vivo FDB transfection

Electroporation experiments were performed on FDB muscles from wild-type and knockout animals. The animals were anesthetized by an intraperitoneal injection of xylazine (Xilor) (20 mg/Kg) and Zoletil (10 mg/Kg). 7 µl of hyaluronidase (2 mg/ml) (Sigma-Aldrich) was injected in the feet of anesthetized mice to soften muscle tissue underneath the epidermis. After 50 min, we injected 15 µg of plasmid DNA (shRNA against LC3, TLR9; IkB -AA-) and after 10 min electric pulses were applied by two stainless needles placed at 1 cm from each other (100 V/cm) (100 Volts/cm, 20 pulses, 1 s intervals). Muscles were analyzed 10 days later. No evidence of necrosis or inflammation were observed after the transfection procedure. Oligos were cloned into the pSUPER vector (Brummelkamp et al., 2002.) or into Invitrogen BLOCK-IT Pol II miR RNAi Expression Vectors. For validation of shRNA constructs, MEF cells were maintained in DMEM/10%FBS and transfected with shRNA constructs using Lipofectamine 2000 (Invitrogen) according to the manufacturer's instructions. Cells were lysed 72 hours later, and immunoblotting was performed as described below.
The sequences of the Oligos Used for siRNA Production are listed in Table 1

2.17. In vivo tibialis transfection

Mice were co-transfected with a short hairpin for panFoXO and relative control plasmid. *In vivo* transfection of tibialis anterior (TA) muscle was carried out using the NEPA21 Super Electroporator with settings: 21 voltage, 20 ms pulse

length, 200 ms pulse internal, a total of five pulses. At least five mice were electroporated. The right TA muscle was electroporated with shpanFOXO and the control vectors pBI-CMV1-GFP Muscles were collected 12 days after transfection.

2.18. Force measurements

In vivo force measurements were performed as described previously (Blaauw et al, FASEB 2009). Briefly, mice were anesthetized and stainless steel electrodes wires were placed on either side of the sciatic nerve. Torque production of the plantar flexors was measured using a muscle lever system (Model 305c; Aurora Scientific, Aurora ON, Canada). The force-frequency curves were determined by increasing the stimulation frequency in a stepwise manner, pausing for 30 s between stimuli to avoid effects due to fatigue. Force was normalized to the muscle mass as an estimate of specific force. Following force measurements, animals were sacrificed by cervical dislocation and muscles were dissected and weighed.

2.19. Mitochondria oxidative stress measurements

Mitochondrial targeted HyPer (Hydrogen Peroxide sensor) was used as an indicator of mitochondrial redox status. Briefly, adult FDB muscles were transfected by electroporation with mt-HyPer plasmid. After 7 days of transfection, single-muscle fibers were isolated from the control and knockout mice. Mt-HyPer fluorescence (excitation: 420 and 488 nm, emission: 515 nm) was measured for 8 min every 10 s and upon treatment with H2O2. The ratio of fluorescence intensities was determined by ImageJ software.

2.20. Single Fibers Isolation and Mitochondrial Membrane Potential analyses

Mitochondrial membrane potential was measured in isolated transfected fibers from flexor digitorum brevis (FDB) muscles as previously described (Mammucari et al., 2007; Zhao et al., 2007). Briefly, FDB myofibers were placed

in 1 ml Tyrode's buffer and loaded with 2,5nM TMRM (Molecular Probes) supplemented with 1µM cyclosporine H (a P-glycoprotein inhibitor) for 30 min at 37°C. Myofibers were then observed at Olympus IMT-2 inverted microscope (Melville, NY) equipped with a CellR imaging system. Sequential images of TMRM fluorescence were acquired every 60 s with a 20X 0,5, UPLANSL N A objective (Olympus). At the times indicated by arrows, oligomycin (Olm, 5 µM) (Sigma) or the protonophore carbonyl cyanide p-trifluoromethoxyphenylhydrazone (FCCP, 4 µM) (Sigma) were added to the cell culture medium. Images were acquired, stored and analysis of TMRM fluorescence over mitochondrial regions of interest was performed using ImageJ software (http://rsb.info.nih.gov/ij/). When stated, isolated FDB fibers were stained with a rabbit polyclonal anti-TOM20 (Santa Cruz 1:200) and were further analyzed by confocal microscopy.

2.21. Plasma measurements

Plasma was obtained from blood collected from controls and OPA1-null mice. Blood FGF21 levels were determined using Rat/Mouse FGF21 Enzyme-linked Immunosorbent ELISA-Kit (Millipore, EZRMFGF21-26K). OPA1 KO mice FGF21 relative quantification was normalized to controls. Data are expressed as fold increase of controls. Blood IL-6 (Millipore, EZMIL6), TNF-alfa (Millipore, EZMTNFA), IL-1 (Thermofisher, EMIL1A) IL-1 (Thermofisher, EM2IL1B) were measured following the manufacturer's instructions. Data are expressed in pg/mL. Glucose measurement was performed at 9 a.m. in fed condition, with the One Touch Ultra Easy glucose meter (LifeScan Inc.). Data are expressed in mg/dL.

2.22. Exercise experiments

In this study 18, months-old mice performed a concentric exercise on a treadmill (Biological Instruments, LE 8710 Panlab Technology 2B), with 10° incline. Mice were trained for one week, 1 hour per day at a constant speed of 18 cm/s. Then, aged mice treatment

2.23. Glucose and insulin tolerance tests

Mice fasted for 8 h before analysis during their normal rest/fasting phase. Blood glucose was measured using a Glucocard G^+ meter (Arkray Factory, Shiga, Japan). Glucose tolerance tests (GTT) and insulin tolerance tests (ITT) were performed at ZT12, For GTT, mice were injected i.p. with glucose (2 g/kg body weight). Blood glucose was measured at 0, 10, 20, 30, 60 and 120 min via the tail vein. For ITT, mice were injected i.p. with human insulin (0.75 U/kg body weight; Sigma) and blood glucose was measured at 10, 0, 10, 20, 30, 60, and 90 min via the tail vein.

2.24. Autophagic flux quantification

Autophagic flux was monitored in a fed condition using colchicine (C9754, Sigma-Aldrich) as previously described (Milan et al. 2015). Briefly, HSA $OPA1^{-/-}$ and $OPA1^{f/f}$ mice were treated, by i.p. injection, with vehicle or with 0,4mg/ kg colchicine. The treatment was administered twice, at 24 h and at 12 h before muscle collection.

QUANTIFICATION AND STATISTICAL ANALYSIS

Statistical analysis

All data are expressed as means ±SEM. Statistical analysis was performed using one-tailed or two-tailed Student's t-test. Normal distribution of the variables of interest was checked using the Shapiro-Wilk test. For experiments in which more than two groups should be compared, 2-way analysis of variant (ANOVA) was used. When ANOVA revealed significant differences, further analysis was performed using Bonferroni's multiple comparison test.. Linear regression models were used to verify the linear correlation between variables. T-test was performed on the slopes of the regressions to verify their significance (GraphPad). Statistical significance was set at $p<0.05$.were considered statistically significant for $p\leq0.05$ or $p\leq0.01$. Regression linear analysis was done using an F test (GraphPad).

3. PART I: PUBLISHED DATA

Mitochondrial dysfunction occurs during aging, but its impact on tissue senescence is unknown. Here, we find that sedentary but not active seniors display an age-related decline in the mitochondrial protein, optic atrophy 1 (OPA1), that is associated with muscle loss. Conditional and inducible muscle-specific Opa1 deletion alters mitochondrial morphology and promotes lethality. In adult mice, acute muscle-specific deletion of Opa1 induces a precocious aging phenotype and premature death. The key factor in this pathological process is FGF21, a pleiotropic mitokine. Upon simultaneous deletion of Opa1 and fgf21, mice do not display anymore premature aging.

Article

Cell Metabolism

Age-Associated Loss of OPA1 in Muscle Impacts Muscle Mass, Metabolic Homeostasis, Systemic Inflammation, and Epithelial Senescence

Graphical Abstract

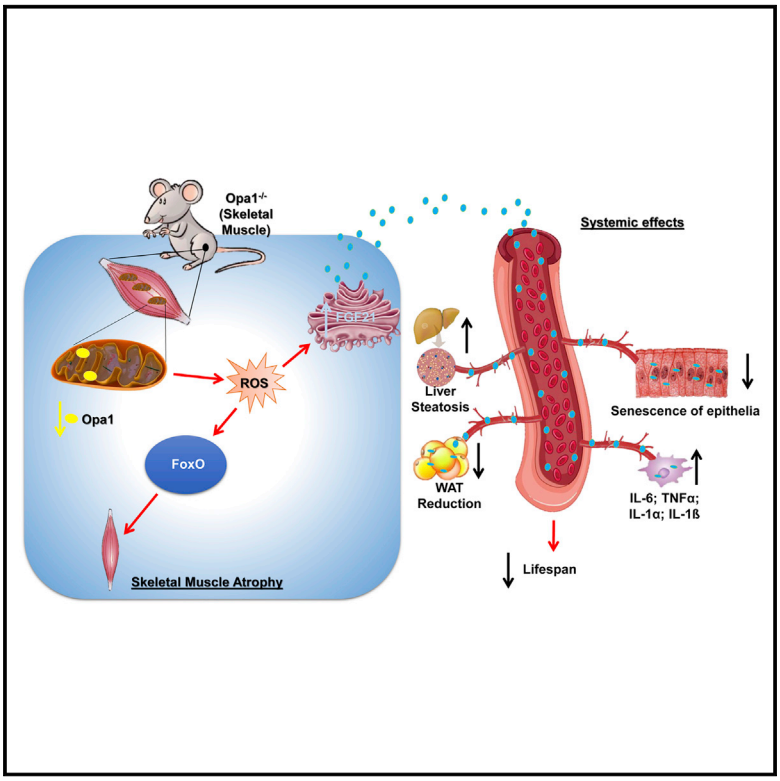

Authors

Caterina Tezze, Vanina Romanello, Maria Andrea Desbats, ..., Leonardo Salviati, Luca Scorrano, Marco Sandri

Correspondence

luca.scorrano@unipd.it (L.S.), marco.sandri@unipd.it (M.S.)

In Brief

Aging has been reported to be accompanied by changes in mitochondrial dynamics, but the impact on tissue senescence is unknown. Tezze et al. show that deletion of Opa1 impacts muscle mass, metabolic homeostasis, systemic inflammation, and epithelial senescence and identify FGF21 as the culprit of precocious aging and premature death.

Highlights

- OPA1 is a physical activity sensor that is downregulated during aging sarcopenia
- Muscle OPA1 controls general metabolism and epithelial senescence via FGF21
- Inhibition of muscle OPA1 induces a systemic pro-inflammatory status
- OPA1 controls protein breakdown/synthesis, muscle stem cells and fiber innervation

Tezze et al., 2017, Cell Metabolism *25*, 1374–1389
June 6, 2017
http://dx.doi.org/10.1016/j.cmet.2017.04.021

CellPress

Cell Metabolism
Article

Age-Associated Loss of OPA1 in Muscle Impacts Muscle Mass, Metabolic Homeostasis, Systemic Inflammation, and Epithelial Senescence

Caterina Tezze,[1,2,10] Vanina Romanello,[1,2,10] Maria Andrea Desbats,[3] Gian Paolo Fadini,[1] Mattia Albiero,[1] Giulia Favaro,[1,2] Stefano Ciciliot,[1] Maria Eugenia Soriano,[1,4] Valeria Morbidoni,[3] Cristina Cerqua,[3] Stefan Loefler,[5] Helmut Kern,[5] Claudio Franceschi,[6] Stefano Salvioli,[7] Maria Conte,[7] Bert Blaauw,[2] Sandra Zampieri,[2] Leonardo Salviati,[3,8] Luca Scorrano,[1,4,*] and Marco Sandri[1,2,9,11,*]

[1]Venetian Institute of Molecular Medicine, via Orus 2, 35129 Padova, Italy
[2]Department of Biomedical Science, University of Padova, via G. Colombo 3, 35100 Padova, Italy
[3]Clinical Genetics Unit, Department of Woman and Child Health, University of Padova, Via Giustiniani 3, 35128 Padova, Italy
[4]Department of Biology, University of Padova, Via U. Bassi 58B, 35121 Padova, Italy
[5]Ludwig Boltzmann Institute of Electrical Stimulation and Physical Rehabilitation, Wilhelminenspital, Montleartstrasse 37, A-1171 Wien, Austria
[6]IRCCS, Institute of Neurological Sciences of Bologna, 40139 Bologna, Italy
[7]Department of Experimental, Diagnostic and Specialty Medicine (DIMES), University of Bologna, 40126 Bologna, Italy
[8]Istituto di Ricerca Pediatria, IRP, Città della Speranza, Corso Stati Uniti 4, 35129 Padova, Italy
[9]Department of Medicine, McGill University, Montreal, QC H4A 3J1, Canada
[10]These authors contributed equally
[11]Lead Contact
*Correspondence: luca.scorrano@unipd.it (L.S.), marco.sandri@unipd.it (M.S.)
http://dx.doi.org/10.1016/j.cmet.2017.04.021

SUMMARY

Mitochondrial dysfunction occurs during aging, but its impact on tissue senescence is unknown. Here, we find that sedentary but not active humans display an age-related decline in the mitochondrial protein, optic atrophy 1 (OPA1), that is associated with muscle loss. In adult mice, acute, muscle-specific deletion of *Opa1* induces a precocious senescence phenotype and premature death. Conditional and inducible *Opa1* deletion alters mitochondrial morphology and function but not DNA content. Mechanistically, the ablation of *Opa1* leads to ER stress, which signals via the unfolded protein response (UPR) and FoxOs, inducing a catabolic program of muscle loss and systemic aging. Pharmacological inhibition of ER stress or muscle-specific deletion of FGF21 compensates for the loss of *Opa1*, restoring a normal metabolic state and preventing muscle atrophy and premature death. Thus, mitochondrial dysfunction in the muscle can trigger a cascade of signaling initiated at the ER that systemically affects general metabolism and aging.

INTRODUCTION

Mitochondria are crucial organelles in the production of energy and in the control of signaling cascades. A machinery of pro-fusion and -fission proteins regulates their morphology and subcellular localization. Both mechanisms are evolutionarily conserved from yeast to humans. In mammals, mitofusin (MFN) 1 and 2 and optic atrophy protein 1 (OPA1) are required for fusion of the outer mitochondrial membrane and inner mitochondrial membrane (Romanello and Sandri, 2016). OPA1 requires MFN1 to regulate mitochondrial fusion, but on the other hand, oligomerization of OPA1 regulates apoptosis by controlling cristae remodeling and cytochrome *c* redistribution (Cipolat et al., 2006; Frezza et al., 2006). The maintenance of a dynamic mitochondrial network is particularly important for cells with a complex and highly structured cytosol, such as neurons and cardiac and skeletal muscles constituted by post-mitotic cells that do not divide. While tissues with high cell turnover can dilute the damaged/altered mitochondria among the dividing cells, the post-mitotic tissues use the fusion/fission machinery to preserve or restore mitochondrial function. Alternatively, post-mitotic organs activate selective autophagy to remove the irreversibly injured mitochondria (mitophagy). A failure of these systems predisposes to tissue dysfunction and degeneration. Mouse knockouts (KO) for each of the pro-fusion genes (*Mfn1*, *Mfn2*, and *Opa1*) are lethal to embryos because of mitochondrial dysfunction (Chen et al., 2003; Davies et al., 2007). Muscle-specific KO mice for *Mfn1* and *Mfn2* are viable at birth, although they display profound defects of muscle growth characterized by mitochondrial dysfunction, reduction of mitochondrial DNA (mtDNA) in skeletal muscle, and accumulation of point mutations and deletions in the mitochondrial genome that cause death within 6–8 weeks of age (Chen et al., 2010). In humans, mutations in *MFN2* and *OPA1* genes cause two neurodegenerative diseases, Charcot-Marie-Tooth type 2A (CMT2A) and dominant optic atrophy (DOA), respectively (Alexander et al., 2000; Delettre et al., 2000; Züchner et al., 2004). CMT2A is an inherited neuropathy that is clinically characterized by muscle atrophy. Heterozygous missense recessive mutations of OPA1 genes

cause DOA with a muscle involvement revealed as an aspecific myopathy with mitochondrial features (Amati-Bonneau et al., 2008; Schaaf et al., 2011). Interestingly, the first case of homozygous missense mutation has been reported in two sisters that died at 2 and 10 months of age showing myopathy, encephalopathy, and cardiomyopathy (Spiegel et al., 2016). The muscle biopsies of these sisters revealed 50% reduction of OPA1 protein, a decrease in the activity of all the respiratory chain complexes, and an important mtDNA depletion (80%). Therefore, mutations in fusion genes result in brain and muscle dysfunction.

Skeletal muscle is a major site of metabolic activity and the most abundant tissue in the human body, accounting for almost 50% of the total mass. Being the largest protein reservoir, muscle serves as a source of amino acids to be utilized for energy production by various organs during catabolic periods. Importantly, skeletal muscle is an important modulator of general metabolism since it plays an important role in glucose, amino acid, and lipid homeostasis. Recent data in *Drosophila* show that maintenance of a functional proteostasis specifically in muscles, but not in white adipose tissue, during aging reverberates to the whole organism, leading to an extension of lifespan (Demontis et al., 2014; Demontis and Perrimon, 2010). Therefore, a new concept is emerging from this and other studies that considers the metabolic adaptations occurring in skeletal muscles as disease modifier/controller (Baskin et al., 2015). Indeed, growing evidence suggests that muscle-derived growth factor or cytokines, known as myokines, modulate systemic physiology (Demontis et al., 2013). Importantly, exercise by preserving and ameliorating muscle metabolism is able to counteract the body deterioration by improving function of multiple organs (Neufer et al., 2015). However, the mechanistic insights that link muscle contraction to organ function and longevity are still unknown. Here we show that deletion of *Opa1* in skeletal muscle results in a lethal phenotype that is even more severe than *Mfn1/2* double KO. This phenotype results from suppression of myogenesis, impaired protein synthesis and activation of protein breakdown. Importantly, several of these features were recapitulated in inducible muscle-specific *Opa1* KO mice that additionally show multiple-organ senescence and precocious aging.

RESULTS

Age-Related Muscle Loss in Humans and Mice Is Associated with Decreased OPA1 Expression

Aging has been reported to be accompanied by numerous functional alterations of mitochondria, including changes of mitochondrial dynamics (Ibebunjo et al., 2013). Thus, we tested whether mitochondria-shaping factors are reduced in humans. A decline of *Mfn1/2*, *Opa1*, and *Drp1* transcripts was found in muscle biopsies of old sedentary (sarcopenic) subjects (Figure 1A and Table S1). Since exercise counteracts most of the age-related features, including the decline in muscle mass/force, we tested whether a long-life regular exercise was able to prevent the reduction of these genes (Figure 1A). Expression of the mitochondria-shaping genes was maintained in muscle biopsies of senior sportsmen. Similar to transcript level, we further confirmed that OPA1, MFN1, and DRP1 proteins were reduced in sedentary subjects and that regular exercise was able to counteract this decline (Figures 1B, S1A, and S1B). When we explored whether the decrease of mitochondrial shaping proteins correlates with muscle mass loss in elderly people, we found a significant correlation only for OPA1 and not for DRP1 or MFN1 (Figure 1C). Similarly, muscle force drop significantly correlates with decrease of OPA1 expression but not of DRP1 or MFN1 (Figure 1D). This association is independent of fiber type (Figures S1C and S1D). Consistently with human data, aged mice displayed a significant reduction of OPA1 in muscles (Figures 1E and S1E). Importantly, 1 week of exercise training is sufficient to reactivate OPA1 expression in muscles of aged mice (Figure 1E). Overall, these findings suggest a causative role of mitochondrial dynamic impairment that correlated with the decreased OPA1 expression and age-related muscle loss and weakness.

Muscle-Specific *Opa1* Deletion in Newborns Blocks Animal Growth and Is Lethal

Given the important decrease of OPA1 during aging and the fact that there is no animal model of conditional *Opa1* KO in postmitotic tissues, we generated a muscle-specific *Opa1* KO mouse line. Muscles in newborns showed a 50% decrease in transcript level and 70% reduction of OPA1 protein (Figures S2A and S2B) specifically in the muscle. Importantly, these mice died within 9 days of postnatal life (Figure 2A) even when they were artificially fed, suggesting that nutrition was not the cause of death. During the first 8 days of postnatal life, the $Opa1^{-/-}$ mice showed an impairment of total body growth, resulting in smaller animals (Figure S2C). These animals displayed hypoglycemia under nonfasting conditions (Figure 2B). The size of the muscles was decreased because of reduced fiber size (Figure S2D) that results in an increased amount of fibers per area (Figure 2C). The $Opa1^{-/-}$ mice did not show decrease of total fiber number (Figure S2E), suggesting that myogenesis and myotube formation are not perturbed, but that postnatal myofiber growth is affected by OPA1 ablation.

Muscle-Specific OPA1 Ablation Alters Mitochondrial Function and Morphology

To understand the molecular mechanisms behind the observed phenotype, we monitored mitochondrial ultrastructure. Electron microscopy revealed a disorganized sarcomere arrangement with Z-disk misalignment, empty spaces between myofibrils, and accumulation of lipid droplets (Figure S2F, left and middle panels). Mitochondria of $Opa1^{-/-}$ were smaller in size than controls, and cristae were dilated (Figure S2F, right panels). However, the mtDNA content per nuclear genome did not differ between the two genotypes (Figure S2H), suggesting that total mitochondrial content was not decreased. Consistent with the mtDNA analyses, the mitochondrial mass revealed by TOM20 and porin proteins was not affected in $Opa1^{-/-}$ (Figure S2I). We then verified whether OPA1 ablation caused compensatory changes in the levels of the other mitochondria-shaping machinery members. PGC1α and Mfn1 transcripts were upregulated, whereas the level of the fission protein DRP1 was not increased (Figures S2I and S2J). At the bioenergetic level, complex I-dependent respiration was reduced, and supercomplexes were destabilized in OPA1-deficient muscles (Figures 2D, 2E, and S2G).

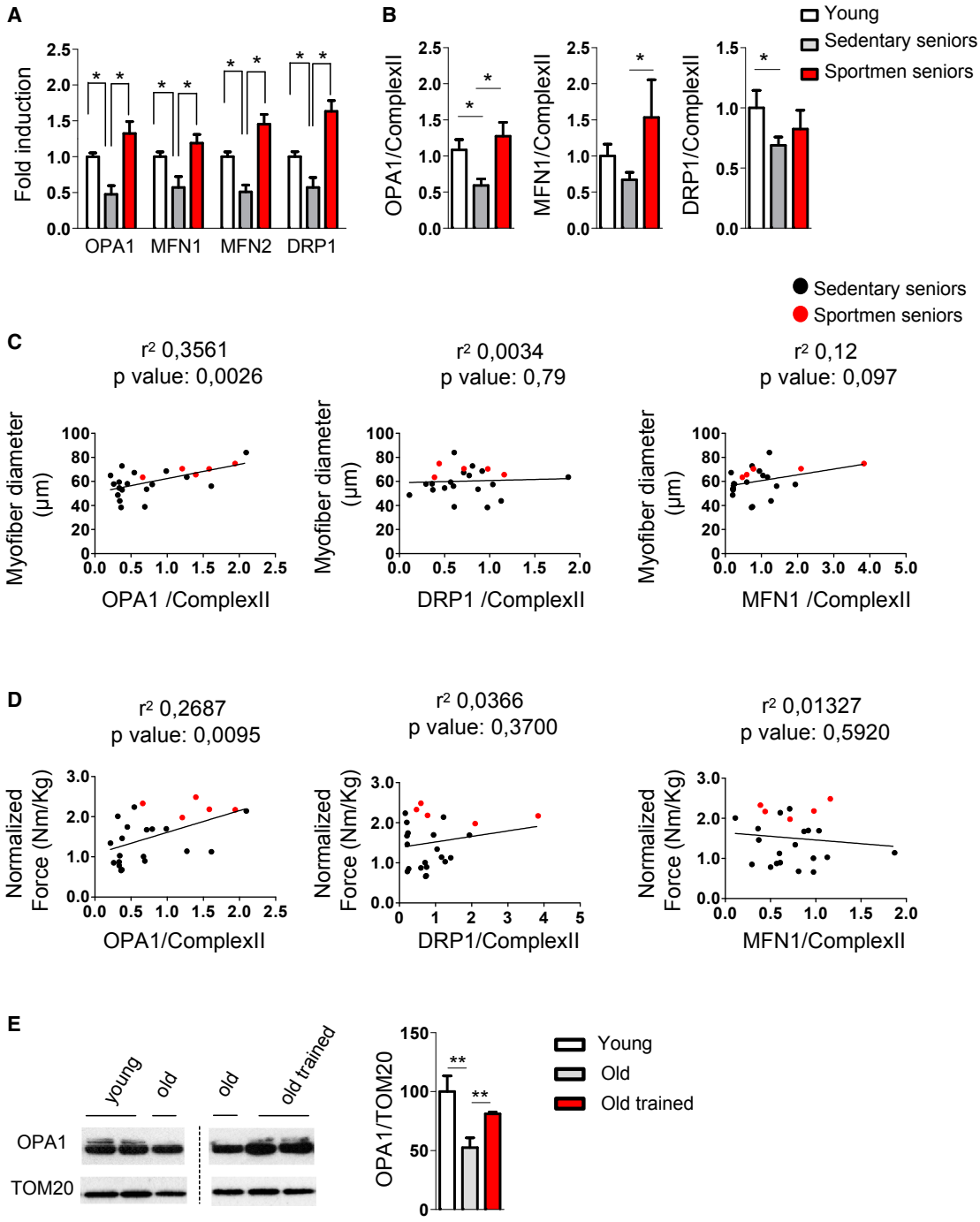

Figure 1. OPA1 Expression Is Reduced during Aging in Sarcopenic Patients

(A) Mitochondria-shaping machinery is downregulated in sarcopenia and maintained by lifelong exercise. Quantitative PCR analysis of mitochondrial dynamics transcripts from human muscle biopsies of 5 young subjects, 7 sedentary seniors, and 11 senior sportsmen is shown. Data represent mean ± SEM and are normalized for GAPDH.

(B) Densitometric analysis of OPA1/Complex II, MFN1/Complex II, and DRP1/Complex II signal ratios revealed by immunoblotting. Data represent mean ± SEM of four independent experiments (young = 5, sedentary seniors = 19, senior sportsmen = 5).

(C) Linear regression analysis including OPA1, DRP1, and MFN1 expression levels and myofiber size in elderly persons (n = 24). Red spots depict senior sportsmen.

(D) Linear regression showing that decrease of OPA1 but not of DRP1 or MFN1 levels correlates with muscle weakness in elderly persons (n = 24). Red spots depict senior sportsmen.

(E) Representative immunoblot and densitometric analysis of OPA1 in homogenates of tibialis anterior muscles from young (6 months old, n = 6), old (18 months old, n = 9) and old trained mice (18 months old, n = 6). Data are expressed as mean ± SEM; *$p \leq 0.05$, **$p < 0.01$.

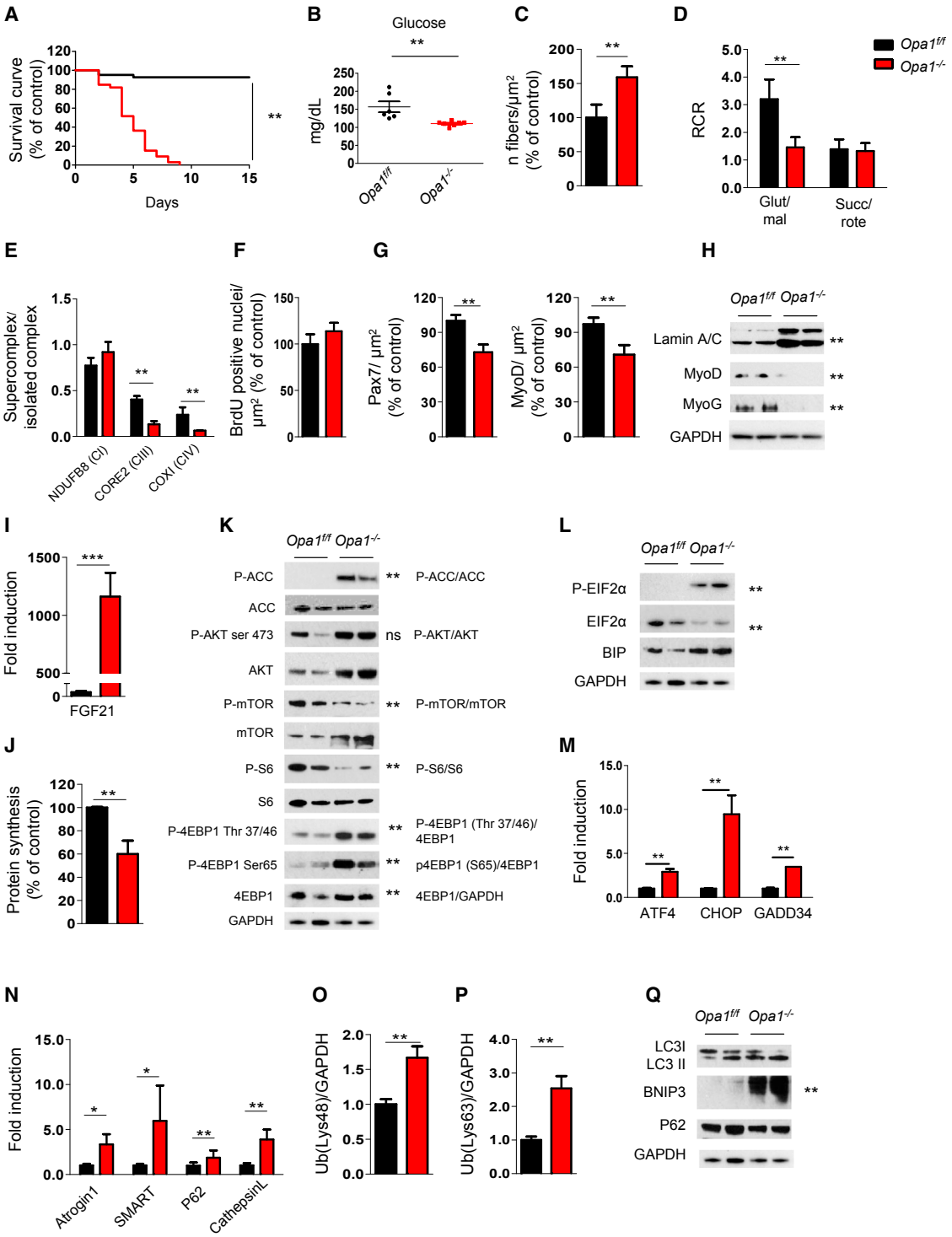

Figure 2. OPA1 Deletion Induces a Lethal Phenotype Characterized by Mitochondrial Dysfunction, Reduction of Myogenic Stem Cells, Decreased Protein Synthesis, and Activation of Protein Breakdown

(A) Kaplan-Meier survival curve of *Opa1*$^{f/f}$ and *Opa1*$^{-/-}$ littermates (n = 37 for each group) indicates that muscle-specific OPA1 deletion results in lethality by post-natal day 9. **p < 0.01.

(B) Blood glucose levels in control and knockout mice (*Opa1*$^{f/f}$ n = 6; *Opa1*$^{-/-}$ n = 7). Data represent mean ± SEM, **p < 0.01.

(C) Analysis of the number of fibers normalized per muscle area (µm^2). Data represent mean ± SEM for n = 6, **p < 0.01.

(D) Respiratory control ratio (RCR) of mitochondria energized with 5 mM/2.5 mM glutamate/malate (GLU/MAL) or 10 mM succinate (SUCC/ROTE). Data represent average ± SEM of three independent experiments (n = 9 per each condition), **p < 0.01.

(legend continued on next page)

Inhibition of OPA1 Reduces Muscle Stem Cells, Inhibits Protein Synthesis, and Induces Atrophy-Related Genes and Protein Breakdown

Muscle growth during the first 2 weeks of postnatal life depends on fusion of muscle stem cell to growing myotube and on protein synthesis (Schiaffino et al., 2013). First, we checked whether OPA1 deletion in myofiber affected muscle stem cell renewal and myogenic differentiation. Proliferative rate, revealed by BrdU incorporation, did not differ between the two genotypes (Figure 2F). However, immunostaining for Pax7, a marker of the quiescent muscle stem cells, revealed a significant reduction of positive cells in *Opa1*$^{-/-}$ (Figure 2G). Accordingly, MyoD-positive myoblasts were also decreased (Figure 2G). Western blot analyses confirmed that the markers of myoblast proliferation, MyoD, and differentiation, myogenin, were significantly reduced in KO mice (Figures 2H and S3A). We then explored the involvement of myostatin pathway in stem cell loss, but immunoblotting for pSmad3 ruled out myostatin/TGFβ members (Figure S2K). Since levels of apoptosis were similar in *Opa1*$^{f/f}$ and *Opa1*$^{-/-}$ muscles (Figure S2L), we concluded that muscle stem cells were likely depleted and unable to self-renew, suggesting a link between mitochondrial fusion and muscle stem cell maintenance.

The sole muscle stem cell dysfunction could not explain the generalized observed small animal size. When we monitored the growth hormone (GH)/IGF1 axis that controls cellular proliferation in most tissues, including muscle, we found a significant reduction in hepatic expression of one of the most important GH targets, IGF1 (Figure S2M). However, muscle expression of IGF1 was not reduced in *Opa1*$^{-/-}$ animals (not shown). Alternatively, the cytokine fibroblast growth factor (FGF) 21 could be the culprit, given its ability to induce GH resistance. Indeed, FGF21 transcript was 1,000-fold induced in *Opa1*$^{-/-}$ muscles compared to *Opa1*$^{f/f}$ (Figure 2I).

Since GH has an important anabolic function, we checked in vivo whether protein synthesis was altered in *Opa1*$^{-/-}$. A SunSET analysis revealed a 50% protein synthesis reduction in *Opa1* KO (Figures 2J and S2N). Interestingly, *Opa1*$^{-/-}$ muscle displayed an increase of total and phospho-Akt (pAkt), which was not sufficient to maintain the phosphorylation of mTOR and of its downstream target S6 (Figures 2K and S3B). Consistent with these data, the downstream target of AMPK, ACC, was hyper-phosphorylated, supporting the concept of an undergoing energy stress that inhibits mTOR. However, when we monitored 4EBP1, a second mTOR downstream target, we found an increase of p4EBP1 in two different sites (Figure 2K). The inconsistency of the Akt/mTOR/4EBP1/S6 axis suggests that other regulators are involved in the observed translation impairment, such as ribosome assembly, controlled by initiation factors, among which eIF2α is the most critical one. When eIF2α is phosphorylated (p-eIF2α), ribosome assembly is blocked and general protein synthesis is shut down. During ER stress, the unfolded protein response (UPR) kinase PERK phosphorylates eIF2α, leading to protein synthesis blockage. Levels of p-eIF2α and of the chaperone Bip/Grp78, a downstream target of UPR, were indeed increased in *Opa1*$^{-/-}$ (Figures 2L and S3C). Moreover, we observed that PERK-dependent UPR triggered the activation of the transcription factor ATF4 and the transcription of several genes including Bip, GADD34, CHOP, and FGF21 (Figures 2M and 2I). Thus, UPR activation in *Opa1*$^{-/-}$ muscles accounts for the reduction of translation (Figure 2J) and activates, via FGF21 (Figure 2I), a catabolic condition.

Since cell size is determined by the balance between protein synthesis and degradation, we also monitored the status of the ubiquitin-proteasome and autophagy-lysosome systems. The atrophy-related ubiquitin ligases atrogin-1 and SMART (Milan et al., 2015) were induced (Figures 2N, S2O, and S2P), resulting in an increase of lysine 48 poly-ubiquitinated proteins (Figures 2O and S2Q). Interestingly, lysine 63 poly-ubiquitinated proteins were also significantly increased in *Opa1*$^{-/-}$ (Figures 2P and S2R). Since lysine 63 poly-ubiquitinated proteins are also autophagy substrates, we checked the autophagy system by monitoring the recruitment of LC3 on autophagosomes (LC3 lipidation) and expression of autophagy-related genes. Despite the induction of p62 and cathepsin L genes and Bnip3 protein (Figures S2S and 2Q), the lipidated LC3 (LC3 II) was not significantly increased, suggesting that autophagosome number is not enhanced at this time point (Figures 2Q and S3D). In conclusion, *Opa1* deletion during early postnatal life leads to a defect of muscle growth caused by a block of muscle stem cell renewal and protein synthesis and a concomitant induction of proteasome-dependent protein breakdown.

(E) Densitometric quantification of Blue Native-PAGE of respiratory chain supercomplexes (RCS) that were normalized for individual respiratory chain complexes. Data represent mean ± SEM, n = 3, **p < 0.01.

(F) BrdU incorporation in *Opa1*$^{f/f}$ and *Opa1*$^{-/-}$ muscles. Data represent mean ± SEM, n = 4.

(G) Pax7-positive muscle stem cells and MyoD-positive myoblast were revealed by immunohistochemistry and normalized for muscle area. Data are mean ± SEM for n = 4, **p < 0.01.

(H) Representative immunoblot of muscle homogenates of three independent experiments. Lamin A/C, MyoD, and myogenin (MyoG) were normalized for GAPDH expression. Statistical significance after densitometric analysis is indicated on the right, **p < 0.01.

(I) Quantitative RT-PCR of FGF21 expression in *Opa1*$^{-/-}$ muscles. Data represent mean ± SEM, ***p < 0.001, n = 4.

(J) Quantification of puromycin incorporation in skeletal muscles. In vivo SUnSET technique demonstrates a significant reduction of protein synthesis in *Opa1*$^{-/-}$ muscles. Data are mean ± SEM of three independent experiments (*Opa1*$^{f/f}$ n = 5; *Opa*$^{-/-}$ n = 7), **p < 0.01.

(K) Immunoblots of protein extracts from newborn muscles for the indicated antibodies. Representative immunoblots of three independent experiments are shown. Statistical analysis of the densitometric ratio is indicated on the right, n = 7 per each, ns: not significant, **p < 0.01.

(L and M) Representative immunoblots (L) and quantitative RT-PCR (M) showing activation of the UPR pathway in *Opa1*$^{-/-}$. Data are mean ± SEM of three independent experiments, **p < 0.01.

(N) Quantitative RT-PCR analysis of FoxO-target genes. Data are mean ± SEM for n = 6, **p < 0.01.

(O and P) Densitometric quantification of lysine 48 (Lys48; O) and lysine 63 (Lys63; P) poly-ubiquitinated proteins from controls and *Opa1*$^{-/-}$ muscles. Data are mean ± SEM, n = 4, **p < 0.01.

(Q) Representative immunoblot of three independent experiments of autophagy-related proteins. Data are mean ± SEM, **p < 0.01.

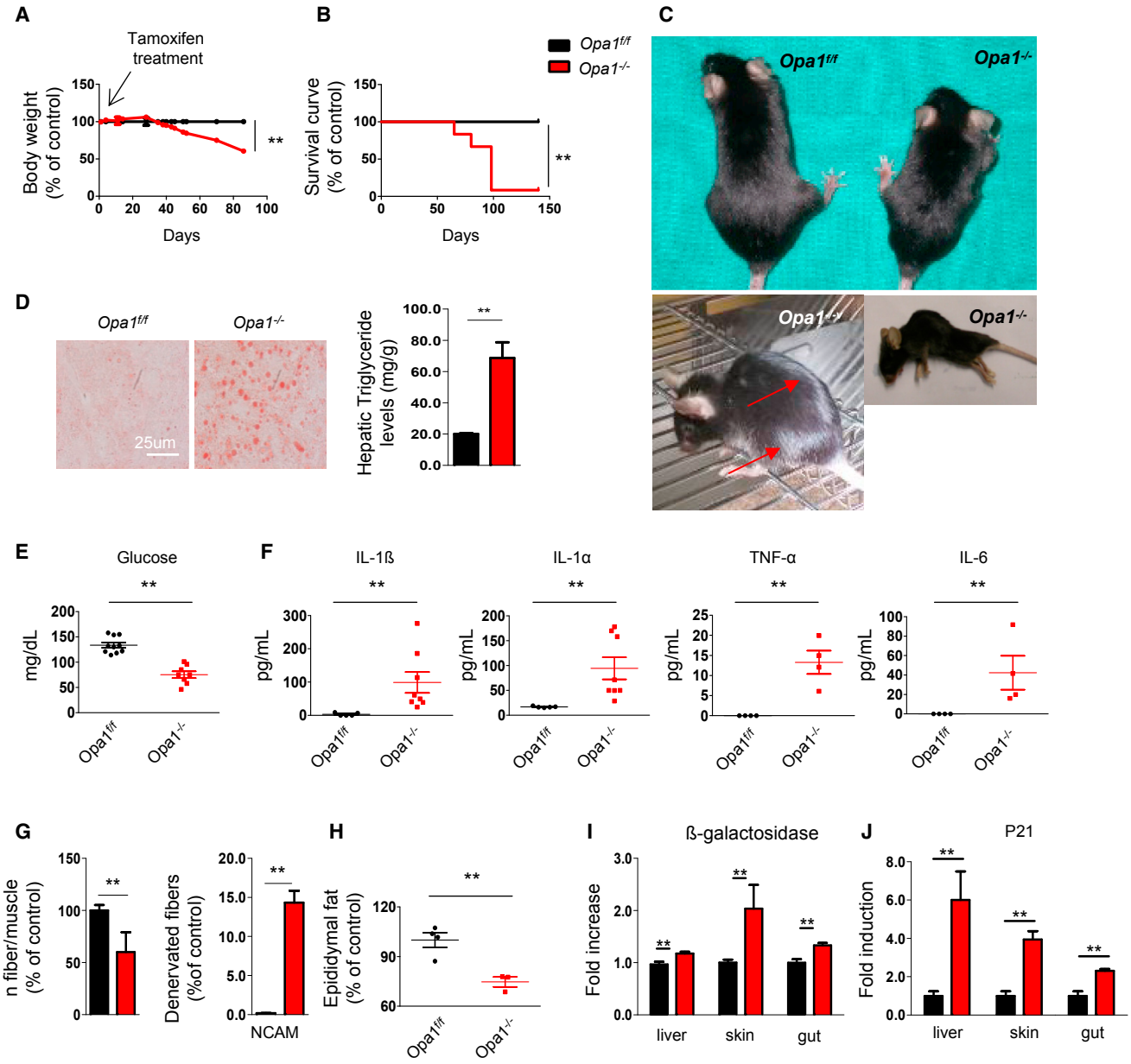

Figure 3. Acute Deletion of OPA1 in Adult Muscles Leads to Metabolic Changes, Precocious Senescence, and Degeneration of Multiple Organs

(A) Growth curve of *Opa1*$^{f/f}$ (black) and *Opa1*$^{-/-}$ (red) mice after tamoxifen treatment. KO mice start to lose body weight after 30 days from the beginning of the treatment. Data are mean ± SEM (*Opa1*$^{f/f}$ n = 20, *Opa1*$^{-/-}$ n = 19), **p < 0.01.

(B) Kaplan-Meier survival curve of *Opa1*$^{f/f}$ and *Opa1*$^{-/-}$ adult animals (n = 10 for each group) indicates that muscle-specific OPA1 deletion results in lethality within 3 months from the beginning of the tamoxifen treatment.

(C) Eight-month-old *Opa1*$^{-/-}$ mice show a reduction of total body size (upper panel), white hairs (left bottom panel), and kyphosis (right bottom panel).

(D) Lipid content shown by oil red O staining of a representative liver cryosection reveals liver steatosis in *Opa1*$^{-/-}$ adult animals (left panel). Triglyceride content is increased in liver of *Opa1*$^{-/-}$. Data are mean ± SEM for n = 5, **p < 0.01.

(E) Glycemia is reduced in fed knockout mice (*Opa1*$^{f/f}$ n = 10, *Opa1*$^{-/-}$ n = 8). Data are mean ± SEM, **p < 0.01.

(F) Blood levels of the inflammatory cytokines IL6, IL1α, IL1β, and TNFα (*Opa1*$^{f/f}$ n = 5, *Opa1*$^{-/-}$ n = 8). Data are mean ± SEM, **p < 0.01.

(G) Quantification of myofiber number (left graph) and of denervated NCAM-positive fibers. Data represent mean ± SEM, *Opa1*$^{f/f}$ n = 3, *Opa1*$^{-/-}$ n = 4, **p < 0.01.

(H) Epididymal fat content analysis indicates the reduction of white adipose tissue in OPA1 null animals. Data represent mean ± SEM for n = 4, **p < 0.01.

(I and J) β-galactosidase (I) and p21 (J) are significantly increased in liver, skin, and gut. Data represent mean ± SEM (n = 10), **p < 0.01.

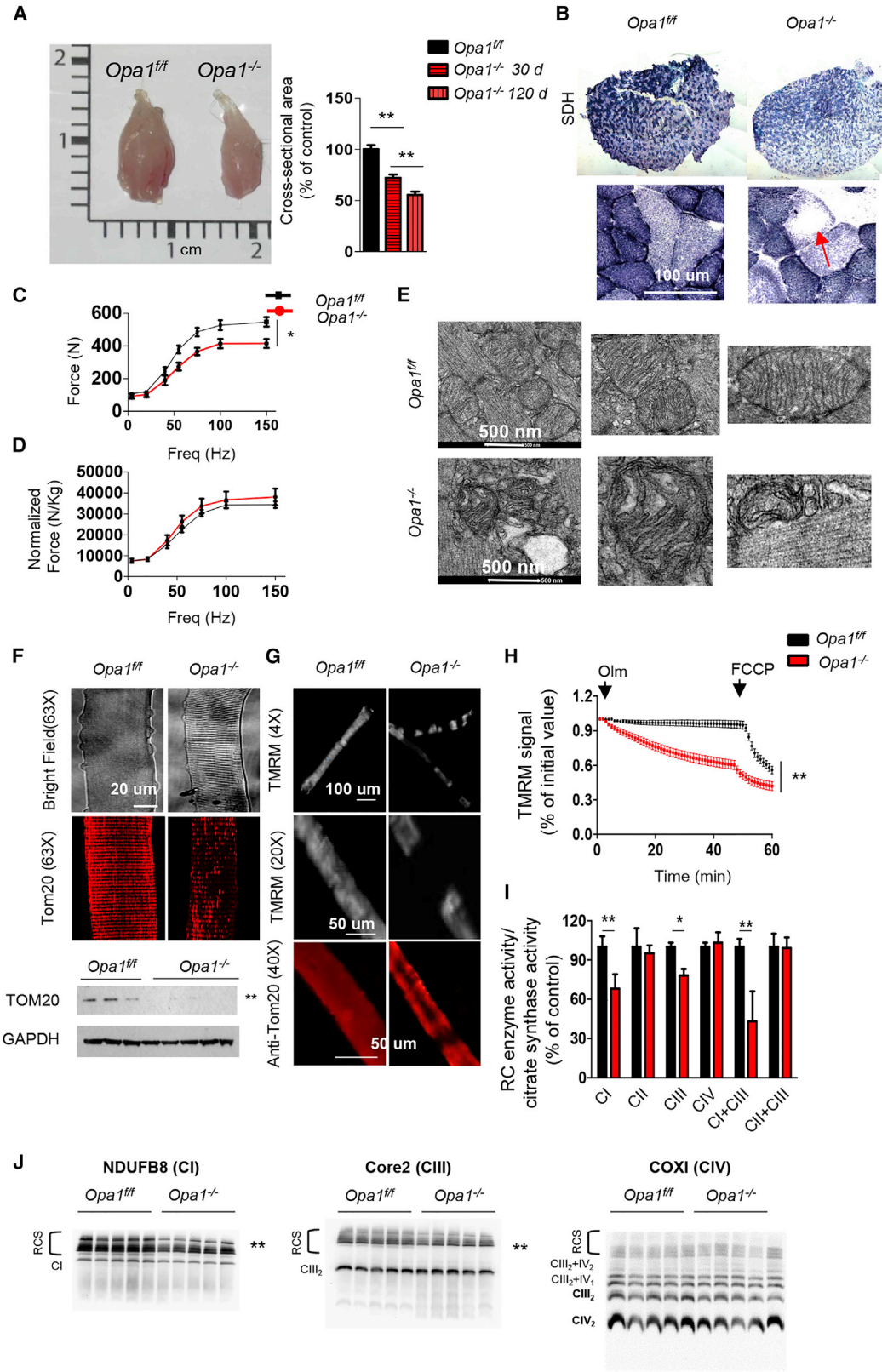

Figure 4. Acute Deletion of OPA1 in Adult Animals Causes Muscle Atrophy and Weakness and Alters Mitochondrial Morphology and Function

(A) Left panel: representative picture of gastrocnemius muscles from *Opa1*$^{f/f}$ and *Opa1*$^{-/-}$ mice. Right panel: myofiber cross-sectional area analysis of controls and *Opa1*$^{-/-}$ at 30 and at 120 days from the induction, respectively. Values are mean ± SEM from at least five muscles in each group, **p < 0.01.

(legend continued on next page)

Acute *Opa1* Deletion in the Skeletal Muscle Reverberates to the Whole Body, Leading to a Precocious Aging Phenotype that Culminates with Animal Death

Due to the severe phenotype of conditional *Opa1*$^{-/-}$ mice, which impaired further analyses in adulthood, we generated a tamoxifen-inducible muscle-specific OPA1 KO mouse. Tamoxifen treatment of 5-month-old mice efficiently reduced OPA1 transcript and protein (Figures S4A and S4B). Importantly, within 50 days from tamoxifen treatment, mice started to lose weight (Figure 3A), and they died within 3 months (Figure 3B), showing a precocious aging phenotype. Mice of 8 months show white hairs and kyphosis (Figure 3C); liver steatosis (Figure 3D); low glucose levels (Figure 3E); high inflammatory cytokines such as IL6, IL1α, IL1β, and TNFα in blood (Figure 3F); loss of myofiber innervation, revealed by myofiber disappearance and increase of NCAM positive fibers (Figure 3G); and disappearance of white adipose tissue (Figure 3H). To further support the aging phenotype, we checked several markers of aging like β-galactosidase and p21. Both are significantly increased in liver, skin, and gut (Figures 3I and 3J). Since the inflammatory cytokine IL6 is also produced by skeletal muscle, we checked whether muscles participate in the systemic inflammation. Interestingly, expression of IL6 and IL1α but not of TNFα or IL1β was strongly upregulated in *Opa1*$^{-/-}$ mice (Figure S4C). Therefore, acute inhibition of OPA1 in adult muscles leads to metabolic changes, systemic inflammatory response, and precocious epithelial senescence that culminate with animal death.

Acute Opa1 Deletion Induces Muscle Loss and Weakness

The body weight reduction was secondary to decreased size of glycolytic fibers and adipose tissue loss (Figures 4A, 3H, and S4D). Morphological analyses showed no features of myofiber degeneration such as center-nucleated fibers or inflammation, suggesting that the decrease of muscle mass was due to atrophy (Figure S4E). Quantification of myofiber size indicated that *Opa1*$^{-/-}$ myofibers were smaller than controls in a time-dependent manner (Figure 4A). Succinate dehydrogenase (SDH) staining was reduced (Figure 4B) and revealed a pattern of localization that resembled central core disease, where regions of myofiber cytoplasm are devoid of mitochondria (Figure 4B). Next we measured the force generated by gastrocnemius muscle in living animals. Maximal absolute force (tetanic force) was significantly reduced (Figure 4C), whereas the specific force (i.e., force normalized for muscle mass) was not significantly affected in KO mice (Figure 4D), indicating an increased loss of sarcomeric proteins. To explain the lipolysis, we checked whether browning of WAT occurred and found an upregulation of UCP1, a well-known marker of brown adipose tissue (Figure S4F). *Opa1*$^{-/-}$ mice showed an improved glucose tolerance and insulin sensitivity (Figure S4G) because glucose uptake in liver, but not in muscles or WAT, is enhanced (Figures S4H–S4K).

Acute Inhibition of *Opa1* Induces Mitochondrial Dysfunction

Analyses of mitochondrial morphology at ultrastructural level confirmed the presence of smaller mitochondria displaying dilated cristae in *Opa1*$^{-/-}$ muscles (Figure 4E). When we stained isolated single adult myofibers for Tom20 (Figure 4F, upper panels), we found that the typical striated pattern of mitochondrial network was absent in *Opa1*$^{-/-}$ fibers where areas were completely unstained. Western blot for mitochondrial proteins and real-time PCR for mtDNA indicated a decreased mitochondrial mass (Figure 4F, lower panel; Figures S4L and S5A). Staining with the potentiometric fluorescent dye tetramethylrhodamine methyl ester (TMRM) revealed a mosaic mitochondrial distribution in the cytoplasm of *Opa1*$^{-/-}$ isolated adult fibers (Figure 4G). Then, we checked the status of the mitochondrial membrane potential ($\Delta\psi m$) in isolated adult fibers of WT and OPA1 KO muscles. As expected, in control mice oligomycin-dependent inhibition of ATP synthase did not alter $\Delta\psi m$ (Figure 4H), and mitochondrial depolarization was achieved after membrane permeabilization by the protonophore carbonylcyanide-p-trifluoromethoxy phenylhydrazone (FCCP). Conversely, mitochondria of *Opa1*$^{-/-}$ fibers underwent a significant depolarization when F_1F_0-ATPase is inhibited by oligomycin (Grumati et al., 2010) (Figure 4H), suggesting that these fibers were at least in part relying on reverse activity of ATP synthase to preserve their membrane potential as a consequence of proton leak-consuming proton motive force. Mechanistically, this dysfunction was caused by the reduction of respiratory chain enzymatic activity and by a destabilization of the respiratory chain supercomplexes (Figures 4I, 4J, and S4M).

Opa1 Deletion Retrogradely Signals to the Nucleus via UPR and FoxO to Induce a Catabolic Condition

We next checked proteostasis in inducible *Opa1*$^{-/-}$. Interestingly, protein synthesis was superimposable in controls and KO mice (Figures S4N and S4O) as well as muscle stem cells

(B) SDH staining showed a reduction of mitochondrial content in *Opa1*$^{-/-}$ that is particularly evident in the center of myofibers (arrow).
(C and D) Force-frequency curves performed in vivo on gastrocnemius muscles. Absence of OPA1 leads to a significant decrease of absolute force (C) but not of maximal specific force (D) generated during tetanic contraction. Data represent mean ± SEM (n = 6), *p < 0.05.
(E) Electron micrographs of EDL muscles of controls and *Opa1*$^{-/-}$.
(F) Upper panel: representative images of adult isolated myofibers at bright field or immunostained for TOM20 showing decreased mitochondrial content in *Opa1*$^{-/-}$. Lower panel: western blot for Tom20 confirms the decrease of mitochondrial mass, **p < 0.01.
(G) Myofibers were stained with the potentiometric dye TMRM.
(H) Absence of OPA1 induces mitochondrial depolarization. Isolated adult fibers were loaded with TMRM. Oligomycin and the protonophore FCCP were added at the indicated time points. TMRM staining was monitored in at least 40 fibers per condition, data are mean ± SEM, **p < 0.01.
(I) Mitochondrial respiratory chain (RC) enzymatic activities from muscles of *Opa1*$^{f/f}$ and *Opa1*$^{-/-}$. Data were normalized to citrate synthase (CS) activity and were plotted as percentage of controls, data are mean ± SEM for n = 8, *p < 0.05; **p < 0.01.
(J) Representative Blue Native-PAGE gels showing respiratory chain supercomplexes (RCS). CI subunit NDUFB8 (left panel), CIII-Core2 protein 2 (middle panel), and CIV subunit COXI (right panel). n = 10; *p < 0.05; **p ≤ 0.01. CI, Complex I; CII, Complex II; CIII, Complex III; CIV, Complex IV; CI+CIII, Complex I plus Complex III; CII+CIII, Complex II plus Complex III.

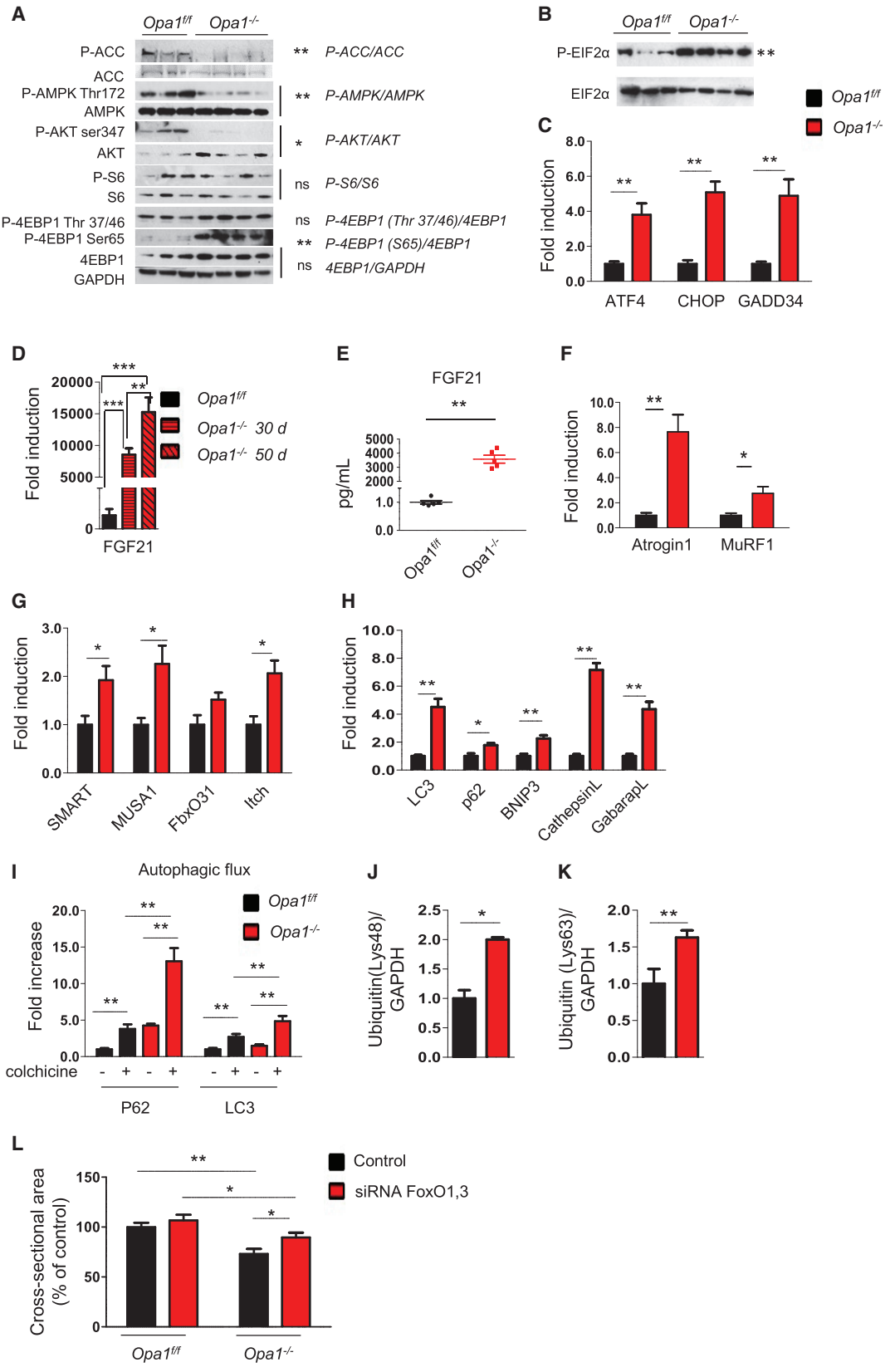

(legend on next page)

and myogenesis (Figures S4P–S4R). Monitoring the signaling pathways related to protein synthesis, we found that pAkt was decreased, whereas pAMPK was reduced, leading to an increase of serine 65 p4EBP1 (Figures 5A and S5B), that was not sufficient to enhance translation because of UPR activation. In fact, p-eIF2α was increased, as was expression of ATF4, GADD34, and CHOP genes (Figures 5B, 5C, and S5C). Importantly, FGF21 was massively upregulated in a time-dependent manner, leading to an important raise of circulating FGF21 in the blood (Figures 5D and 5E). The FGF21 induction occurs specifically in skeletal muscles and not in other tissues such as liver or WAT (Figure S6A). Interestingly, Klotho (KLB) and FGF receptors (FGFR) were expressed in skeletal muscles and were upregulated in *Opa1*$^{-/-}$ fibers (Figure S6B), but not in the other tissues, with the exception of KLB in the skin (Figures S6C–S6F).

According to muscle loss, several atrophy-related genes were significantly induced (Figures 5F and 5G) and a robust activation of autophagy was observed (Figures 5H, 5I, and S6G), leading to an increase of lysine 48 and lysine 63 poly-ubiquitinated proteins (Figures 5J and 5K). Interestingly, oxidative stress, revealed by the level of carbonylated proteins, was significantly increased in *Opa1*$^{-/-}$ mice (Figures S6H and S6I). To further support the mitochondrial-dependent oxidative stress, we transfected adult muscles of *Opa1*$^{-/-}$ and *Opa1*$^{f/f}$ with a mitochondrial targeted fluorescent ROS sensor (mt-roGFP) (Lo Verso et al., 2014) and found that mitochondria of *Opa1*$^{-/-}$ produced more ROS than controls (Figure S6J). Our results indicate that acute *Opa1* ablation triggers an atrophy program that enhances protein breakdown. Since FoxOs are master regulators of autophagy and ubiquitin-proteasome system (Milan et al., 2015) and are activated by oxidative stress and Akt inhibition, we hypothesized an involvement of these factors in *Opa1*$^{-/-}$. Indeed, inhibition of FoxOs, in vivo, by RNAi was sufficient to reduce muscle atrophy in *Opa1*$^{-/-}$ (Figure 5L).

Chemical Chaperone Treatment Blunts UPR and Prevents Muscle Loss

To explain how an alteration of mitochondrial shape affects a nuclear program of aging and muscle atrophy, we addressed the potential pathogenetic involvement of UPR. We acutely treated our inducible *Opa1*$^{-/-}$ mice with TUDCA, an established chemical chaperone known to counteract ER stress. TUDCA blunted p-eIF2α and improved pAkt as well as reduced FGF21 expression in *Opa1*$^{-/-}$ (Figures 6A–6C and S5D). Accordingly, expression of some atrophy-related ubiquitin ligases (Atrogin1, Itch, and SMART) and autophagy-related genes (e.g., LC3, GabarapL, and Bnip3) was reduced by TUDCA (Figures 6D and 6E). When we prolonged the treatment throughout the time during which muscles undergo atrophy, the observed reduction of XBP1 splicing and FGF21 induction (Figure 6F) was accompanied by the maintenance of mitochondrial content (Figures 6G and 6H) but not function (Figure S7A). Body weight loss was partially spared (Figure S7B) because muscle wasting, but not WAT loss, was greatly prevented (Figures 6I and S7C).

Oxidative Stress Links Mitochondria to UPR

Since acute inhibition of OPA1 results in an increased oxidative stress, we reason that mitochondria-derived ROS may connect OPA1 deficiency with ER stress and UPR activation. To test this hypothesis, we treated the inducible KO mice with Trolox, a vitamin E analog with a potent anti-oxidant action. The treatment started 10 days before the beginning of weight loss. Trolox blunted the oxidative stress (Figures S7D and S7E), restored a normal ER function (Figure 6J), and completely prevented FGF21 induction in *Opa1*$^{-/-}$ mice (Figure 6K). However, mitochondrial dysfunction was not rescued by TROLOX (Figure S7A). Importantly, the antioxidant treatment preserved *Opa1*$^{-/-}$ from body weight loss (Figure 6L). Both skeletal muscle mass and WAT were maintained by Trolox in *Opa1*$^{-/-}$ (Figures 6M and 6N). Similar results were obtained by treating mice with a mitochondrial-targeted ROS scavenger named Mito-TEMPO (Lo Verso et al., 2014). Consistent with TUDCA and TROLOX data, Mito-TEMPO prevented protein oxidation, reduced FGF21 induction, blocked the atrophy program, restored an almost normal muscle mass, and partially prevented body weight loss, but did not affect white adipose tissue loss (Figures S7F–S7L). Thus, oxidative stress is the trigger that induces an ER-dependent atrophic program when OPA1 is acutely reduced.

Muscle-Dependent FGF21 Controls General Metabolism and Aging

To address the relevance of muscle-derived FGF21 in the context of *Opa1*$^{-/-}$ phenotype, we generated double Tamoxifen-inducible muscle-specific OPA1/FGF21 KO (*Opa1*$^{-/-}$ *Fgf21*$^{-/-}$) mice. Acute and simultaneous deletion of *Opa1* and

Figure 5. Acute OPA1 Inhibition Does Not Affect Protein Synthesis but Triggers an Atrophy Program

(A) Total protein extracts from adult muscles were immunoblotted with the indicated antibodies. Representative immunoblots of two independent experiments are shown. Statistical significance after densitometry is indicated on the right. Data are mean ± SEM, *p < 0.05, **p < 0.01.

(B) p-eIF2α and total eIF2α immunoblots of muscle homogenates of three independent experiments. Statistical significance after densitometry is indicated on the right. Data are mean ± SEM, **p ≤ 0.01.

(C) Quantitative RT-PCR of genes downstream of UPR. Data are mean ± SEM, n = 5, **p < 0.01.

(D) Quantitative RT-PCR of FGF21 in OPA1-deficient muscles. Data are mean ± SEM, n = 4, **p < 0.01, ***p < 0.001.

(E) FGF21 plasma levels in *Opa1*$^{-/-}$ mice were determined by ELISA (n = 6). **p < 0.01.

(F–H) Quantitative RT-PCR of several atrophy-related genes belonging to the ubiquitin proteasome (F and G) and autophagy-lysosome systems (H). Data are mean ± SEM, n = 5, *p < 0.05, **p < 0.01.

(I) Autophagy flux is increased in basal condition in OPA1-deficient muscles. Inhibition of autophagosome-lysosome fusion by colchicine treatment induces higher increase of p62 and LC3II band in OPA1 null than control muscles. Data are mean ± SEM, n = 5, **p ≤ 0.01.

(J and K) Densitometric quantification of lysine 48 (Lys48) and of lysine 63 (Lys63) poly-ubiquitinated proteins of muscle extracts from *Opa1*$^{f/f}$ and *Opa1*$^{-/-}$. Data are mean ± SEM, n = 8, *p < 0.05, **p ≤ 0.01.

(L) *Opa1*$^{-/-}$ mice and *Opa1*$^{f/f}$ were transfected in vivo with scramble or siRNA against FoxO1/3. Inhibition of FoxOs by RNAi prevented muscle atrophy in *Opa1*$^{-/-}$ muscles. n = 6 per each group. Data are mean ± SEM, *p < 0.05, **p < 0.01.

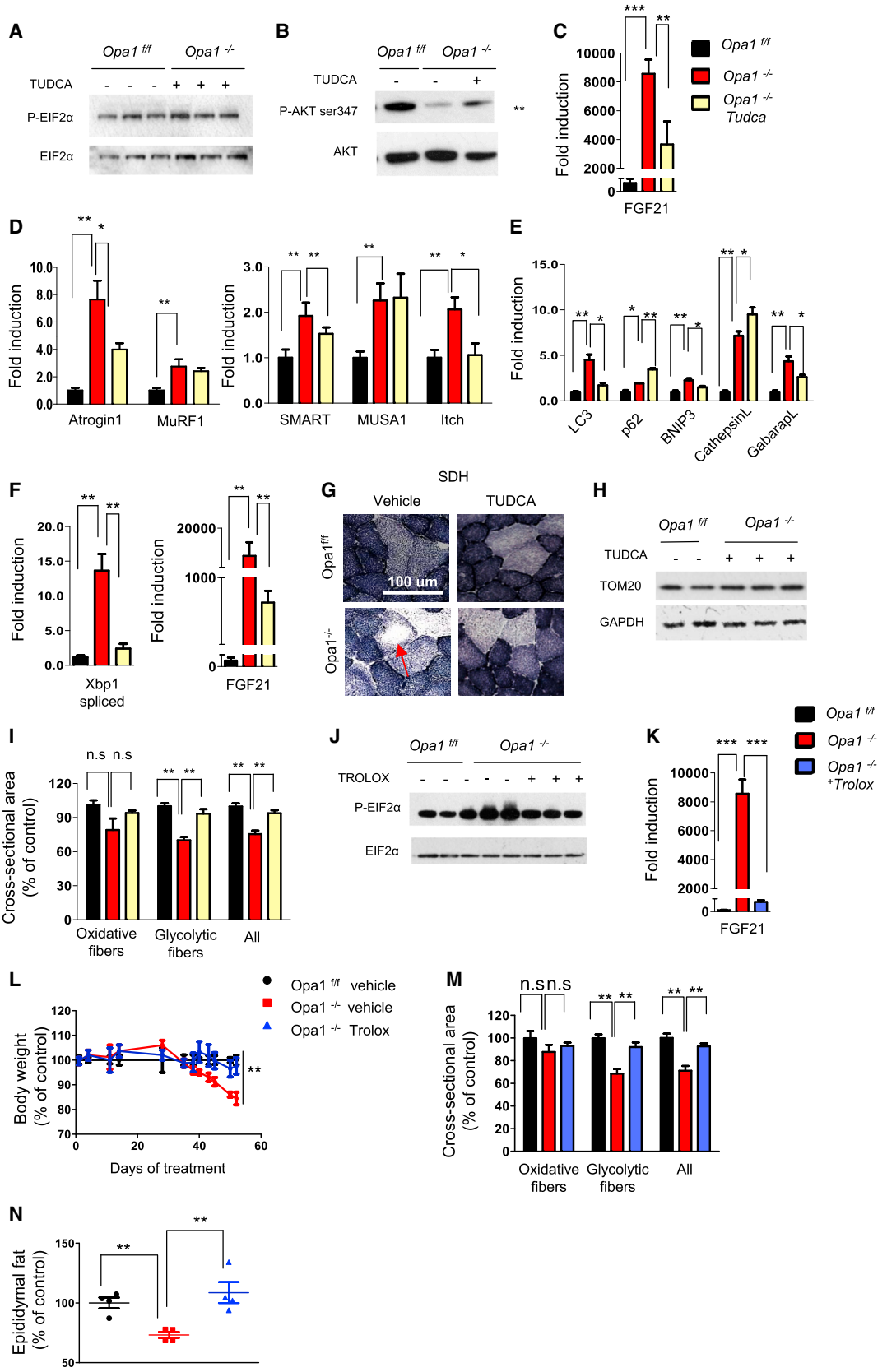

(legend on next page)

Fgf21 restored normal blood levels of FGF21 (Figure 7A). Double KO mice are partially protected from body weight loss (Figures 7B and S7M) because muscle mass and white adipose tissue are, in part, spared (Figures 7C and 7D). The lipolysis is not completely blocked in *Opa1*$^{-/-}$*Fgf21*$^{-/-}$, because UCP1 is still induced in WAT and muscles are still atrophic, because atrogin1 expression in double KO is less than *Opa1*$^{-/-}$ but higher than controls (Figures S7N and S7O). Although Complex III activity is improved, mitochondria are still dysfunctional after the deletion of both FGF21 and OPA1, with a significant reduction of Complex I activity and of respiration (Figures S7A and S7P–S7R). Importantly, the aging phenotype was completely reverted by FGF21 deletion. Mice did not show any more white hairs and kyphosis (Figure 7E), liver steatosis was prevented, glycemia was restored to normal level, inflammatory cytokines were now in normal blood range (Figures 7F–7H), and muscle expression of IL6 and IL1α was normalized (Figure S7S). Loss of motorneurons and innervation, revealed by NCAM staining, was prevented (Figure 7I). Additionally, markers of aging such as β-galactosidase activity and p21 expression were normalized to control levels in several tissues (Figures 7J and 7K). Finally, the simultaneous deletion of *Opa1* and *Fgf21* prevented the precocious death of *Opa1*$^{-/-}$ mice (Figure 7L).

FGF21 Serum Level Increases with Aging in Humans

To corroborate our animal findings, we tested the blood levels of FGF21 in a human cohort ranging from 19 to 103 years old. A highly significant correlation between FGF21 serum levels and age was found (Figure 7M). Thus, muscle-derived FGF21 is an important player in regulation of whole-body metabolism and in senescence but is only partially involved in muscle loss where FoxOs are dominant.

DISCUSSION

Here we have identified how OPA1 in muscles triggers a cascade of signaling that reverberates to the whole body, affecting general metabolism and aging. We have also translated our data to humans and shown that mitochondrial shaping proteins decline during aging in old sedentary people, both as transcripts and proteins. However, among the different fusion and fission genes, only OPA1 expression correlates with age-dependent muscle loss and weakness. Our data confirm previous observations that proteins of mitochondrial dynamics decrease with aging in sedentary rodents and humans (Ibebunjo et al., 2013; Joseph et al., 2012). Furthermore, we have also found that exercise can prevent this decline. Therefore, altogether these findings strongly suggest that a functional mitochondrial network is critical for muscle-mass maintenance and healthy aging. At the moment the question of how mitochondria affect aging and lifespan remains up for debate (Wang and Hekimi, 2015), as does how physical activity counteracts unhealthy aging (Neufer et al., 2015). The generation of inducible muscle-specific OPA1 and double FGF21/OPA1 KO mice enables us to shed a light on these issues. Indeed, we have identified the link that connects mitochondria to systemic metabolic changes, organ function, and longevity. The recent findings that muscle metabolism overcomes a mitochondrial problem in the heart and prevents the onset of dilated cardiomyopathy and heart failure (Wai et al., 2015) suggest that muscles may play a role in general metabolism and tissue function. This is an emerging concept that considers the metabolic adaptations occurring in skeletal muscles as disease modifier/controller (Baskin et al., 2015) and explains why physical activity elicits several beneficial effects in many different diseases. Indeed, exercise by preserving and ameliorating mitochondrial function and muscle metabolism affects the release of myokines and metabolites that systemically counteract organ deterioration. We identified FGF21 as one of these factors that, when chronically expressed at high levels in adulthood, greatly contributes to a pro-senescence metabolic shift. At the moment, whether FGF21 is beneficial or detrimental is debated, especially when related to heart function in humans (Chou et al., 2016; Li et al., 2016). Interestingly, high levels of serum FGF21 have been found in a child affected by progeria (Suomalainen et al., 2011), and circulating levels of FGF21 have been shown to increase with age in humans (Hanks et al., 2015). FGF21 is now recognized and used as a diagnostic marker in patients with mitochondrial myopathy (Lehtonen et al., 2016) who clearly are not longer lived. Importantly, while inhibition of FGF21 greatly ameliorates the precocious aging phenotype of OPA1 KO mice, it shows minor beneficial effects on muscle mass, suggesting that FGF21 mediates systemic

Figure 6. TUDCA and Trolox Treatments Prevent ER Stress, Reduce FGF21 Induction, and Spare Muscle Mass

(A and B) Representative immunoblots of three independent experiments of p-eIF2α (A) and pAkt (B) in KO animals treated with TUDCA compared to untreated OPA1 null mice. Statistical significance after densitometry is indicated on the right. Data are mean ± SEM, n = 6, **p < 0.01.

(C) Quantitative RT-PCR demonstrated a significant reduction of FGF21 expression in TUDCA-treated (5 days) animals. Data are mean ± SEM, n = 5, **p < 0.01, ***p < 0.001.

(D and E) Quantitative RT-PCR analysis of atrophy-related genes. Data are mean ± SEM, n = 5, *p < 0.05, **p < 0.01.

(F) Quantitative RT-PCR shows the significant reduction of both spliced XBP1 and FGF21 expression when animals were treated with TUDCA for 2 weeks. Data are mean ± SEM, n = 6, **p < 0.01.

(G) Representative SDH staining shows the maintenance of normal mitochondrial content in TUDCA-treated *Opa1*$^{-/-}$.

(H) Representative immunoblots of TOM20.

(I) Quantification of cross-sectional area of *Opa1*$^{f/f}$ and *Opa1*$^{-/-}$ myofibers treated or not with TUDCA. Values are mean ± SEM from at least 4 muscles in each group, **p < 0.01.

(J) Representative immunoblots of p-eIF2α after Trolox treatment in OPA1 null mice. n = 3.

(K) Quantitative RT-PCR of FGF21 expression in Trolox-treated mice. Data are mean ± SEM, n = 7, ***p < 0.001.

(L) Growth curve of control and *Opa1*$^{-/-}$ mice. Trolox prevented the body weight loss of *Opa1*$^{-/-}$. Data are mean ± SEM (*Opa1*$^{f/f}$ n = 20, *Opa1*$^{-/-}$ n = 19, *Opa1*$^{-/-}$ + TROLOX n = 10), **p < 0.01.

(M) Quantification of cross-sectional area of controls and OPA1 knockout myofibers treated or not with Trolox. Values are mean ± SEM from at least four muscles in each group, **p < 0.01, n.s.: not significant.

(N) Epididymal white adipose tissue content of controls and *Opa1*$^{-/-}$ mice treated or not with Trolox (n = 6 in each group). Data are mean ± SEM, **p < 0.01.

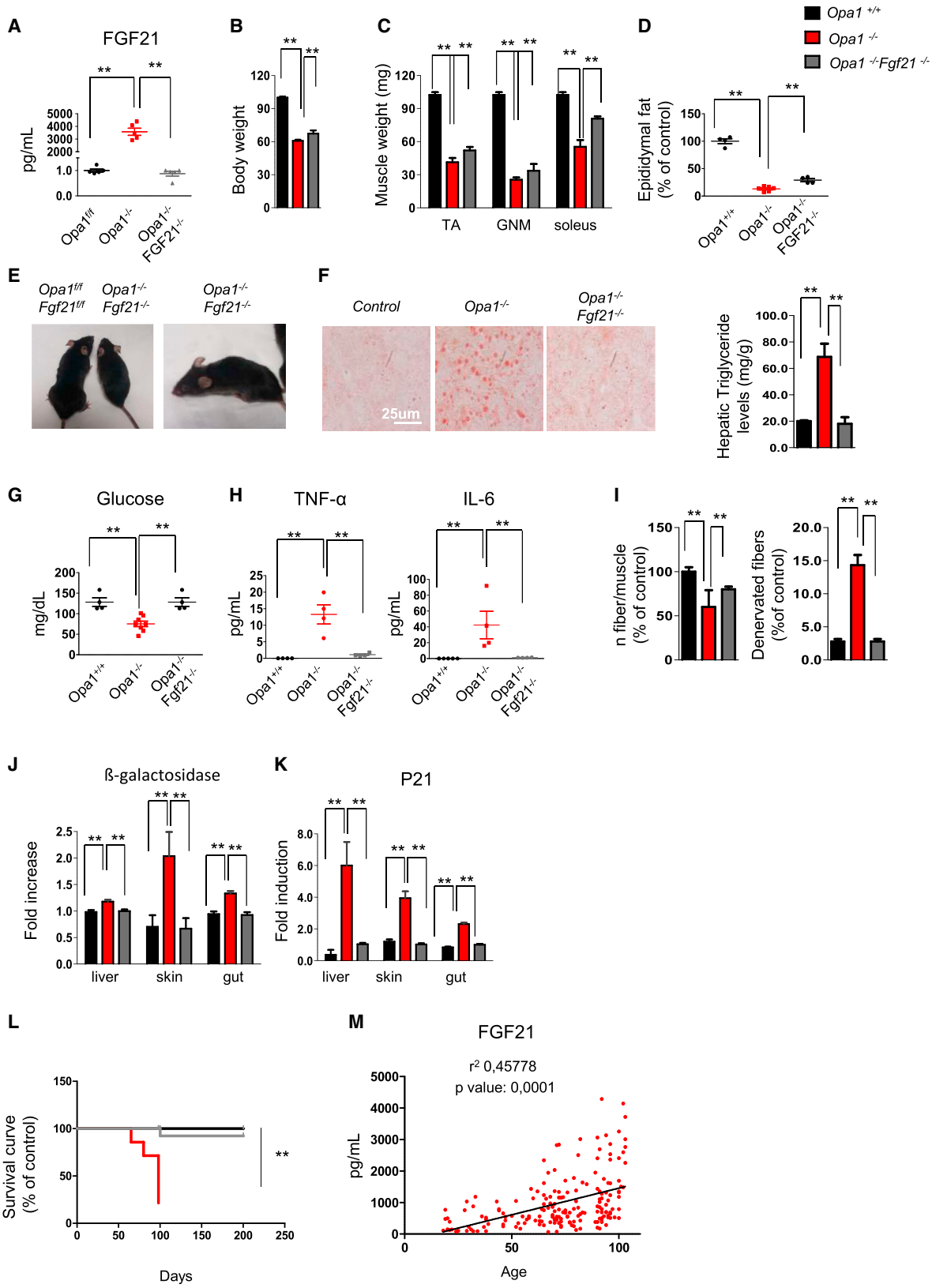

(legend on next page)

metabolic changes while other signaling, e.g., FoxO, is responsible for protein breakdown and muscle loss. The marginal effect on muscle mass explains why FGF21 deletion in newborns did not rescue the lethal phenotype of conditional OPA1 KO mice that die as a result of breathing problems (data not shown). These data also support the concept that FGF21 needs the presence of other factors that synergize to trigger the precocious senescence phenotype of OPA1 KO mice. The finding that OPA1 deletion induces IL6 and IL1α expression in muscles and blood suggests that a concomitant pro-inflammatory status may be permissive for the pro-aging action of FGF21. Since IL6 is known to be detrimental for human health when chronically elevated, the concomitant increase of FGF21 and IL6 can explain the systemic effects on aging that were not reported when FGF21 is expressed from liver or adipose tissue. A further point is that the outcome can be dictated by plasma FGF21 levels. Interestingly, FGF21 blood levels detected in the inducible OPA1 model (Figure 5E) are superimposable with several values found in the blood of very old human subjects (Figure 7M). Indeed, our data in humans do find a highly significant correlation between FGF21 serum levels and age. Importantly, unhealthy aged people that suffer from sarcopenia/frailty syndrome are in a strong catabolic (fasting-like and FGF21-like) condition, with an important anabolic resistance that inhibits muscle recovery after an injury. All together, these observations sustain a detrimental action of muscle-derived FGF21 more than a beneficial effect.

The phenotype of the *Opa1*$^{-/-}$ described here does not completely match with those of other pro-fusion proteins or with constitutive deletion of the Opa1 gene. Total OPA1 KO mice are lethal, but heterozygous OPA1$^{+/-}$ are viable and have been used to study the role of this gene in exercise performance (Caffin et al., 2013). Hemizygous mice for OPA1 do have problem in training-induced mitochondrial biogenesis but, surprisingly, do not show any problem in physical activity. However, this model suffers from the fact that adaptations and compensations occur in muscle as well as in other tissues consequent to the constitutive reduction of OPA1 from zygote formation. Indeed, mitochondria morphology in these mice is not consistent with a fusion problem, since mitochondria are bigger than wild-type mice, and there are no abnormalities in cristae shape, supporting the concept that something happened during embryological/neonatal development to compensate for the 50% reduction of OPA1 protein (Caffin et al., 2013). More interesting are the data from conditional KO of mitofusin genes. A reduced muscle mass has been also reported in mice ablated for both *Mfn1* and *Mfn2*, although analyses of muscle stem cell and of protein synthesis were not shown (Chen et al., 2010). Importantly, the muscle-specific deletion of *Mfn1*/*Mfn2* genes was performed by using the same driver that we used here for conditional OPA1 ablation, but only some phenotypes appear to be in common. The similarities include a defect of muscle growth, the presence of low blood glucose levels at basal condition, and a reduced mitochondrial function. However, while Chen and colleagues interpret this as a consequence of depleted mtDNA, we observed it only following prolonged fusion inhibition in the model of inducible OPA1 ablation, whereas the impairment in cristae shape and mitochondrial supercomplex assembly was conversely an early consequence and could explain the observed reduced mitochondrial function. We believe that our data corroborate a model in which mtDNA depletion is a consequence of chronic fusion inhibition (Cogliati et al., 2013). Our findings also place autophagic removal of the small abnormal mitochondria in the pathway leading to reduced mtDNA content following fusion ablation, thereby dissociating the myopathic phenotype from mtDNA decrease and suggesting that mitochondrial dysfunction can be amplified by mitochondrial depletion.

In conclusion, our findings point to mitochondria dynamics in muscle as a signaling hub that, by modulating nuclear gene expression programs, not only controls muscle mass but systemically reverberates, affecting lipid homeostasis, inflammation, and the senescence of different tissues.

STAR★METHODS

Detailed methods are provided in the online version of this paper and include the following:

- KEY RESOURCES TABLE
- CONTACT FOR REAGENT AND RESOURCE SHARING
- EXPERIMENTAL MODEL AND SUBJECT DETAILS
  - Human subjects
  - Plasma Human samples
  - Mouse models

Figure 7. Acute Simultaneous Deletion of OPA1 and FGF21 Reverted Precocious Epithelial Senescence, Systemic Inflammation, and Premature Death

(A) FGF21 plasma levels in OPA1/FGF21-KO, determined by ELISA, are significantly decreased compared to OPA1-deficient animals. Data are mean ± SEM, n = 4, **p < 0.01.

(B) Body weight measured 120 days after the beginning of tamoxifen treatment. Data are mean ± SEM, n = 5, **p < 0.01.

(C) Muscle weight of controls, *Opa1*$^{-/-}$, and *Opa1*$^{-/-}$*Fgf21*$^{-/-}$. Data are mean ± SEM, n = 4, **p < 0.01. TA, tibialis anterior; GNM, gastrocnemius.

(D) Epididymal fat is higher in *Opa1*$^{-/-}$*Fgf21*$^{-/-}$ than in *Opa1*$^{-/-}$ mice. Data are mean ± SEM (controls n = 4, *Opa1*$^{-/-}$ n = 8, *Opa1*$^{-/-}$*Fgf21*$^{-/-}$ n = 4), **p < 0.01.

(E) Eight-month-old *Opa1*$^{-/-}$*Fgf21*$^{-/-}$ show reduction of animal size (left panel) but do not show white hairs and kyphosis (right panel).

(F) Left panel: representative images of oil red O staining in liver cryosections. Right panel: Quantification of liver triglyceride content. Data are mean ± SEM, n = 4, **p < 0.01.

(G) Fasting blood glucose is restored to normal level in *Opa1*$^{-/-}$*Fgf21*$^{-/-}$ mice. Data are mean ± SEM (*Opa1*$^{f/f}$ n = 4, *Opa1*$^{-/-}$ n = 8, *Opa1*$^{-/-}$*Fgf21*$^{-/-}$ n = 4), **p < 0.01.

(H) Blood inflammatory cytokines are back to control level in *Opa1*$^{-/-}$*Fgf21*$^{-/-}$ mice. Data are mean ± SEM, n = 4, **p < 0.01.

(I) Quantification of fibers number per muscle (left panel) and denervated NCAM-positive fibers (right panel) in *Opa1*$^{-/-}$, *Opa1*$^{-/-}$*Fgf21*$^{-/-}$, and controls. Data are mean ± SEM, n = 5, **p < 0.01.

(J and K) Quantification of β-galactosidase and p21 levels. Data represent mean ± SEM, n = 4, **p < 0.01.

(L) Survival curve of control, *Opa1*$^{-/-}$, and *Opa1*$^{-/-}$*Fgf21*$^{-/-}$mice. Data are mean ± SEM (controls n = 19, *Opa1*$^{-/-}$ n = 20, *Opa1*$^{-/-}$*Fgf21*$^{-/-}$ n = 15), **p < 0.01.

(M) Regression analysis between age and FGF21 plasma levels of human subjects ranging from 19 to 103 years old. Data represent mean ± SEM, n = 180.

SUPPLEMENTAL INFORMATION

Supplemental Information includes seven figures and three tables and can be found with this article online at http://dx.doi.org/10.1016/j.cmet.2017.04.021.

AUTHOR CONTRIBUTIONS

C.T. and V.R. generated the inducible and muscle-specific knockout mice, performed experiments, and analyzed and interpreted data. C.T., V.R., L. Salviati, L. Scorrano, and M.S. designed experiments, discussed data, and wrote the manuscript. M.A.D., M.A., G.F., S.C., M.E.S., V.M., C.C., M.C., B.B., and S.Z. contributed to experiments and data collection. G.P.F., S.L., H.K., C.F., S.S., and L. Salviati provided reagents and materials and discussed data. M.S. and L. Scorrano supervised the work.

ACKNOWLEDGMENTS

This work was supported by CARIPARO Foundation 2010 Excellence Project to M.S. and to L. Scorrano; by ERC (282310-MyoPHAGY), AFM-Telethon (19524), Italian Ministry of Education (MiUR) (PRIN 2010/2011), Foundation Leducq, AIRC (17388), and RISE (645648) to M.S.; by CARIPARO Foundation Starting Grant to V.R. and M.S.; by Telethon Italy (GPP10005, GGP12162, GGP14187), ERC (FP7-282280), EU FP7 (CIG PCIG13-GA-2013-618697), and MiUR (FIRB AUTOMED RBAP11Z3YA_005) to L. Scorrano; and by Telethon Italy (GGP13222, GGP14187) and Fondazione CARIPARO to L. Salviati. We acknowledge Prof. Chiara Romualdi (Department of Biology, University of Padua) for help with statistical analyses.

Received: August 16, 2016
Revised: December 22, 2016
Accepted: April 17, 2017
Published: May 25, 2017

REFERENCES

Alexander, C., Votruba, M., Pesch, U.E., Thiselton, D.L., Mayer, S., Moore, A., Rodriguez, M., Kellner, U., Leo-Kottler, B., Auburger, G., et al. (2000). OPA1, encoding a dynamin-related GTPase, is mutated in autosomal dominant optic atrophy linked to chromosome 3q28. Nat. Genet. *26*, 211–215.

Amati-Bonneau, P., Valentino, M.L., Reynier, P., Gallardo, M.E., Bornstein, B., Boissière, A., Campos, Y., Rivera, H., de la Aleja, J.G., Carroccia, R., et al. (2008). OPA1 mutations induce mitochondrial DNA instability and optic atrophy 'plus' phenotypes. Brain *131*, 338–351.

Baskin, K.K., Winders, B.R., and Olson, E.N. (2015). Muscle as a "mediator" of systemic metabolism. Cell Metab. *21*, 237–248.

Blaauw, B., Canato, M., Agatea, L., Toniolo, L., Mammucari, C., Masiero, E., Abraham, R., Sandri, M., Schiaffino, S., and Reggiani, C. (2009). Inducible activation of Akt increases skeletal muscle mass and force without satellite cell activation. FASEB J *23*, 3896–3905.

Caffin, F., Prola, A., Piquereau, J., Novotova, M., David, D.J., Garnier, A., Fortin, D., Alavi, M.V., Veksler, V., Ventura-Clapier, R., and Joubert, F. (2013). Altered skeletal muscle mitochondrial biogenesis but improved endurance capacity in trained OPA1-deficient mice. J. Physiol. *591*, 6017–6037.

Chen, H., Detmer, S.A., Ewald, A.J., Griffin, E.E., Fraser, S.E., and Chan, D.C. (2003). Mitofusins Mfn1 and Mfn2 coordinately regulate mitochondrial fusion and are essential for embryonic development. J. Cell Biol. *160*, 189–200.

Chen, H., Vermulst, M., Wang, Y.E., Chomyn, A., Prolla, T.A., McCaffery, J.M., and Chan, D.C. (2010). Mitochondrial fusion is required for mtDNA stability in skeletal muscle and tolerance of mtDNA mutations. Cell *141*, 280–289.

Chou, R.H., Huang, P.H., Hsu, C.Y., Chang, C.C., Leu, H.B., Huang, C.C., Chen, J.W., and Lin, S.J. (2016). Circulating Fibroblast Growth Factor 21 is Associated with Diastolic Dysfunction in Heart Failure Patients with Preserved Ejection Fraction. Sci. Rep. *6*, 33953.

Cipolat, S., Rudka, T., Hartmann, D., Costa, V., Serneels, L., Craessaerts, K., Metzger, K., Frezza, C., Annaert, W., D'Adamio, L., et al. (2006). Mitochondrial rhomboid PARL regulates cytochrome c release during apoptosis via OPA1-dependent cristae remodeling. Cell *126*, 163–175.

Cogliati, S., Frezza, C., Soriano, M.E., Varanita, T., Quintana-Cabrera, R., Corrado, M., Cipolat, S., Costa, V., Casarin, A., Gomes, L.C., et al. (2013). Mitochondrial cristae shape determines respiratory chain supercomplexes assembly and respiratory efficiency. Cell *155*, 160–171.

Davies, V.J., Hollins, A.J., Piechota, M.J., Yip, W., Davies, J.R., White, K.E., Nicols, P.P., Boulton, M.E., and Votruba, M. (2007). Opa1 deficiency in a mouse model of autosomal dominant optic atrophy impairs mitochondrial morphology, optic nerve structure and visual function. Hum. Mol. Genet. *16*, 1307–1318.

Delettre, C., Lenaers, G., Griffoin, J.M., Gigarel, N., Lorenzo, C., Belenguer, P., Pelloquin, L., Grosgeorge, J., Turc-Carel, C., Perret, E., et al. (2000). Nuclear gene OPA1, encoding a mitochondrial dynamin-related protein, is mutated in dominant optic atrophy. Nat. Genet. *26*, 207–210.

Demontis, F., and Perrimon, N. (2010). FOXO/4E-BP signaling in Drosophila muscles regulates organism-wide proteostasis during aging. Cell *143*, 813–825.

Demontis, F., Piccirillo, R., Goldberg, A.L., and Perrimon, N. (2013). The influence of skeletal muscle on systemic aging and lifespan. Aging Cell *12*, 943–949.

Demontis, F., Patel, V.K., Swindell, W.R., and Perrimon, N. (2014). Intertissue control of the nucleolus via a myokine-dependent longevity pathway. Cell Rep. *7*, 1481–1494.

Frezza, C., Cipolat, S., Martins de Brito, O., Micaroni, M., Beznoussenko, G.V., Rudka, T., Bartoli, D., Polishuck, R.S., Danial, N.N., De Strooper, B., and Scorrano, L. (2006). OPA1 controls apoptotic cristae remodeling independently from mitochondrial fusion. Cell *126*, 177–189.

Frezza, C., Cipolat, S., and Scorrano, L. (2007). Organelle isolation: functional mitochondria from mouse liver, muscle and cultured fibroblasts. Nat. Protoc. *2*, 287–295.

Goodman, C.A., Mabrey, D.M., Frey, J.W., Miu, M.H., Schmidt, E.K., Pierre, P., and Hornberger, T.A. (2011). Novel insights into the regulation of skeletal muscle protein synthesis as revealed by a new nonradioactive in vivo technique. FASEB J. *25*, 1028–1039.

Grumati, P., Coletto, L., Sabatelli, P., Cescon, M., Angelin, A., Bertaggia, E., Blaauw, B., Urciuolo, A., Tiepolo, T., Merlini, L., et al. (2010). Autophagy is

defective in collagen VI muscular dystrophies, and its reactivation rescues myofiber degeneration. Nat. Med. *16*, 1313–1320.

Hanks, L.J., Gutiérrez, O.M., Bamman, M.M., Ashraf, A., McCormick, K.L., and Casazza, K. (2015). Circulating levels of fibroblast growth factor-21 increase with age independently of body composition indices among healthy individuals. J. Clin. Transl. Endocrinol. *2*, 77–82.

Ibebunjo, C., Chick, J.M., Kendall, T., Eash, J.K., Li, C., Zhang, Y., Vickers, C., Wu, Z., Clarke, B.A., Shi, J., et al. (2013). Genomic and proteomic profiling reveals reduced mitochondrial function and disruption of the neuromuscular junction driving rat sarcopenia. Mol. Cell. Biol. *33*, 194–212.

Joseph, A.M., Adhihetty, P.J., Buford, T.W., Wohlgemuth, S.E., Lees, H.A., Nguyen, L.M., Aranda, J.M., Sandesara, B.D., Pahor, M., Manini, T.M., et al. (2012). The impact of aging on mitochondrial function and biogenesis pathways in skeletal muscle of sedentary high- and low-functioning elderly individuals. Aging Cell *11*, 801–809.

Lehtonen, J.M., Forsström, S., Bottani, E., Viscomi, C., Baris, O.R., Isoniemi, H., Höckerstedt, K., Österlund, P., Hurme, M., Jylhävä, J., et al. (2016). FGF21 is a biomarker for mitochondrial translation and mtDNA maintenance disorders. Neurology *87*, 2290–2299.

Li, Q., Zhang, Y., Ding, D., Yang, Y., Chen, Q., Su, D., Chen, X., Yang, W., Qiu, J., and Ling, W. (2016). Association Between Serum Fibroblast Growth Factor 21 and Mortality Among Patients With Coronary Artery Disease. J. Clin. Endocrinol. Metab. *101*, 4886–4894.

Lo Verso, F., Carnio, S., Vainshtein, A., and Sandri, M. (2014). Autophagy is not required to sustain exercise and PRKAA1/AMPK activity but is important to prevent mitochondrial damage during physical activity. Autophagy *10*, 1883–1894.

Mammucari, C., Milan, G., Romanello, V., Masiero, E., Rudolf, R., Del Piccolo, P., Burden, S.J., Di Lisi, R., Sandri, C., Zhao, J., et al. (2007). FoxO3 controls autophagy in skeletal muscle in vivo. Cell Metab. *6*, 458–471.

Masiero, E., Agatea, L., Mammucari, C., Blaauw, B., Loro, E., Komatsu, M., Metzger, D., Reggiani, C., Schiaffino, S., and Sandri, M. (2009). Autophagy is required to maintain muscle mass. Cell Metab. *10*, 507–515.

Milan, G., Romanello, V., Pescatore, F., Armani, A., Paik, J.H., Frasson, L., Seydel, A., Zhao, J., Abraham, R., Goldberg, A.L., et al. (2015). Regulation of autophagy and the ubiquitin-proteasome system by the FoxO transcriptional network during muscle atrophy. Nat. Commun. *6*, 6670.

Neufer, P.D., Bamman, M.M., Muoio, D.M., Bouchard, C., Cooper, D.M., Goodpaster, B.H., Booth, F.W., Kohrt, W.M., Gerszten, R.E., Mattson, M.P., et al. (2015). Understanding the Cellular and Molecular Mechanisms of Physical Activity-Induced Health Benefits. Cell Metab. *22*, 4–11.

Romanello, V., and Sandri, M. (2016). Mitochondrial Quality Control and Muscle Mass Maintenance. Front. Physiol. *6*, 422.

Šarabon, N., Loefler, S., Cvecka, J., Sedliak, M., and Kern, H. (2013a). Strength training in elderly people improves static balance: a randomized controlled trial. Eur. J. Transl. Myol. *23*, 85–89.

Šarabon, N., Rošker, J., Fruhmann, H., Burggraf, S., Loefler, S., and Kern, H. (2013b). Reliability of maximal voluntary contraction related parameters measured by a portable isometric knee dynamometer. Phys. Med. Rehabil. Kuror. *23*, 22–27.

Schaaf, C.P., Blazo, M., Lewis, R.A., Tonini, R.E., Takei, H., Wang, J., Wong, L.J., and Scaglia, F. (2011). Early-onset severe neuromuscular phenotype associated with compound heterozygosity for OPA1 mutations. Mol. Genet. Metab. *103*, 383–387.

Schiaffino, S., Dyar, K.A., Ciciliot, S., Blaauw, B., and Sandri, M. (2013). Mechanisms regulating skeletal muscle growth and atrophy. FEBS J. *280*, 4294–4314.

Schmidt, E.K., Clavarino, G., Ceppi, M., and Pierre, P. (2009). SUnSET, a nonradioactive method to monitor protein synthesis. Nat. Methods *6*, 275–277.

Spiegel, R., Saada, A., Flannery, P.J., Burté, F., Soiferman, D., Khayat, M., Eisner, V., Vladovski, E., Taylor, R.W., Bindoff, L.A., et al. (2016). Fatal infantile mitochondrial encephalomyopathy, hypertrophic cardiomyopathy and optic atrophy associated with a homozygous OPA1 mutation. J. Med. Genet. *53*, 127–131.

Spinazzi, M., Casarin, A., Pertegato, V., Salviati, L., and Angelini, C. (2012). Assessment of mitochondrial respiratory chain enzymatic activities on tissues and cultured cells. Nat. Protoc. *7*, 1235–1246.

Suomalainen, A., Elo, J.M., Pietiläinen, K.H., Hakonen, A.H., Sevastianova, K., Korpela, M., Isohanni, P., Marjavaara, S.K., Tyni, T., Kiuru-Enari, S., et al. (2011). FGF-21 as a biomarker for muscle-manifesting mitochondrial respiratory chain deficiencies: a diagnostic study. Lancet Neurol. *10*, 806–818.

Wai, T., García-Prieto, J., Baker, M.J., Merkwirth, C., Benit, P., Rustin, P., Rupérez, F.J., Barbas, C., Ibañez, B., and Langer, T. (2015). Imbalanced OPA1 processing and mitochondrial fragmentation cause heart failure in mice. Science *350*, aad0116.

Wang, Y., and Hekimi, S. (2015). Mitochondrial dysfunction and longevity in animals: Untangling the knot. Science *350*, 1204–1207.

Zampieri, S., Pietrangelo, L., Loefler, S., Fruhmann, H., Vogelauer, M., Burggraf, S., Pond, A., Grim-Stieger, M., Cvecka, J., Sedliak, M., et al. (2015). Lifelong physical exercise delays age-associated skeletal muscle decline. J Gerontol A Biol Sci Med Sci *70*, 163–173.

Zhao, J., Brault, J.J., Schild, A., Cao, P., Sandri, M., Schiaffino, S., Lecker, S.H., and Goldberg, A.L. (2007). FoxO3 coordinately activates protein degradation by the autophagic/lysosomal and proteasomal pathways in atrophying muscle cells. Cell Metab. *6*, 472–483.

Züchner, S., Mersiyanova, I.V., Muglia, M., Bissar-Tadmouri, N., Rochelle, J., Dadali, E.L., Zappia, M., Nelis, E., Patitucci, A., Senderek, J., et al. (2004). Mutations in the mitochondrial GTPase mitofusin 2 cause Charcot-Marie-Tooth neuropathy type 2A. Nat. Genet. *36*, 449–451.

STAR★METHODS

KEY RESOURCES TABLE

REAGENT or RESOURCE	SOURCE	IDENTIFIER
Antibodies		
mouse anti-Bromodeoxyuridine	Roche	11170376001
mouse anti-Pax 7	Hybridoma Bank	Pax7
rabbit anti-phospho-Akt (Ser473)	Epitomics	EP2109Y
rabbit anti-total Akt	Cell Signaling	#9272
rabbit anti-phospho-S6	Cell Signaling	#2215
rabbit anti-total S6	Cell Signaling	#2217
rabbit anti-LC3 B	Sigma	L7543
rabbit anti-P62	Sigma	P0067
rabbit anti-phospho-AMPKα (Thr172)	Cell Signaling	#2531
rabbit anti-total AMPKα	Cell Signaling	#2532
rabbit anti-phospho-4EBP1 (Ser65)	Cell Signaling	#9451
rabbit anti-phospho-4EBP1 (Thr37/46)	Cell Signaling	#9459
rabbit anti-total 4EBP1	Cell Signaling	#9452
rabbit anti-phospho-ACC	Cell Signaling	#3661
rabbit anti-phospho-mTOR	Cell Signaling	#5536
rabbit anti-mTOR	Cell Signaling	#2983
mouse anti-GAPDH	Abcam	ab8245
mouse anti-puromycin	Hybridoma Bank	PMY-2A4
mouse anti-ubiquitinylated proteins (FK2)	Millipore	#04-263
rabbit anti-ubiquitin,lys63-specific (clone Apu3)	Millipore	#05-1308
rabbit anti-MyoD	Santa Cruz	sc-32758
mouse anti-MyoG	Millipore	MAB3876
mouse anti-Lamin A/C (N-18)	Santa Cruz	sc-6215
rabbit anti-phospho-eIF2α	Abcam	ab 32157
rabbit anti-eIF2α	Cell Signaling	#9722
rabbit anti-BIP/GRP78	BD	610979
mouse anti-OPA1	BD	612606
mouse anti-Drp1	BD	611738
rabbit anti-TOM20	Santa Cruz	Sc-11415
mouse anti-Bnip3	Sigma	B7931
mouse anti-complexII	Invitrogen	459200
rabbit anti-phospho-Smad3	Epitomics	Ep #1880-1
rabbit anti-phospho-smad1/5/8	Cell Signaling	#9511
mouse anti-Bnip3	Sigma	B7931
mouse anti-complexII	Invitrogen	459200
rabbit anti-phospho-Smad3	Epitomics	Ep #1880-1
rabbit anti-phospho-smad1/5/8	Cell Signaling	#9511
mouse MFN1	Abcam	Ab57602
mouse MFN2	Abcam	Ab56889
Rabbit ACC	Cell Signaling	3662S
mouse NDUF 88	Abcam	ab110242
mouse CORE2	Abcam	ab14745
goat anti-mouse Cy3	Jackson Laboratory	115-165-003

(*Continued on next page*)

Continued

REAGENT or RESOURCE	SOURCE	IDENTIFIER
goat anti mouse IgG	Bio-Rad	1706516
goat anti rabbit IgG	Bio-Rad	1706515
Biological Samples		
Human biopsies		EK 07-057-0407; EK 08-102-0608
Human plasma		EU FP6 Project "GeHA"; EU FP7 Project "MYOAGE"
Chemicals, Peptides, and Recombinant Proteins		
Tamoxifen food	Harlan	Td55125
Tudca	Tokyo Chemical Industry	Cas 302-95-4
Trolox	Sigma-Aldrich	Cas 53188-07-1
Mito tempo	Enzolife Science	ALX-400-150-M005
5-Bromo-20 -deoxyuridine	Sigma-Aldrich	Cat#B9285
Protease Inhibitor	Sigma-Aldrich	Cat#P8340
Phosphatase Inhibitor Cocktail 2	Sigma-Aldrich	Cat#P5276
Phosphatase Inhibitor Cocktail 3	Sigma-Aldrich	Cat#P0044
Pierce BCA Protein Assay Kit	Thermo Fisher	Cat#23225
SYBR Green Supermix	Bio-Rad	Cat#1725274
Colchicine	Sigma-Aldrich	09754
Critical Commercial Assays		
Mouse IL6 ELISA Kit	MERCK Millipore	EZMIL6
Mouse TNFα ELISA Kit	MERCK Millipore	EZMTNFA
Mouse IL1a ELISA Kit	Thermo Fisher	EMIL1A
Mouse IL1b ELISA Kit	Thermo Fisher	EMIL1B
Rat/Mouse FGF-21 ELISA Kit	MERCK Millipore	EZRMFGF21-26K
Human FGF-21 ELISA Set (10 × 96 T)	Aviscera Bioscience	SK00145-10
Coating buffer, blocking buffer, concentrated diluition buffer, antibody diluent solution, HRP diluent solution	Aviscera Bioscience	CS01, BS-01, BD01, BD18, BD06
2-Deoxyglucose (2DG) Uptake Measurement Kit	Cosmo Bio	CSR-OKP-PMG-K01TE
Experimental Models: Organisms/Strains		
MLC1f-Cre-Opa1f/f /BL6	Sandri Lab	N/A
HSA-Cre-ER-Opa1f/f /BL6	Sandri Lab	N/A
HSA-Cre-ER-Opa1f/f –Fgf21f/f /BL6	Sandri Lab	N/A
Oligonucleotides		
Primers for qPCR, see Table S3		
Recombinant DNA		
Mt-roGPF1: ro1 with mitochondrial targeting sequence in pEGFP-N1, pRA306	S.J. Remington (University of Oregon)	N/A
pSUPER FoxO1/3	Mammucari et al., 2007	N/A
Software and Algorithms		
ImageJ Software		N/A
Prism 7 software (GraphPad software)		N/A

CONTACT FOR REAGENT AND RESOURCE SHARING

Further information and requests for resources and reagents should be directed to and will be fulfilled by the Lead Contact, Marco Sandri (marco.sandri@unipd.it).

EXPERIMENTAL MODEL AND SUBJECT DETAILS

Human subjects

All participants were healthy volunteers and declared not to have any specific physical/disease issues. The specific exclusion criteria were body mass index $\geq$ 40kg/m2; previous knee replacement; recent deep vein thrombosis or any infection; myopathy; neurologic, pulmonary, or symptomatic cardiovascular diseases; vertigo or impaired cognitive function; recent or past cancer; rheumatism; or any other relevant limitations of the musculoskeletal system. All participants were informed about the testing procedures and the possible risks, and written informed consent had to be signed prior to inclusion in this study. In addition, ethical approval was obtained from the ethical commission of the municipality of Vienna (EK 07-057-0407) and (EK08-102-0608).

Nutritional status before skeletal muscle biopsy consisted in daily routine. Muscle biopsy collection was performed quite at the same time in the morning between 10.00 and 11.00 from the Vastus Lateralis of three different groups of male subjects as described (Zampieri et al., 2015): Young subjects (23 to 34 years of age) performing moderate training activities; sedentary seniors (53 to 82 years of age), either inactive healthy subjects performing only routine daily activities or seniors with knee arthropathy, and senior sportsmen: (66 to 72 years of age) who routinely practiced (lifelong) sport activities more 3 to 5 times a week (one –to –two hours per session). 15 mg of muscle tissue were sufficient to perform both, proteins and RNA extraction.

Plasma Human samples

The human samples used in this study were obtained from volunteers of different ages, ranging from 19-103 years-old. recruited in the framework of the EU FP6 Project "GeHA – Genetics of Healthy Ageing"; the EU FP7 Project "MYOAGE – Understanding and combating age-related muscle weakness"; and the Italian National Project "PRIN2009CB4C9F - Ruolo della epigenetica e della genetica del DNA mitocondriale nella longevità: studi su soggetti con più di 105 anni di età (semi-supercentenari)."

The study protocols were approved by the local Ethical Committees responsible for the Bologna unit, respectively:

- for the GeHA study: Sant'Orsola-Malpighi University Hospital (Bologna), ethical clearance n. 118/2004/U/Tess issued on 20/07/2004;
- for the MYOAGE study: Istituto Ortopedico Rizzoli (Bologna) ethical clearance n. 10823 issued on 26/04/2010;
- for the PRIN study: Sant'Orsola-Malpighi University Hospital (Bologna) ethical clearance n. 22/2007/U/Tess issued on 27/02/2007, amendment n. EM 157/2011/U issued on 25/11/2011.

Inclusion/ Exclusion criteria

MYOAGE samples from 24-96 years-old subjects: Healthy subjects. Exclusion criteria were: to be non-autonomous in the dayly living activities, to be unable to walk a distance of 250 m, presence of morbidity (neurologic disorders, metabolic diseases, rheumatic diseases, recent malignancy, heart failure, severe chronic obstructive pulmonary disease (COPD), haemocoagulative syndromes), use of medication (immunosuppressive drugs, insulin), immobilization for 1 week during last 3 months, and orthopedic surgery during the last 2 years or still causing pain or functional limitation.

Hip replacement subjects: Subjects who underwent surgery for hip dysplasia. Age (> 20 years) and the ability to provide informed consent and to cooperate with the study personnel were inclusion criteria, while exclusion criteria were presence of diseases, i.e., chronic kidney and/or liver diseases, bleeding disorders, severe type 2 diabetes, rheumatic diseases, osteoarthritis, neuromuscular disorders, malignancies and systemic infections, other than chronic steroid use, major psychological problems or history of alcohol or drug abuse, evidence of prior surgery in the involved hip.

GEHA samples: Inclusion criteria of participants: i) they should be at least 90 years of age (a nonagenarian); ii) they should have a living sibling who also is a nonagenarian; iii) they should be able to understand the scope of the project.

PRIN2009CB4C9F samples: Inclusion criteria: 100+ years old subjects

For FGF21 detection the HUMAN FGF-21 IMMMUNOASSAY CAT NUM DF2100 (R&D SYSTEMS) kit was used. To obtain sufficient technical replicates for the Elisa assay, at least 300 ul of plasma samples were needed.

Mouse models

Animals were handled by specialized personnel under the control of inspectors of the Veterinary Service of the Local Sanitary Service (ASL 16 - Padova), the local officers of the Ministry of Health. All procedures are specified in the projects approved by the Italian Ministero Salute, Ufficio VI (authorization number 1060/2015 PR). Muscles were removed at various time periods and frozen in liquid nitrogen for subsequent analyses.

To generate constitutive muscle-specific OPA1 knockout (KO) animals, mice bearing *Opa1* floxed alleles (*Opa1*$^{f/f}$) (Cogliati et al., 2013) were crossed with transgenic mice expressing Cre under the control of a Myosin Light Chain 1 fast promoter (MLC1f-Cre) and kept in a homozygous mating system. Experiments were performed on newborns at post-natal day 7 or 8. Cre-negative littermates were used as controls.

A second KO model with inducible muscle-specific deletion of OPA1 was obtained by crossing the *Opa1*$^{f/f}$ line with mice carrying Cre-ER driven by human skeletal actin promoter (HSA). Tamoxifen-induced Cre LoxP recombination was activated by oral administration of tamoxifen-containing chow (Tam400/Cre ER Harlan) which was provided ad libitum for 5 weeks. A third KO model was obtained by crossing HSA- *Opa1*$^{f/f}$ line with *Fgf21*$^{f/f}$. Tamoxifen-induced CreLoxP recombination was activated by oral administration

of tamoxifen-containing chow (Tam400/Cre ER Harlan) which was given ad libitum for 5 weeks. Animals with food intake received indicatively, 1 mg of tamoxifen per day. Mice were housed in individual cages in an environmentally controlled room (23°C, 12-h light–dark cycle) with ad libitum access to food and water. All experiments were performed on 3- to 18-month-old male (17–32 g) and female mice (16–26 g). Mice of the same sex and age were used for each individual experiment. Muscles were collected at different times: 30, 50 or 120 days after the beginning of the tamoxifen diet. Cre-negative littermates, also receiving tamoxifen treatment were used as controls. *Fgf21* floxed (*Fgf21*$^{f/f}$) were purchased by The Jackson Laboratory and crossed with HSA- *Opa1*$^{f/f}$ Cre positive.

PCR genotyping was performed with the following primers:
OPA1 Fw: CAGTGTTGATGACAGCTCAG
OPA1 Rv: CATCACACACTAGCTTACATTTGC
FGF21 Fw: AGGAGGCTAGGGCTTGACTCT
FGF21 Rw: TGACAGGGTCTCAGGTTCAA
Cre Fw: CACCAGCCAGCTATCAACTCG
Cre Rv: TTACATTGGTCCAGCCACCAG

METHOD DETAILS

Gene expression analyses

Total RNA was prepared from muscles using TRIzol (Invitrogen). Complementary DNA was generated from 0.4 μg of RNA reverse-transcribed with SuperScript III Reverse Transcriptase(Invitrogen). Duplicates of cDNA samples were then amplified on the 7900HT Fast Real-Time PCR System (Applied Biosystems) using the Power SYBR Green RT-PCR kit (Applied Biosystems). All data were normalized to GAPDH and to actin expression and plotted in arbitrary units as mean ± SEM. The oligonucleotide primers used are shown in table S3.

Immunoblotting

Muscles were lysed and immunoblotted as previously described (Mammucari et al., 2007). Blots were stripped using Restore western blotting stripping buffer (Pierce) according to the manufacturer's instructions and probed again when necessary. List of antibodies is indicated in the key resources table

β-galactosidase assay

In vitro β-galactosidase measurement was performed on different tissues (liver, skin and gut). Lysates were prepared using T-PER Tissue Protein Extraction Reagent (cat n78510, Thermofisher) then Pierceβ-Galactosidase Assay Reagent (Product No. 75705) and β-Galactosidase Assay Stop Solution (Product No. 75706) to develop the reaction.

Imaging and Transmission Electron Microscopy

Cryosections of both P8 newborns hindlimb cross-sections and adult TA were stained for H&E and SDH. Total myofiber number was calculated from entire hindlimb cross-section based on assembled mosaic image (20X magnification). CSA was performed on adult TA as described (Mammucari et al., 2007). ATPase staining: Serial cryosections (8 μm) from human muscle biopsies were mounted on polysine glass slides, air-dried, and stained either with hematoxylin and eosin (H&E) or conventional techniques for myofibrillar ATPases to evaluate muscle fiber type. For ATPase stains, slow-type fibers are dark, whereas fast-type fibers are lightly stained following preincubation at pH 4.35. Fiber type grouping is identified on the basis that one myofiber is surrounded by fibers of the same phenotype. Morphometric analyses were performed on stained cryosections using Scion Image for Windows version Beta 4.0.2 (2000 Scion Corporation) (Zampieri et al., 2015). For immunostaining, we used antibodies specific for Pax7 (1:20, Hybridoma Bank), BrdU (1:40, Roche) and TOM20 (1:100, Santa Cruz). The secondary antibodies, goat anti-mouse Cy3 were obtained from Jackson lab. Hoechts co-staining, allowed to identify subsarcolemmal position of myonuclei.

For electron microscopy, we used conventional fixation-embedding procedures based on glutaraldehyde-osmium fixation and Epon embedding.

Measurement of MtDNA Copy Number

Total gastrocnemius DNA was isolated using Puregene Cell and Tissue Kit(QIAGEN) and was amplified using specific primers for mtCOXII and 18S by real-time PCR using the Power SYBR Green RT-PCR kit (Applied Biosystems). The mtDNA copy number was calculated using 18S amplification as a reference for nuclear DNA content.

Mitochondrial Assays

Muscle mitochondria from the indicated genotype were isolated as described (Frezza et al., 2007). To detect RCS, Blue Native PAGE was performed by resuspending mitochondrial pellets in Native Buffer (Invitrogen) plus 4% Digitonin (SIGMA) to a final concentration of 10 μg/μl and incubated for 1 hr on ice. After 20 min of centrifugation at 16,000 g, the supernatant was collected and one-third of

digitonin percentage of Sample Buffer 5% G250 (Invitrogen) was added. Then 50 μg of mitochondrial membrane proteins was loaded and run on a 3%–12% Bis-Tris gel (Invitrogen) as described in the NativePAGE Novex® Bis-Tris Gel System manual. Western blot was performed using a Trans-Blot transfer cell (Bio-Rad) at 4°C O/N. List of antibodies is depicted in Table S2.

To measure respiration, mitochondria (1 mg/ml) were incubated in Experimental Buffer (EB: 150 mM KCl, 10 mM Tris Mops,10 mM EGTA-Tris, 10mM ATP). When indicated, mitochondria were transferred into a Clark's type oxygen electrode chamber and 5mM glutamate/2.5 mM malate or 2 mM rotenone/10 mM succinate were added. Basal O2 consumption was recorded (state 2) and after 2 min 100 mMADP was added (state 3), followed by 2.5 mg/ml oligomycin (state 4) and 200 mMFCCP (state 3u). Assesment of mitochondrial respiratory chain enzymatic activities on muscles was determined as described (Spinazzi et al., 2012). Results were normalized to citrate synthase enzymatic activity.

Protein Carbonyls Detection

Carbonylation of muscle proteins were detected by using the OxyBlot Protein Oxidation Detection Kit (Millipore, s7150) (Masiero et al., 2009). Quantification analysis was performed with ImageJ Software and all values were normalized for the housekeeping GAPDH.

Torque measurement and testing

An isometric measurement on a dynamometer (S2P Ltd., Lubljana, Slovenia) with 90° hip flexion and 60° knee flexion (full knee extension = 0°) was performed as described (Šarabon et al., 2013a, 2013b) three times at each leg to assess the maximal isometric torque of the left and right knee extensors. The mean of the best values of each leg were taken for further analyses.

The time up and go test (TUGT) was performed to evaluate mobility and function in activities of daily living. Briefly, the subjects were asked to stand up from a standard chair, walk 3 m, turn around, walk back to the chair, and sit down again all as fast as possible.

VAS-48h (visual analog scale in rest and during activity) and WOMAC (Western Ontario and McMaster Universities Arthritis Index) questionnaire were performed to evaluate pain in the activities of daily living in the last 48h prior to the assessment.

MOUSE STUDIES

Mitochondrial oxidative stress measurement

Mt-roGFP1, which measures the thiol/disulfide equilibrium in the mitochondrial matrix, was used as an indicator of mitochondrial redox status, as previously described (Lo Verso et al., 2014). Briefly, Adult FDB muscles were transfected by electroporation with mt-roGFP1 plasmid. After 7 d of transfection single muscle fibers were isolated from control and knock-out mice. Mt-roGFP1 fluorescence (excitation: 405 and 480 nm, emission: 535 nm, 20 × objective) was measured for 5 min every 10 s and upon H_2O_2. The ratio of fluorescence intensities (exc 405/480) was determined by ImageJ Software.

In vivo protein synthesis measurements

In vivo protein synthesis was measured by using the SUnSET technique (Goodman et al., 2011; Schmidt et al., 2009). Mice were anesthetized and then given an intraperitoneal injection of 0.040 μmol/g puromycin dissolved in 100 μL of PBS. At exactly 30 min after injection, muscles were collected and frozen in liquid N2 for WB analysis using a mouse IgG2a monoclonal anti-puromycin antibody (clone 12D10, 1:5000).

In vivo drug treatments

KO and control mice received TUDCA (Tokyo Tanabe, Tokyo, Japan) at a dose of 500 mg/kg twice a day (8:00 AM and 8:00 PM) by oral administration for 5 days or 2 weeks.

Mice were intraperitoneally injected daily for 5 days or 2 weeks with 30 mg/kg of TROLOX (6-hydroxy-2,5,7,8-tetramethylchroman-2-carboxylic acid).

Mito-TEMPO (Enzo Life Science, ALX-430-150-M005) at a dose of 1.4 mg/kg was administered through an intraperitoneal injection every day for 5 days or 2 weeks

Force measurements

In vivo force measurements were performed as described previously (Blaauw et al., 2009). Briefly, mice were anesthetized and stainless steel electrodes wires were placed on either side of the sciatic nerve. Torque production of the plantar flexors was measured using a muscle lever system (Model 305c; Aurora Scientific, Aurora ON, Canada). The force–frequency curves were determined by increasing the stimulation frequency in a stepwise manner, pausing for 30 s between stimuli to avoid effects due to fatigue. Force was normalized to the muscle mass as an estimate of specific force. Following force measurements, animals were sacrificed by cervical dislocation and muscles were dissected and weighed.

Single Fibers Isolation and Mitochondrial Membrane Potential analyses

Mitochondrial membrane potential was measured in isolated transfected fibers from flexor digitorum brevis (FDB) muscles as previously described (Mammucari et al., 2007; Zhao et al., 2007). Briefly, FDB myofibers were placed in 1 mL Tyrode's buffer and loaded

with 2.5 nM TMRM (Molecular Probes) supplemented with 1μM cyclosporine H (a P-glycoprotein inhibitor) for 30 min at 37°C. Myofibers were then observed at Olympus IMT-2 inverted microscope (Melville, NY) equipped with a CellR imaging system. Sequential images of TMRM fluorescence were acquired every 60 s with a 20X 0.5, UPLANSL N A objective (Olympus). At the times indicated by arrows, oligomycin (Olm, 5 μM) (Sigma) or the protonophore carbonyl cyanide p-trifluoromethoxyphenylhydrazone (FCCP, 4 μM) (Sigma) were added to the cell culture medium. Images were acquired, stored and analysis of TMRM fluorescence over mitochondrial regions of interest was performed using ImageJ software (https://imagej.nih.gov/ij/). When stated, isolated FDB fibers were stained with a rabbit polyclonal anti-TOM20 (Santa Cruz 1:200) and were further analyzed by confocal microscopy.

Plasma measurements

Plasma was obtained from blood collected from controls and OPA1 null mice. Blood FGF21 levels were determined using Rat/Mouse FGF21 Enzime-linked Immunosorbent ELISA-Kit (Millipore, EZRMFGF21-26K). OPA1 KO mice FGF21 relative quantification was normalized to controls. Data are expressed as fold increase of controls. Blood IL-6 (Millipore, EZMIL6), TNF-α (Millipore, EZMTNFA), IL-1α (Thermofisher, EMIL1A) IL-1β (Thermofisher, EM2IL1B) were measured following the manufacturer's instructions. Data are expressed in pg/mL. Glucose measurement was performed at 9 a.m. in fed condition, with the One Touch Ultra Easy glucose meter (LifeScan Inc.). Data are expressed in mg/dL.

Exercise experiments

In this study 18 months-old mice performed concentric exercise on a treadmill (Biological Instruments, LE 8710 Panlab Technology 2B), with 10° incline. Mice were trained for one week, 1 hr per day at constant speed of 18 cm/s

Glucose and insulin tolerance tests

Mice were fasted for 8 hr before analysis during their normal rest/fasting phase. Blood glucose was measured using a Glucocard G^+ meter (Arkray Factory, Shiga, Japan). Glucose tolerance tests (GTT) and insulin tolerance tests (ITT) were performed at ZT12, For GTT, mice were injected i.p. with glucose (2 g/kg body weight). Blood glucose was measured at 0, 10, 20, 30, 60 and 120 min via the tail vein. For ITT, mice were injected i.p. with human insulin (0.75 U/kg body weight; Sigma) and blood glucose was measured at 10, 0, 10, 20, 30, 60, and 90 min via the tail vein.

Autophagic flux quantification

Autophagic flux was monitored in fed condition using colchicine (C9754, Sigma-Aldrich) as previously described (Milan et al., 2015). Briefly, HSA $OPA1^{-/-}$ and $OPA1^{f/f}$ mice were treated, by i.p. injection, with vehicle or with 0,4mg/ kg colchicine. The treatment was administered twice, at 24 hr and at 12 hr before muscle collection.

In vivo Glucose uptake

Glucose uptake was measured using a non-radioactive colorimetric method (Saito K and Minokoshi Y et al. Analytical Biochem 412: 9-17, 2011), by means of the 2-deoxyglucose uptake measurement kit (Cosmo Bio Co., LTD, Tokyo, Japan). Mice were fasted 5 hr before the beginning of the experiment. Mice were then injected intraperitoneally with a solution containing D-glucose (1 g/Kg) and 2-deoxy-D-glucose (0.027 g/Kg). One hour after injection, mice were killed by cervical dislocation, and tissues (soleus, tibialis anterior, liver, epidydimal white adipose tissue) were rapidly removed, weighed and placed in ice cold Tris-HCl (10mM, pH8) buffer. Muscles from left and right legs were separately processed. Entire soleus and tibialis anterior muscles, 50-100 mg of liver and 100-200 mg of adipose tissue were used for the assay. Tissues were subsequently homogenized in 1ml of Tris-HCl (10mM, pH8) with TissueLyser II (QIAGEN), by shaking at maximum speed for 3 min, and heated at 95°C for 15 min. Samples were then centrifuged at 16000 g for 15 min at 4°C to remove tissue debris. Supernatants were finally collected, and a portion was diluted in 20μl (final volume; 2μl for soleus, 5μl for tibialis anterior, 1μl for liver and 10μl for WAT) with the sample dilution buffer provided with the kit. The assay was then performed following manufacturer's instructions.

QUANTIFICATION AND STATISTICAL ANALYSIS

Statistical analysis

All data are expressed as means ± SEM. Statistical analysis was performed using one-tailed or two-tailed Student's t test. Normal distribution of the variables of interest was checked using the Shapiro-Wilk test. For experiments in which more than two groups should be compared, 2-way analysis of variant (ANOVA) was used. When ANOVA revealed significant differences, further analysis was performed using Bonferroni's multiple comparison test. Differences between groups were considered statistically significant for $p \leq 0.05$ or $p \leq 0.01$. Linear regression models were used to verify the linear correlation between variables. t test were performed on the slopes of the regressions to verify their significance (GraphPad). Statistical significance was set at $p < 0.05$ were considered statistically significant for $p \leq 0.05$ or $p \leq 0.01$. Regression linear analysis was done using an F test (GraphPad). n, mean and SEM are reported within the figure legends.

Cell Metabolism, Volume *25*

Supplemental Information

Age-Associated Loss of OPA1 in Muscle Impacts Muscle Mass, Metabolic Homeostasis, Systemic Inflammation, and Epithelial Senescence

Caterina Tezze, Vanina Romanello, Maria Andrea Desbats, Gian Paolo Fadini, Mattia Albiero, Giulia Favaro, Stefano Ciciliot, Maria Eugenia Soriano, Valeria Morbidoni, Cristina Cerqua, Stefan Loefler, Helmut Kern, Claudio Franceschi, Stefano Salvioli, Maria Conte, Bert Blaauw, Sandra Zampieri, Leonardo Salviati, Luca Scorrano, and Marco Sandri

Fig. S1

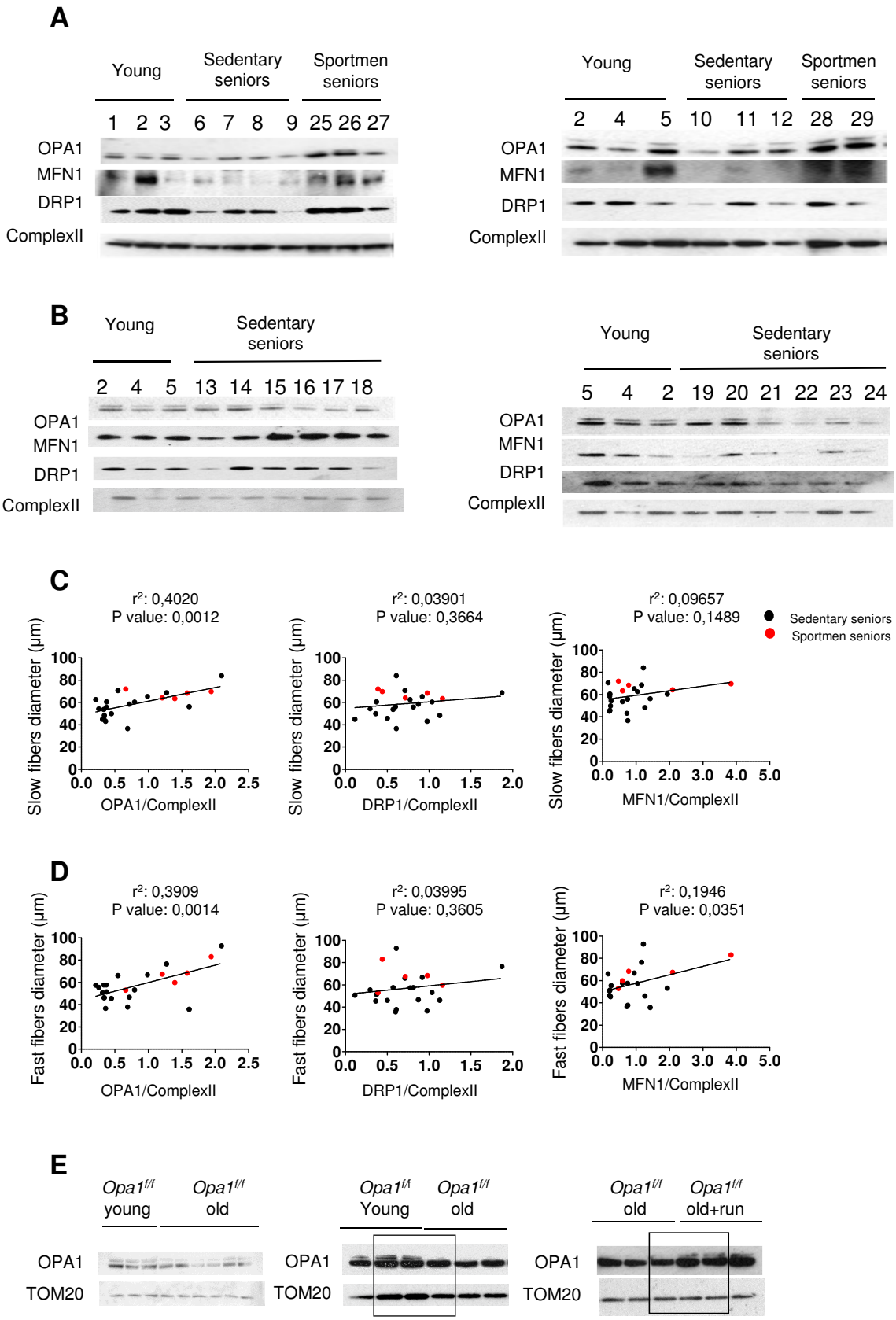
A
Young
Sedentary seniors
Sportmen seniors
1 2 3 6 7 8 9 25 26 27
OPA1
MFN1
DRP1
ComplexII
Young
Sedentary seniors
Sportmen seniors
2 4 5 10 11 12 28 29
OPA1
MFN1
DRP1
ComplexII
B
Young
Sedentary seniors
2 4 5 13 14 15 16 17 18
OPA1
MFN1
DRP1
ComplexII
Young
Sedentary seniors
5 4 2 19 20 21 22 23 24
OPA1
MFN1
DRP1
ComplexII
C
r²: 0,4020
P value: 0,0012
Slow fibers diameter (µm)
OPA1/ComplexII
r²: 0,03901
P value: 0,3664
Slow fibers diameter (µm)
DRP1/ComplexII
r²: 0,09657
P value: 0,1489
Slow fibers diameter (µm)
MFN1/ComplexII
Sedentary seniors
Sportmen seniors
D
r²: 0,3909
P value: 0,0014
Fast fibers diameter (µm)
OPA1/ComplexII
r²: 0,03995
P value: 0,3605
Fast fibers diameter (µm)
DRP1/ComplexII
r²: 0,1946
P value: 0,0351
Fast fibers diameter (µm)
MFN1/ComplexII
E
Opa1f/f young
Opa1f/f old
OPA1
TOM20
Opa1f/f Young
Opa1f/f old
OPA1
TOM20
Opa1f/f old
Opa1f/f old+run
OPA1
TOM20

Figure S1 – OPA1 expression is reduced during ageing in sarcopenic patients - Related to Figure 1

A-B) Immunoblots of human muscle homogenates. On the top of each blot is indicated the number of the relative sample loaded. Further information related to the subjects can be find in the supplementary tables S1 and S2. MNF1, OPA1 and DRP1 were normalized for complex II expression levels. **C-D)** Linear regression analysis between OPA1, DRP1 and MFN1 expression levels and slow (C) and fast (D) myofiber size in elderly persons, (n=23) **E)** Uncropped scans of the western blots presented in Figure 1E. Muscle homogenates of tibialis anterior muscles from young, old and old trained mice were immunoblotted for the indicated antibodies. young (6 months-old n=6), old (18 months-old n=9) and old trained mice (18 months-old n=6).

Fig. S2

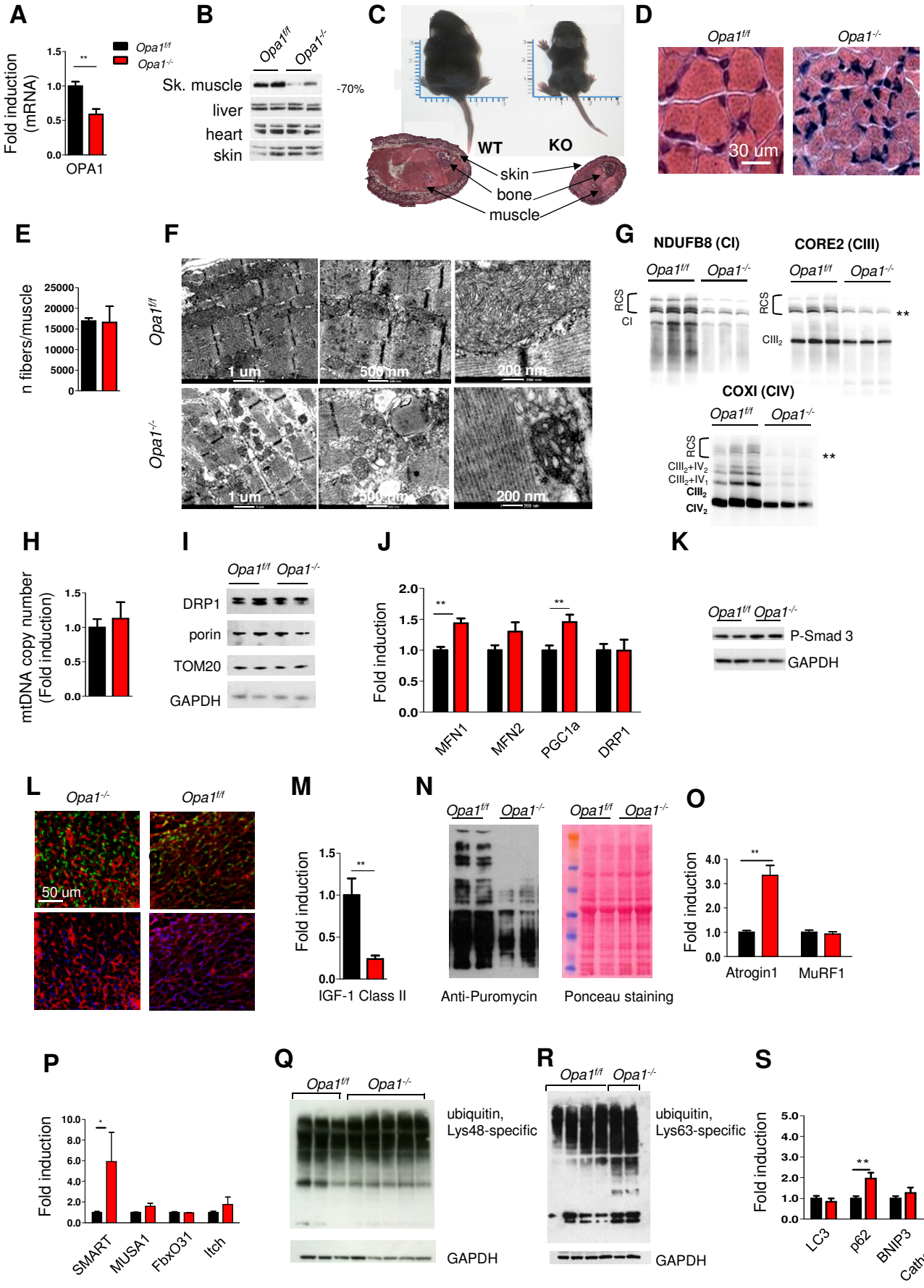
A
Fold induction (mRNA)
Opa1f/f
Opa1-/-
OPA1
B
Opa1f/f
Opa1-/-
Sk. muscle
liver
heart
skin
-70%
C
WT
KO
skin
bone
muscle
D
Opa1f/f
Opa1-/-
30 um
E
n fibers/muscle
F
Opa1f/f
Opa1-/-
1 um
500 nm
200 nm
G
NDUFB8 (CI)
CORE2 (CIII)
COXI (CIV)
RCS
CI
CIII2
CIII2+IV2
CIII2+IV1
CIV2
H
mtDNA copy number (Fold induction)
I
DRP1
porin
TOM20
GAPDH
J
Fold induction
MFN1
MFN2
PGC1a
DRP1
K
P-Smad 3
GAPDH
L
50 um
M
IGF-1 Class II
N
Anti-Puromycin
Ponceau staining
O
Atrogin1
MuRF1
P
SMART
MUSA1
FbxO31
Itch
Q
ubiquitin, Lys48-specific
GAPDH
R
ubiquitin, Lys63-specific
GAPDH
S
LC3
p62
BNIP3
CathepsinL
GabarapL

Figure S2- OPA1 deletion affects mitochondria morphology and function, muscle stem cell renewal, protein synthesis and protein breakdown inducing defects in muscle growth and a lethal phenotype - Related to Figure 2

A) OPA1 mRNA and **B)** OPA1 protein levels are downregulated in skeletal muscle and not in other tissues in OPA1-null mice. Each condition represents the mean ± SEM of at least three independent experiments **C)** Upper row: Representative photograph of control and KO littermates at post-natal day 8 showing that *Opa1*$^{-/-}$ mice are smaller than controls. Lower row: Haematoxilin-Eosin (HE) staining of hindlimb cross-section **D)** HE staining of muscles reveals smaller fibers in OPA1 knockout than controls (n=5 per each) **E)** Total number of fibers per muscle. Data represent mean ± SEM (n=4) **F)** Representative electron micrographs of gastrocnemius muscles from MLCOPA1$^{f/f}$ (upper row) and MLCOPA1$^{-/-}$ (lower row). OPA1 deletion leads to altered sarcomeric organization (left panel), lipid droplets accumulation (middle panel) and defects in cristae shape (right panel). Scale bar is indicated at the bottom of each picture **G)** OPA1 deficiency leads to a significant reduction of CIII and CIV assembly in respiratory chain supercomplexes (RCS). Representative Blue Native-PAGE analysis showing RCS developed and normalized for individual respiratory chain complexes. CI subunit NDUFB8 (left panel), CIII-Core2 protein 2 (right panel) and CIV subunit COXI (bottom panel) **H)** Mitochondrial DNA copy number is not affected by OPA1 deletion. Data are normalized to controls; data are mean ± SEM, n=5 **I)** Representative immunoblots for mitochondrial proteins of three independent experiments of muscle homogenates **J)** qRT-PCR revealed changes in expression of different pro-fusion and fission genes. Data are mean ± SEM (n=6) **K)** Phosphorylation of Smad3, revealed no changes in myostatin pathway between controls and OPA1 knockout. Data are mean ± SEM (n=5) **L)** Representative images of TUNEL assay. Similar number of TUNEL positive nuclei per muscles in control and OPA1 knock-out animals was observed (n=5 per each) **M)** qRT-PCR revealed a decrease of IGF-1 expression in the liver of OPA1 knockout mice (n=5) **N)** *In vivo* SUnSET technique demonstrate a significant reduction of protein synthesis in OPA1-ablated mice muscles. Data are mean ± SEM of three independent experiments **O)** qRT-PCR analysis of transcriptional levels of the FoxO-target genes: Atrogin1 and MuRF1 and **P)** SMART, MUSA1, FbxO31 and Itch **Q)** Representative western blots of Lysine 48 (Lys48) and **R)** Lysine 63 (Lys63) poly-ubiquitinated proteins of muscle extracts from controls and OPA1 knockout mice **S)** Transcriptional levels of several autophagy-related genes. Data are mean ± SEM (n=6 per condition) Statistical significance: *p≤ 0,05; **p≤ 0,01 and ***p≤ 0,001. CI: Complex I; CIII: Complex III; CIV: Complex IV; $CIII_2$+CIV_2: Complex III_2 plus Complex IV_2; $CIII_2$+CIV_1: Complex III_2 plus Complex IV_1.

Fig. S3

MLC OPA1- CONDITIONAL MODEL

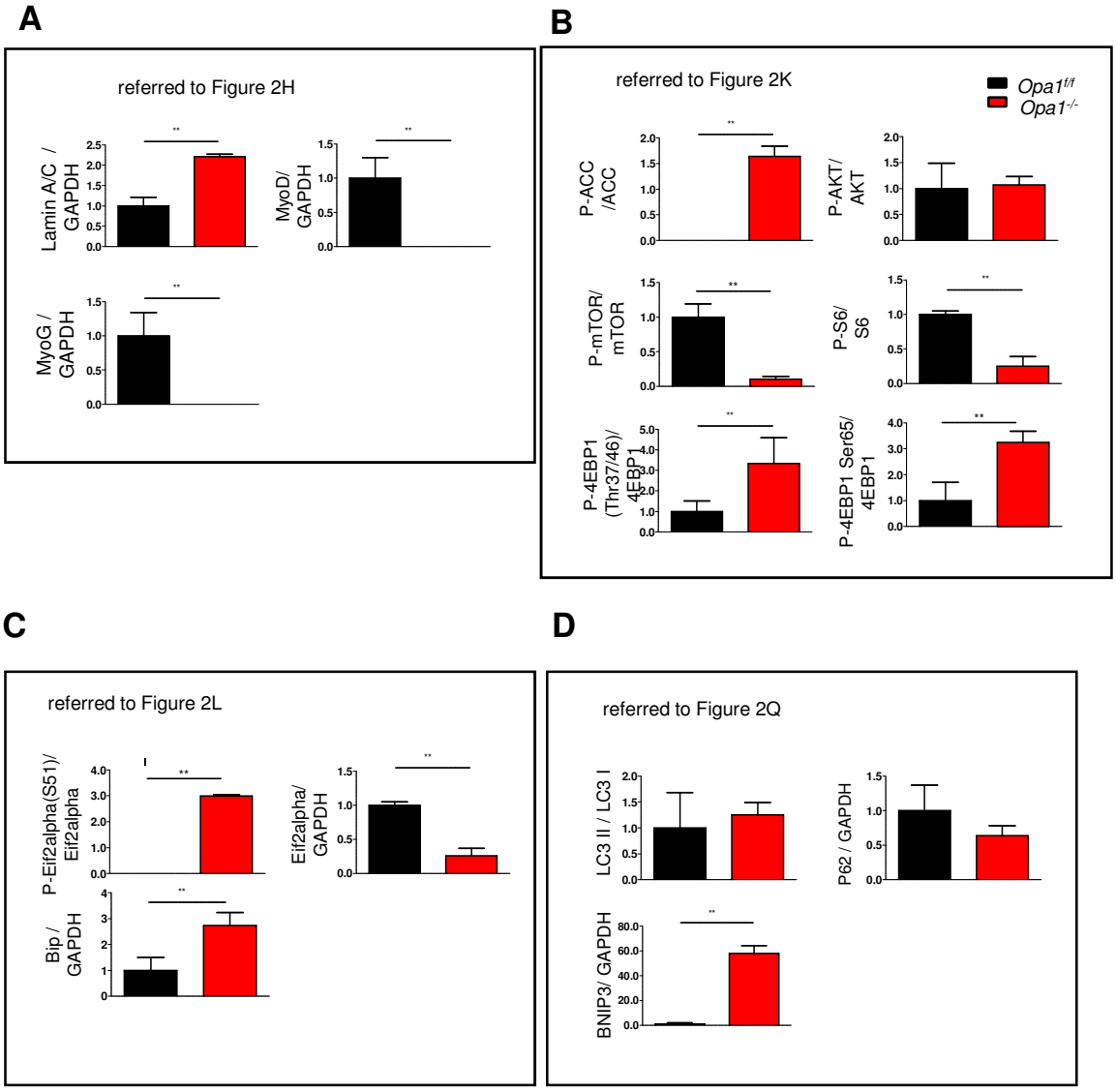

Figure S3 - Densitometric quantification of the western blots related to Figure 2

Fig. S4

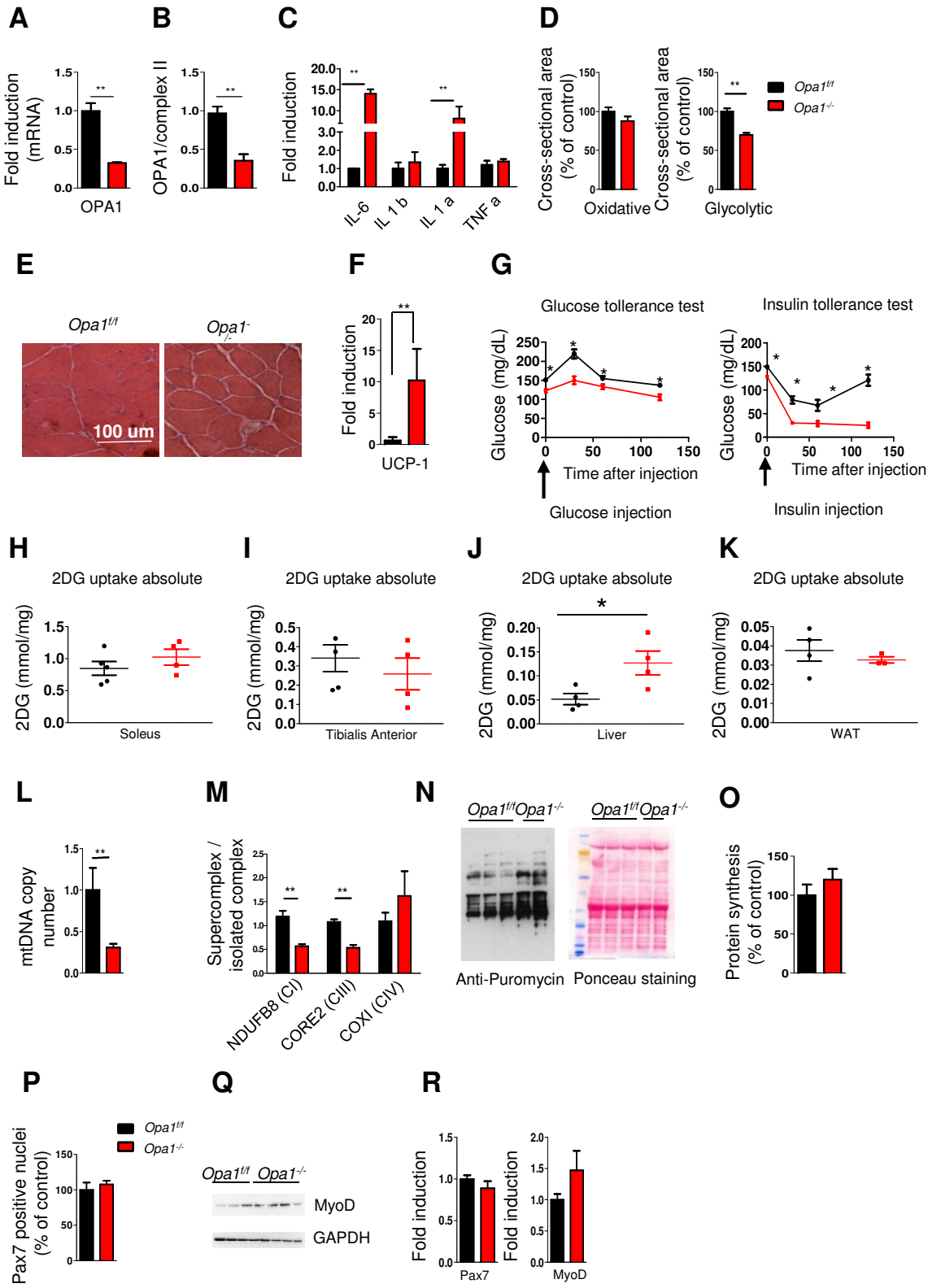
A
Fold induction (mRNA)
OPA1
B
OPA1/complex II
C
Fold induction
IL-6
IL 1 b
IL 1 a
TNF a
D
Cross-sectional area (% of control)
Oxidative
Glycolytic
Opa1f/f
Opa1-/-
E
Opa1f/f
Opa1-/-
100 um
F
Fold induction
UCP-1
G
Glucose tollerance test
Insulin tollerance test
Glucose (mg/dL)
Time after injection
Glucose injection
Insulin injection
H
2DG uptake absolute
2DG (mmol/mg)
Soleus
I
2DG uptake absolute
Tibialis Anterior
J
2DG uptake absolute
Liver
K
2DG uptake absolute
WAT
L
mtDNA copy number
M
Supercomplex / isolated complex
NDUFB8 (CI)
CORE2 (CIII)
COXI (CIV)
N
Opa1f/fOpa1-/-
Opa1f/fOpa1-/-
Anti-Puromycin
Ponceau staining
O
Protein synthesis (% of control)
P
Pax7 positive nuclei (% of control)
Opa1f/f
Opa1-/-
Q
Opa1f/f Opa1-/-
MyoD
GAPDH
R
Fold induction
Pax7
MyoD

Figure S4- Acute deletion of OPA1 in adult muscles reverberates to whole body leading to metabolic changes and to mitochondrial dysfunction - Related to Figure 3 and to Figure 4

A) OPA1 mRNA and **B)** OPA1 protein levels are downregulated in skeletal muscle after tamoxifen-dependent OPA1 deletion. Each condition represents the mean of at least three independent experiments ± SEM **C)** Blood levels of the inflammatory cytokines IL6, IL1a, IL1b and TNFa **D)** Cross-sectional area quantification of both, oxidative and glycolytic fibers in controls and in OPA1-null mice **E)** Representative HE staining of *Opa1$^{f/f}$* and *Opa1$^{-/-}$* mice showing normal morphology, absence of inflammation and no signs of degeneration **F)** qRT-PCR of UCP-1 expression in WAT of *Opa1$^{f/f}$* and *Opa1$^{-/-}$* **G)** Glucose and Insulin tolerance tests performed in *Opa1$^{f/f}$* and *Opa1$^{-/-}$* mice are shown. Data are mean ± SEM of three independent experiments **H-I-J-K)** Graphs show 2-deoxyglucose uptake in vivo in Soleus, Tibialis Anterior, Liver and WAT **L)** Mitochondrial DNA copy number is affected by OPA1 deletion. Data are normalized to controls; (n=3) **M)** OPA1 deficiency leads to a significant reduction of CIII and CIV assembly in respiratory chain supercomplexes (RCS). Quantification of Blue Native-PAGE analysis showing RCS developed and normalized for individual respiratory chain complexes : CI subunit NDUFB8 CIII-Core2 protein 2 and CIV subunit COXI **N)** *In vivo* SUnSET measurements showing no differences of protein synthesis between control and OPA1-deficient adult muscles **O)** Quantification of puromycin-labeled peptides, expressed as a percentage of the values obtained in the control group. Data are mean ± SEM of three independent experiments **P)** Pax7 positive muscle stem revealed by immunohistochemistry and normalized for muscle area and **Q)** MyoD levels detected by western blot (n=4) **R)** qRT-PCR for Pax7 and MyoD expression in adult skeletal muscles of *Opa1$^{f/f}$* and *Opa1$^{-/-}$*; (n=3) Statistical significance; *p≤ 0,05 and **p≤ 0,01. CI: Complex I; CIII: Complex III; CIV: Complex IV.

Fig. S5

HSA OPA1- INDUCIBLE MODEL

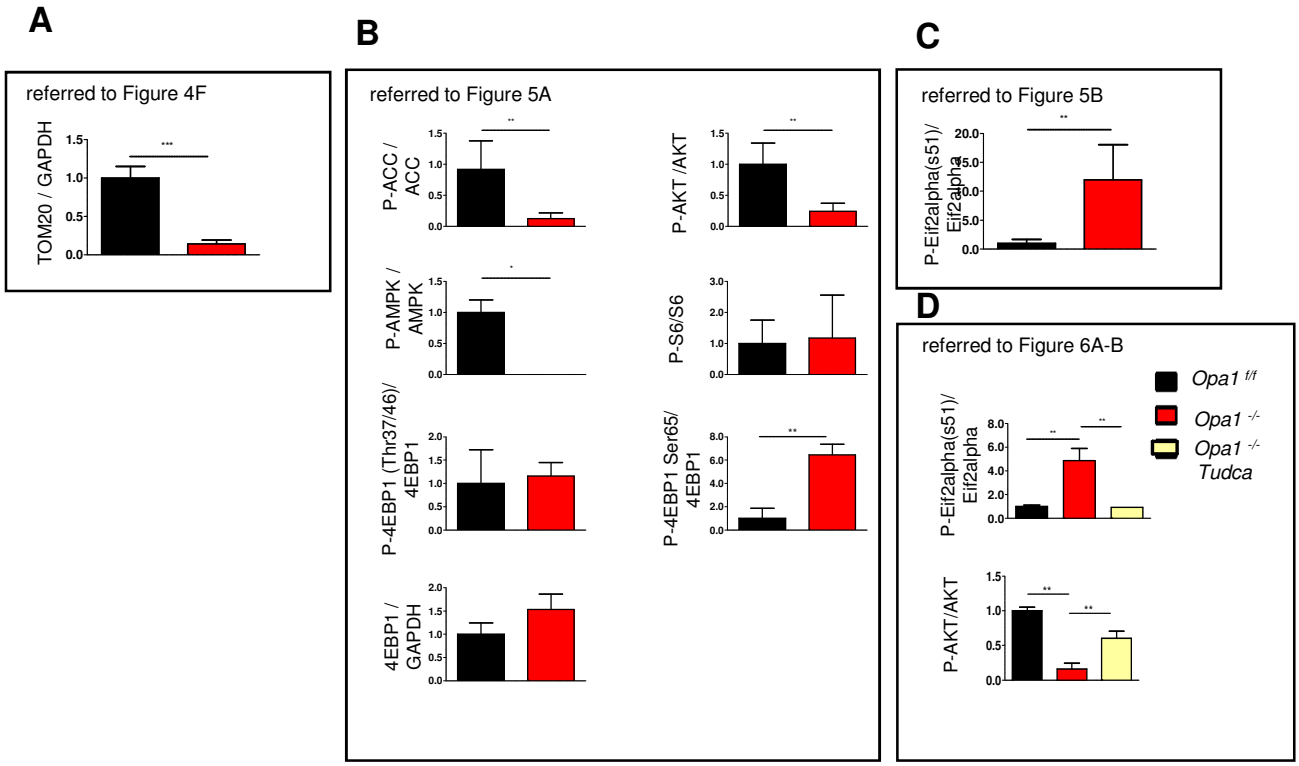

Figure S5 - Densitometric quantification of the western blots related to Figure 4, Figure 5 and Figure 6

Fig. S6

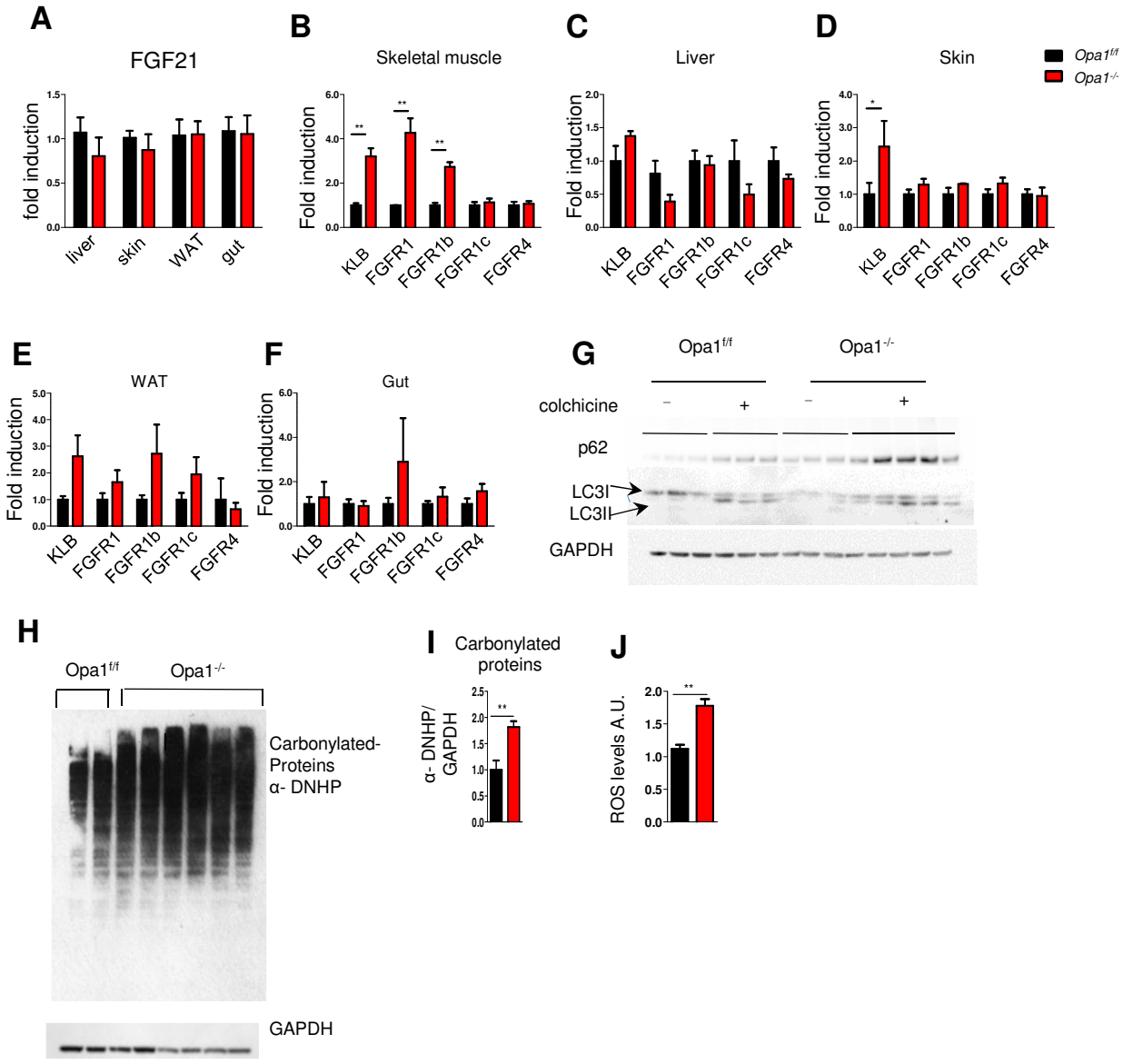
A
FGF21
fold induction
liver
skin
WAT
gut
B
Skeletal muscle
Fold induction
KLB
FGFR1
FGFR1b
FGFR1c
FGFR4
C
Liver
D
Skin
Opa1f/f
Opa1-/-
E
WAT
F
Gut
G
Opa1f/f
Opa1-/-
colchicine
p62
LC3I
LC3II
GAPDH
H
Carbonylated-
Proteins
α- DNHP
GAPDH
I
Carbonylated
proteins
α- DNHP/
GAPDH
J
ROS levels A.U.

Figure S6 - FGF21, Klotho, FGF Receptors, oxidative stress and autophagy flux in OPA1 knockout mice - Related to Figure 5

A) qRT-PCR revealed no changes in FGF21 expression levels in the different tissues analyzed **B-F)** qRT-PCR for different FGF receptors isoforms and KBL in skeletal muscle, liver, skin, WAT and gut (n=6 per each condition per tissue) **G)** Autophagy flux is increased in basal condition in OPA1-deficient muscles. Inhibition of autophagosome–lysosome fusion by colchicine treatment induces more accumulation of p62 and LC3II band in OPA1-null muscles (n=10 per each condition) **H)** Representative oxyblot of *Opa1$^{f/f}$* and *Opa1$^{-/-}$* samples and **I)** its relative quantification **J)** Mitochondrial oxidative stress analysis, measured with Mt-roGFP1sensor.Statistical significance:*p≤ 0,05 and **p≤ 0,01 (n =20 fibers per each condition)

Fig. S7

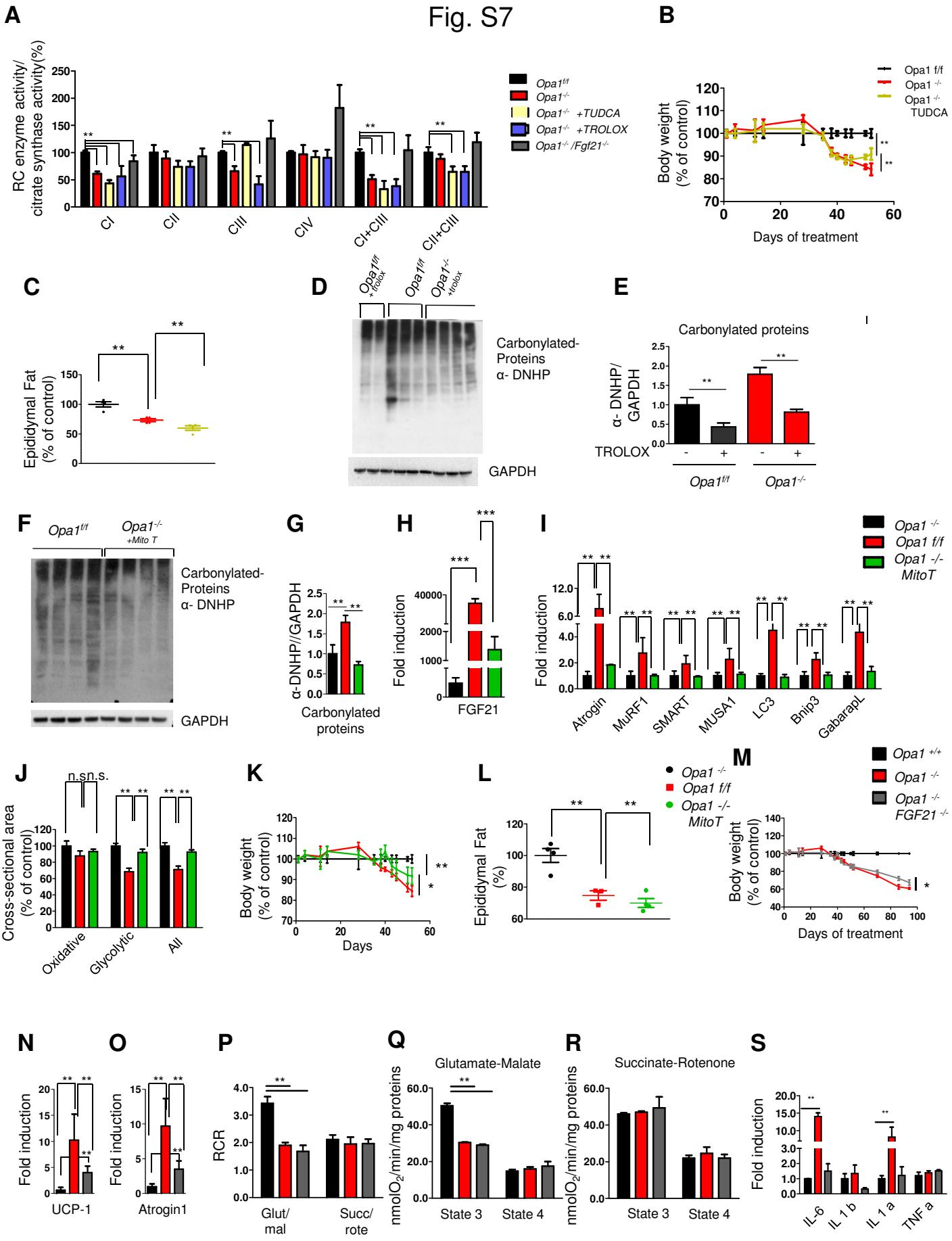
A
RC enzyme activity/ citrate synthase activity(%)
CI
CII
CIII
CIV
CI+CIII
CII+CIII
Opa1f/f
Opa1-/-
Opa1-/- +TUDCA
Opa1-/- +TROLOX
Opa1-/- /Fgf21-/-
B
Body weight (% of control)
Days of treatment
Opa1 f/f
Opa1 -/-
Opa1 -/- TUDCA
C
Epididymal Fat (% of control)
D
Carbonylated-Proteins α- DNHP
GAPDH
E
Carbonylated proteins
α- DNHP/ GAPDH
TROLOX
F
Carbonylated-Proteins α- DNHP
GAPDH
G
α-DNHP//GAPDH
Carbonylated proteins
H
Fold induction
FGF21
I
Fold induction
Atrogin
MuRF1
SMART
MUSA1
LC3
Bnip3
GabarapL
Opa1 -/-
Opa1 f/f
Opa1 -/- MitoT
J
n.s.
Cross-sectional area (% of control)
Oxidative
Glycolytic
All
K
Body weight (% of control)
Days
L
Epididymal Fat (%)
M
Opa1 +/+
Opa1 -/-
Opa1 -/- FGF21 -/-
Body weight (% of control)
Days of treatment
N
Fold induction
UCP-1
O
Fold induction
Atrogin1
P
RCR
Glut/ mal
Succ/ rote
Q
Glutamate-Malate
nmolO2/min/mg proteins
State 3
State 4
R
Succinate-Rotenone
nmolO2/min/mg proteins
State 3
State 4
S
Fold induction
IL-6
IL 1b
IL 1a
TNF a

Figure S7 - Trolox, MitoTempo, TUDCA treatments and acute deletion of FGF21 ameliorate the phenotype of OPA1-/- mice - Related to Figure 6 and to Figure 7

A) Respiratory Complex (RC) enzyme activity normalized for citrate synthase for *Opa1$^{f/f}$*, *Opa1$^{-/-}$*, *Opa1$^{-/-}$*+TUDCA, *Opa1$^{-/-}$*+TROLOX, *Opa1$^{-/-}$/Fgf21$^{-/-}$* **B)** Growth curve of control and *Opa1$^{-/-}$* mice treated or not with the chemical chaperone TUDCA after tamoxifen treatment; (*Opa1$^{f/f}$* n=20, *Opa1$^{-/-}$*+ vehicle n=19, *Opa1$^{-/-}$*+ TUDCA n= 8) **C)** Epididymal fat content measurement (n=4) **D)** Representative oxyblot for TROLOX treatment and **E)** its quantification. Data are mean ± SEM of n= 6 for each condition **F)** Oxyblot of *Opa1$^{f/f}$* and *Opa1$^{-/-}$*+ mito-TEMPO and **G)** its relative quantification **H)** Fgf21 transcriptional levels are reduced in OPA-null mice treated with mito-TEMPO **I)** qRT-PCR of FoxO- target genes. Data are mean ± SEM of three independent experiments **J)** Quantification of cross-sectional area of myofibers from controls, OPA1-knockout and OPA1-deficient mice treated with mito-TEMPO. Values are mean ± SEM from at least 6 muscles in each group K) Growth curve after tamoxifen treatment of control, OPA1$^{-/-}$ and OPA1-null mice treated with mito-TEMPO. Data are mean ± SEM (*Opa1$^{f/f}$* n=20, *Opa1$^{-/-}$*n=19 and *Opa1$^{-/-}$*+ mito-TEMPO n=9) **L)** WAT loss is not prevented by mito-TEMPO treatment **M)** Partial protection from body weight loss in *Opa1$^{-/-}$/Fgf21$^{-/-}$* double knockout mice; (*Opa1$^{f/f}$* n=20, *Opa1$^{-/-}$*n=19 and *Opa1$^{-/-}$/Fgf21$^{-/-}$* n=10) **N)** qRT-PCR of UCP-1 expression in WAT of *Opa1$^{f/f}$*,*Opa1$^{-/-}$* and *Opa1$^{-/-}$ /Fgf21$^{-/-}$* is shown. Data are mean ± SEM of three independent experiments **O)** Atrogin1 transcriptional levels in skeletal muscles of *Opa1$^{f/f}$*,*Opa1$^{-/-}$* and *Opa1$^{-/-}$ /Fgf21$^{-/-}$* is shown. Data are mean ± SEM of three independent experiments **P)** Respiratory control ratio of muscle isolated mitochondria energized with 5mM/2,5mM GLU/MAL or 10mM SUCC. Data represent mean ± SEM of three independent experiments (n=5) **Q-R)** State III and IV of muscle isolated mitochondria energized 5mM/2,5mM GLU/MAL or 10mM SUCC Data represent mean ± SEM of three independent experiments (n=5). **S)** Transcriptional levels of the inflammatory cytokines IL6, IL1a, IL1b and TNFa in skeletal muscle. Statistical significance:*p≤ 0,05 and **p≤ 0,01 n.s.: not significant CI: Complex I; CII: Complex II; CIII: Complex III; CIV: Complex IV; CI+CIII: Complex I plus Complex III; CII+CIII: Complex II plus Complex III

Supplemental tables

Table. S1. Related to Human subjects Fig 1 and S1

		Biopsy number	Age (y)	Weight (kg)	Height (cm)	BMI	TUGT (s)	Maximal isometric torque (Nm/kg)	Weekly training (h)	VAS	WOMAC
	YOUNG	1	27,76944	77	176	24,85795	3,7	4,10	7	0	1,00
		2	23,24167	81	177	25,85464	4,1	2,95	7,5	0	1,00
		3	34,21667	66	172	22,30936	3,95	3,36	5	0	1,00
		4	25,13333	75	169	26,25958	4	2,93	6	0	1,00
		5	26,25278	70,1	179	21,87822	4,1	2,69	3,375	0	1,00
SENIORS	Sedentary	6	67,63288	80	172	27,04164	7,8	1,74	0	0	n/a
		7	69,45205	72	171	24,62296	6,9	1,67	0	2,1	n/a
		8	70,32877	96	190,5	26,45339	8,53	2,24	0	0	1,07
		9	70,60548	95	185	27,75749	5,3	2,01	0	4	3,46
		10	77,70685	118,3	182	35,71429	9,46	1,46	0	0,5	1,96
		11	66,92877	93,5	181	28,54003	4,68	1,70	0	0	2,29
		12	81,89041	89,6	186	25,89895	9,32	1,13	0	0,85	n/a
		13	67,12295	85	181	25,94548	5,9	2,14	0	2,7	3,04
		14	63,39617	83,6	174	27,61263	7,3	1,14	0	5,7	2,88
		15	68,94536	71	182	21,43461	6	1,69	0	3,7	2,96
		16	64,59563	85	187	24,30724	5,9	1,34	0	7,9	3,58
		17	74,88525	68	160	26,5625	6,7	1,03	0	8,2	5,25
		18	79,39071	72,2	162	27,51105	12	0,87	0	8,4	4,50
		19	53,21311	75	150	33,33333	15,4	1,01	0	8,4	7,08
		20	65,46175	72	168	25,5102	9	0,90	0	7,1	4,83
		21	67,87705	98	176	31,6374	14,3	0,68	0	8,5	6,17
		22	62	116	171	39,7	6,7	0,66	0	8,5	6,16
		23	75,9153	88	170	30,44983	9,1	0,85	0	8,3	5,63
		24	78,7623	65	150	28,88889	12,2	0,78	0	7,2	3,88
	Sportmen	25	69,2	73,6	176,0	23,8	4	2,49	16	2,1	2,46
		26	72,3	92,0	180,0	28,4	5	2,18	10	0	1,00
		27	67,0	76,0	174,0	25,1	4,1	2,33	7	0,9	1,21
		28	69,5	81,6	169,5	28,4	5,4	1,98	4,5	0	1,00
		29	66,0	99,0	184,0	29,2	4,34	2,17	9	0	1,00

Table. S2. Related to Human subjects Fig 1 and S1

Criteria	YOUNG	SENIORS	
	n=5	Sedentary n=19	Sportsmen n=5
AGE (y)	27,32 ± 4,19	69,8±7,04 *	68,80±2,42 *
WEIGHT (kg)	73,82 ± 5,87	85,4±15,04	84,4±10,79
HEIGHT (cm)	174,6 ±4,04	173,6±11,78	176,70±5,56
BMI (kg/m2)	24,23±2,02	28,2±4,29	27±2,39
TUGT (s)	4±0,16	8,65±3,02 *	4,6±0,60 #
Maximal isometric torque Nm/kg	3,21±0,56	1,30±0,50 *	2,20±0,19 *, #
Weekly training (h)	5,80±1,65	0 *	9,3±4,29 #
VAS	0	4,85±3,45 *	0,6±0,92 #
WOMAC	1	4,04±1,70 *	1,3±0,63 #

Table. S3. **qPCR primer sequences.** Related to **STAR Methods**

	Forward	Reverse
hOPA1	GGCTCCTGACACAAAGGAAA	TCCTTCCATGAGGGTCCATT
hMFN1	ATATGGAAGACGTACGCAGAC	CCCCTGTGCTTTTTGCTTTC
hMFN2	TTGTCATCAGCTACACTGGC	AACCGGCTTTATTCCTGAGC
hDRP1	GGCGCTAATTCCTGTCATAA	CAGGCTTTCTAGCACTGAGC
hGAPDH	TGCACCACCAACTGCTTAGC	GGCATGGACTGTGGTCATGAG
mOPA1ex2-3	ATACTGGGATCTGCTGTTGG	AAGTCAGGCACAATCCACTT
mDRP1	TCAGATCGTCGTAGTGGGAA	TCTTCTGGTGAAACGTGGAC
mPGC1a	GGAATGCACCGTAAATCTGC	TTCTCAAGAGCAGCGAAAGC
mFGF21	ATGGAATGGATGAGATCTAGAGTTGG	AAGTATGTGCGAGGGCTGT
mATF4	TCCTGAACAGCGAAGTGTTG	ACCCATGAGGTTTCAAGTGC
mCHOP	GCTGGAAGCCTGGTATGAG	ATGTGCGTGTGACCTCTGTT
mGADD34	AGAGAAGACCAAGGGACGTG	CAGCAAGGAATGGACTGTG
mAtrogin-1	GCAAACACTGCCACATTCTCTC	CTTGAGGGGAAAGTGAGACG
mBnip3	TTCCACTAGCACCTTCTGATGA	GAACACCGCATTTACAGAACAA
mCathepsinL	GTGGACTGTTCTCACGCTCAAG	TCCGTCCTTCGCTTCATAGG
SMART (mFbxO21)	TCAATAACCTCAAGGCGTTC	GTTTTGCACACAAGCTCCA
mFbxO31	GTATGGCGTTTGTGAGAACC	AGCCCCAAAATGTGTCTGTA
mGabarapL	CATCGTGGAGAAGGCTCCTA	ATACAGCTGGCCCATGGTAG
mGadd34	AGAGAAGACCAAGGGACGTG	CAGCAAGGAATGGACTGTG
mGAPDH	CACCATCTTCCAGGAGCGAG	CCTTCTCCATGGTGGTGAAGAC
mItch	CCACCCACCCCACGAAGACC	CTAGGGCCCGAGCCTCCAGA
mLC3b	CACTGCTCTGTCTTGTGTAGGTTG	TCGTTGTGCCTTTATTAGTGCATC
MUSA1 (mFbxO30)	TCGTGGAATGGTAATCTTGC	CCTCCCGTTTCTCTATCACG
mMuRF-1	ACCTGCTGGTGGAAAACATC	ACCTGCTGGTGGAAAACATC
mp62	CCCAGTGTCTTGGCATTCTT	AGGGAAAGCAGAGGAAGCTC
mCOXII	GCCGACTAAATCAAGCAACA	CAATGGGCATAAAGCTATGG
m18S	CATTCGAACGTCTGCCCTATCA	GGGTCGGGAGTGGGTAATTTG
mXBP1 splic	AAGAACACGCTTGGGAATGG	ACTCCCCTTGGCCTCCAC
mKlb	: ACACTGTGGGACACAACCTG	AGAGCCAACCCTTCTGATGA
mFgfr1b	GAGTAAGATCGGGCCAGACA	TCACATTGAACAGGGTCAGC
mFgfr1c	GACTCTGGCCTCTACGCTTG	TCGTCGTCGTCATCATCTTC
mFgfr1	ACCAAGAAGAGCGACTTCCA	AACCAGGAGAACCCCAGAGT
mFgfr4	ACTCCATCGGCCTTTCCTAC	TGTTGTCCACGTGAGGTCTT
mUCP-1	ACTGCCACACCTCCAGTCATT	CTTTGCCTCACTCAGGATTGG

4. II PART: UNPUBLISHED DATA

From our publication of 2017 (Tezze et al., 2017) is evident that FGF21 has a key role in the pathological process of Opa1$^{-/-}$ (Tezze et al., 2019) but from the comparison with the other mitochondrial models in our laboratory, it is clear that FGF21 *per se* cannot be the only responsible of all the detrimental features that we observed. Recently, we published two papers in which we studied the consequences of both, a block of fission (Favaro et al., 2019), and a concomitant block of fusion and fission in skeletal muscle (Romanello et al., 2019). Despite mitochondrial dysfunction, alteration in mitochondrial morphology and FGF21 induction, these models, like in Opa1 deleted mice, do not display precocious aging and mortality. Since only the Opa1 model has systemic inflammation, and from our data, this signaling rises from the skeletal muscle compartment, in the unpublished part of this thesis I focus my attention on whether an unopposed mitochondrial fragmentation is connected with innate immunity response, altered metabolism, and premature aging.

5. RESULTS

5.1. Opa1 deletion in skeletal muscle induces the expression of the pro-inflammatory cytokine IL6

Opa1-deleted mice in skeletal muscles showed an increase of circulating pro-inflammatory cytokines when they already display a prematurely aged phenotype at T3 (120days after tamoxifen treatment; see methods "experimental time-line") (Figure 3F in (Tezze et al., 2017a)). Muscle tissue at this time-point display induction of IL-6 and Il-1a, but not of TNF alpha and IL-1b (Figure. S4A in (Tezze et al., 2017a)). Importantly, the deletion of FGF21 in OPA1-null mice reverted the inflammation in both, skeletal muscle, and blood and prolonged lifespan compared to Opa1 ko (Figure 7 and S7s in (Tezze et al., 2017a)). However, it is not clear which are the sources, the kinetics and the role of the different induced cytokines in the Opa1-null phenotype. Macrophages mainly produce the cytokines upon their activation inside the tissues (Arango Duque and Descoteaux, 2014). Thus, to find out the sources of cytokines secretion we initially analyzed their transcript levels in liver and skeletal muscle at the different time points, 30 days (T1-before atrophy), 50 days (T2-during atrophy) and 120 days (T3-premature aging) (see a specific section in methods "experimental time-line). The liver appears to be the source of TNFα and IL1b when mice are already aged (Figure. 5.1 a). However IL6 is produced by the skeletal muscle at T1, T2, and T3 (Figure 5.1 b,c) and it is the only cytokines elevated in the blood before the prematurely aged phenotype (Figure. 5.1 a,b). IL6 is a multifaceted, pleiotropic cytokine that is a central player in the regulation of inflammation, hematopoiesis, immune responses, and host defense mechanisms. Commonly, white adipose tissue (WAT), skeletal muscle, liver, bone marrow, and spleen can secrete IL6 under various conditions (Chen et al., 2013; Makki et al., 2013). IL6 has been considered an adipokine because one-third of circulating IL6 in healthy individuals is estimated to originate from the adipose tissue, (Makki et al., 2013). Indeed, IL6 expression correlates with increased body mass, waist circumference, and free fatty acid levels (Makki et

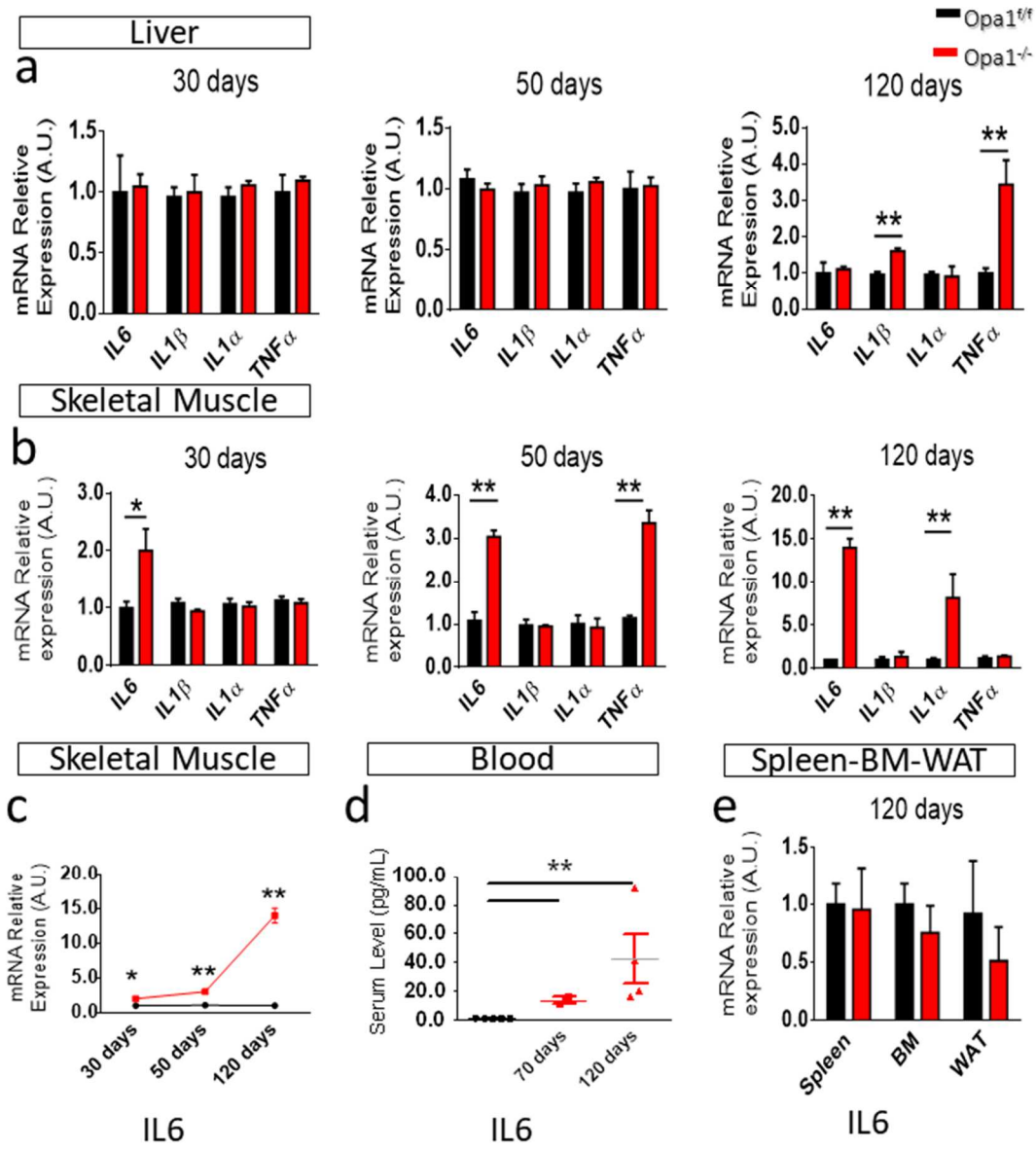

Figure 5.1. Opa1 deletion in skeletal muscle induced the expression of the pro-inflammatory cytokine IL6 a)Quantitative PCR analysis of pro-inflammatory cytokines (IL6, IL1b, IL1a, TNF transcripts from liver b) skeletal muscle; c) Quantitative PCR analysis of IL6 transcripts from and e) spleen, bone marrow (BM), and white adipose tissue (WAT) (n=10) d) Increased IL6 plasma levels in OPA1-null mice were determined by ELISA (n=4).*p≤0.05 **p≤ 0.01

al., 2013). Thus, we investigated the IL6 expression in the white adipose tissue of Opa1$^{-/-}$ but it was unchanged (Figure. 5.1 e).

Spleen and bone marrow, normally involved in the inflammatory response, are not contributing to the IL6 induction as well (Figure. 5.1e). However, the macrophages are not infiltrating the skeletal muscle of Opa1 ko (Tezze et al.,

2017a). For this reason, the central core of this second part of my Ph.D. thesis is to investigate whether the source of IL6 is skeletal muscle cells.

5.2. Opa1 deletion in adult skeletal muscle induces a low chronic grade of systemic inflammation

The natural aging process is associated with a chronic inflammatory phenotype characterized by a systemic induction of proinflammatory cytokines such as IL6. This condition is associated with a chronic inflammatory phenotype characterized by anemia, and hematopoietic stem cells fate (HSC) alteration mainly related to IL6 activity (Pietras, 2017). IL6 and more in general inflammation, are considered key regulators of hematopoietic stem cell fate in health and disease, leading to a chronic overproduction of myeloid cells and, often accompanied by loss of lymphoid output (Pietras, 2017).

In collaboration with Prof Antonella Viola's lab, we checked the hematopoietic stem cell fate in Opa1 ko mice in T3 (premature aging time point). Cytometric analysis of the progenitors, and the myeloid and committed lymphoid cells in the bone marrow niche revealed that the precursors were not altered. Instead, both, myeloid and lymphoid populations were reduced compared to the wild type mice (Figure. 5.2 a). At the same time, in Opa1 ko, there is the accumulation of granulocytes (committed myeloid cells) as well the reduction of lymphocyte (committed lymphoid cells) in the blood (Figure. 5.2 b), and this is compatible with an unbalanced commitment during IL6 stimulation.

From the literature, IL6 is also known to promote anemia, which is related to the induction of hepcidin. This gene when it is increased causes iron deficiency (Wrighting and Andrews, 2006). In the liver of $Opa1^{-/-}$ mice, the transcript of hepcidin is 4 times more induced than in controls (Figure. 5.2 c).

All these data could support the muscle-dependent role of IL6 into the systemic Opa1 ko phenotype. Considering these data we wanted to understand which is the molecular mechanism that links mitochondrial dysfunction to an increase in il6 transcription in skeletal muscle.

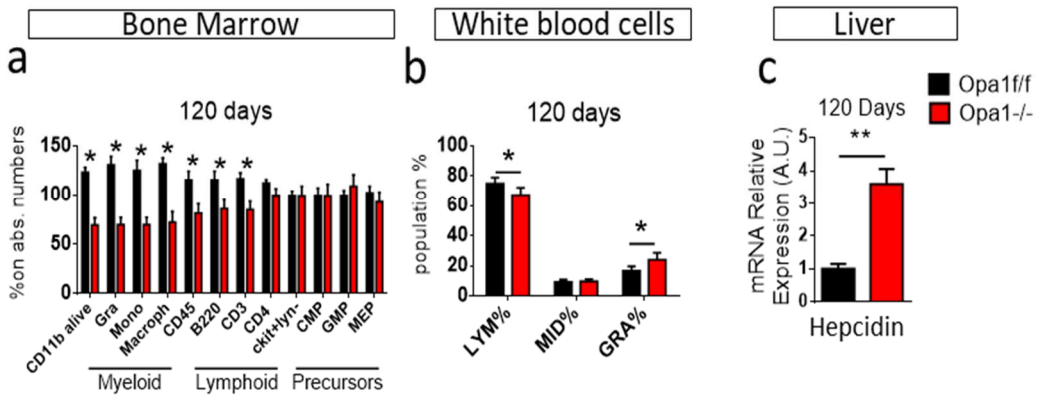

Figure 5.2. System effect of IL6 a) cytometric analysis of bone marrow b) emocrome c) Quantitative PCR analysis of hepcidin transcript from liver (n=4).*p≤0.05 **p≤ 0.01

5.3. Fgf21 triggers IL6 induction via mitophagy

In contrast to muscle-specific Opa1 deletion, the simultaneous ablation of Opa1 and Fgf21 in the adult skeletal muscle reverts the induction of IL6 into the tissue or in the circulation in any time-point (Tezze et al., 2017a). Recently, Fgf21 was reported to control mitophagy in skeletal muscle (Oost et al., 2019). In agreement to a massive Fgf21induction, we found: a) an increase in the autophagic flux in the basal condition in OPA1-deficient muscles, b) a decrease in mitochondrial mass and mtDNA, and c) an exacerbation of mitochondrial fragmentation. All these changes are not present in the double ko Opa1-Fgf21 (Tezze et al., 2017a). Moreover, Drp1 ko mice and Drp1-Opa1 double ko have a block in the autophagy flux, and they do not display IL6 induction (Favaro et al., 2019; Romanello et al., 2019). To explore whether inhibition of mitophagy can be related to IL6 induction in skeletal muscle, we transfected FDB (Flexor digitorum brevis) muscle at T2 with shAtg8, short hairpin for Atg8 (LC3). This plasmid, previously generated and tested in our lab, can promote the knock-down of LC3, an essential gene in autophagosome formation. We decided to perform the experiment of silencing at this time-point because the autophagic flux is increased, IL6 transcript is in the phase of massive induction, and mice are not yet compromised. After 15 days of transfection (at day 65), LC3 downregulation was efficient (Figure 5.3 a), and importantly IL6 induction was

blunted (Figure. 5.3 b). This data suggests a role for mitophagy in IL6 induction in skeletal muscle.

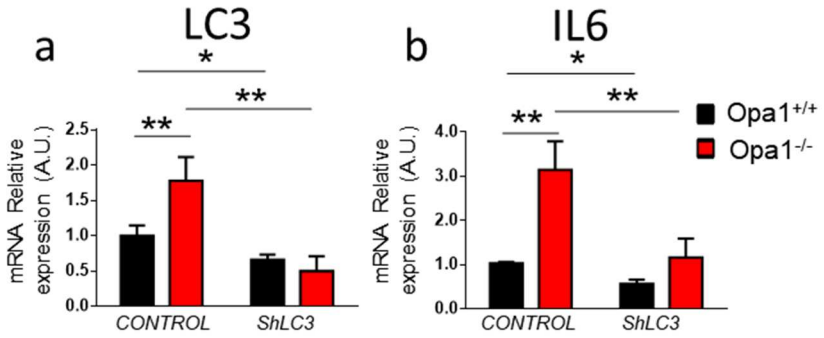

Figure 5.3. Mitophagy triggers IL6 induction a) Quantitative PCR analysis of LC3 IN shLC3 in controls muscles and in shLC3 transfected muscles b) Quantitative PCR analysis of pro-inflammatory cytokine IL6 in controls and in shLC3 b) skeletal muscle;

5.4. TLR9 contributes to IL6 induction

From lysosomal myopathies is emerging that an excessive build-up in autophagosomes is difficult to handle for the cells (Malicdan et al., 2008). Additionally, the failure of autophagic digestion of mitochondrial components such as mtDNA (mitochondrial DNA) can lead to their cytosolic leakage and cause inflammation (Nakai et al., 2007). The mtDNA, an unmethylated dsDNA species of bacterial origin, when it is not correctly recycled has highly immunogenic properties (Caielli et al., 2016; Oka et al., 2012) (Pisetsky, 2016; Zhang et al., 2010). Autophagy malfunction is correlated with undegraded mtDNA, which is then recognized by TLR9 resulting in inflammation (Nakahira et al., 2011). Under basal conditions, TLR9 is localized in the endoplasmic reticulum (ER), and upon different stimulation, it translocates to the membrane of lysosomes where it binds to ligands and initiates cellular inflammation (Latz et al., 2004). TLR9 transcript is upregulated at day 65 in Opa1 ko and it is downregulated upon LC3 silencing (Figure. 5.4 a). To evaluate if TLR9 is involved in IL6 signaling, we transfected FDB at T2 with either shTLR9 and scramble in wt and ko mice. Upon TLR9 knock-down, we found a reduction in IL6 transcript compared to Opa1$^{-/-}$ scramble (Figure 5.4.b-c).

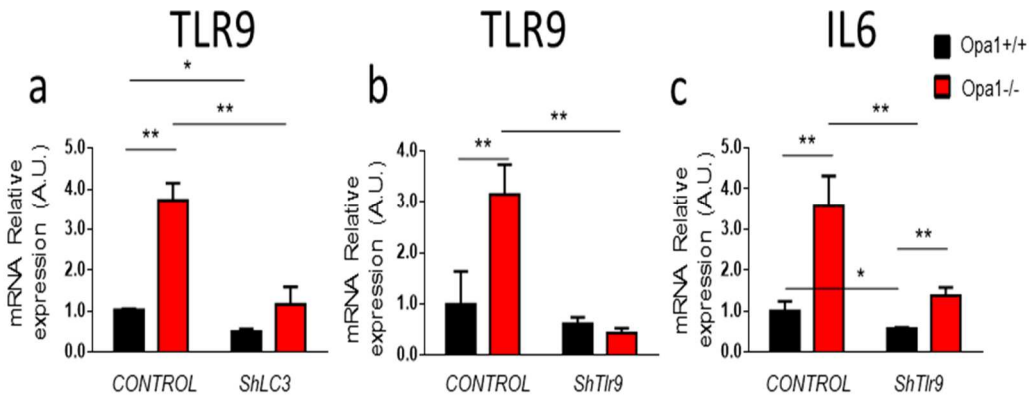

Figure 5.4. TLR9 contributes to IL6 induction a) Quantitative PCR analysis of TLR9 in shLC3 in controls muscles and in shLC3 transfected muscles b) Quantitative PCR analysis of TLR9 in controls and in shTLR9 transfected muscles c) Quantitative PCR analysis of pro-inflammatory cytokine IL6 in controls and in shTLR9 skeletal

5.5. NF-KB modulates IL6 expression

Interaction of TLR9 with mtDNA activates the nuclear factor kappa B (NF-kB) signaling and increases the expression of other pro-inflammatory cytokines such as tumor necrosis factor-a (TNFα), and interleukin IL6 (Julian et al, 2013; Yu & Bennett, 2014; Zhang et al, 2014). Opa1 ko mice display induction of TNFα at 50 days and of IL6 between 30 to 120 days (Figure 5.1 b-c).

Moreover, with the group of Prof. Antonio Zorzano, we published a paper in which, in a different model of Opa1 deletion in skeletal muscle, it was confirmed that there is a connection between Opa1 deficiency, muscle inflammation, and infiltration (Rodríguez-Nuevo et al., 2018). This mouse model was obtained by crossing homozygous Opa1-loxP/loxP mice with a mouse strain expressing Cre recombinase under the control of the myogenin promoter. So the deletion occurs during myogenesis when mice are not already adult. In that constitutive model, there is a massive local infiltration of macrophages that can promote myopathy in mice. They demonstrated that is characterized by enhanced expression of NF-KB target genes, and increased circulating levels of pro-inflammatory cytokines. In our tamoxifen-inducible Opa1 ablation animal

model, the expression of some NF-kB target genes such as NLRP3 and ASC was induced as well at T2, and early under conditions in which muscle mass was normal (Rodríguez-Nuevo et al., 2018, p. 9). To address NF-kB roles in IL6

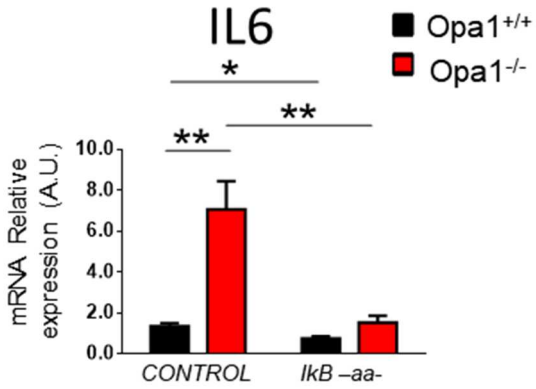

Figure 5.5. NF-kB modulates IL6 expressione Quantitative PCR analysis of pro-inflammatory cytokine IL6 in controls and in IkB superepressor overexpression skeletal muscle; (n=5) *p≤ 0.05 **p≤ 0.01

induction in adult skeletal muscle, we overexpress the constitutively active form of IkB, in which the serin32 and the serin36 were substituted by alanine, in this way NF-kb is sequestered in the cytosol and cannot activate the transcription into the nucleus. Upon NF-kB blocking, IL6 was normalized (Figure. 5.5). Opa1 deficiency causes muscle inflammation, that occurs without macrophage infiltration, which is mediated via activation of NF-KB.

5.6. Mitochondrial ROS activates IL6 transcription in Opa1$^{-/-}$

The transcription factor NF-kappaB plays a critical role in coordinating innate and adaptative immunity, cellular proliferation, apoptosis, and development. Since the discovery in 1991 that NF-kappaB may be activated by $H_{(2)}O_{(2)}$, several laboratories have put a considerable effort into dissecting the molecular mechanisms underlying this activation(Gloire et al., 2006). Oxidative stress is increased in OPA1-null mice mitochondria and treatments with antioxidants ameliorate the muscular and metabolic phenotype (Tezze et al., 2017a).

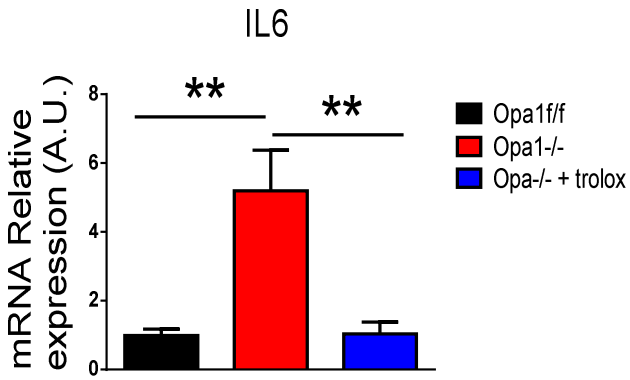

Figure 5.6. Mitochondrial ROS activate IL6 transcription in Opa1-/- Quantitative PCR analysis of pro-inflammatory cytokine IL6 in skeletal muscle of mice treated with Trolox; (n=5) **p≤ 0.01

Thus, we monitored IL6 expression upon *in-vivo* administration of antioxidants. 15 days of Trolox treatment reduced IL6 transcript in skeletal muscle (Figure. 5.6).

5.7. NF-KB treatment in vivo reduces IL6 and ameliorates Opa1 phenotype

To determine if NF-kB has a central role in the controls of IL6 induction *in vivo*, we administer to the mice medical food containing a patented molecule that is able to reduce NFKB activation. We started to treat animals when they are already atrophic T2, and after 3 weeks, we stopped the administration (T70). In this period, in not treated mice the increased of IL6 in skeletal muscle is progressively higher and, the phenotype worsens very quickly. Upon *in vivo* treatment, IL6 is not induced, in skeletal muscle, and not secreted (Figure. 5.7 a-b). Interestingly, before the sacrifice, we measured the physical capacity of these mice. Opa1 ko mice at this time point usually are exercise intolerant. However, after food administration, they were able to run longer (Figure 5.8 a). Usually, muscle-specific Opa1-deleted mice ran only 5 minutes. With NF-kB inhibition, they reached 80 minutes of "walking". Importantly, after NF-kB inhibition IL1β level in the liver is like in the controls, and FGF21 transcript is unchanged.

Altogether our data might support a central role in the promotion of inflammation for the skeletal muscle tissue in Opa1$^{-/-}$.

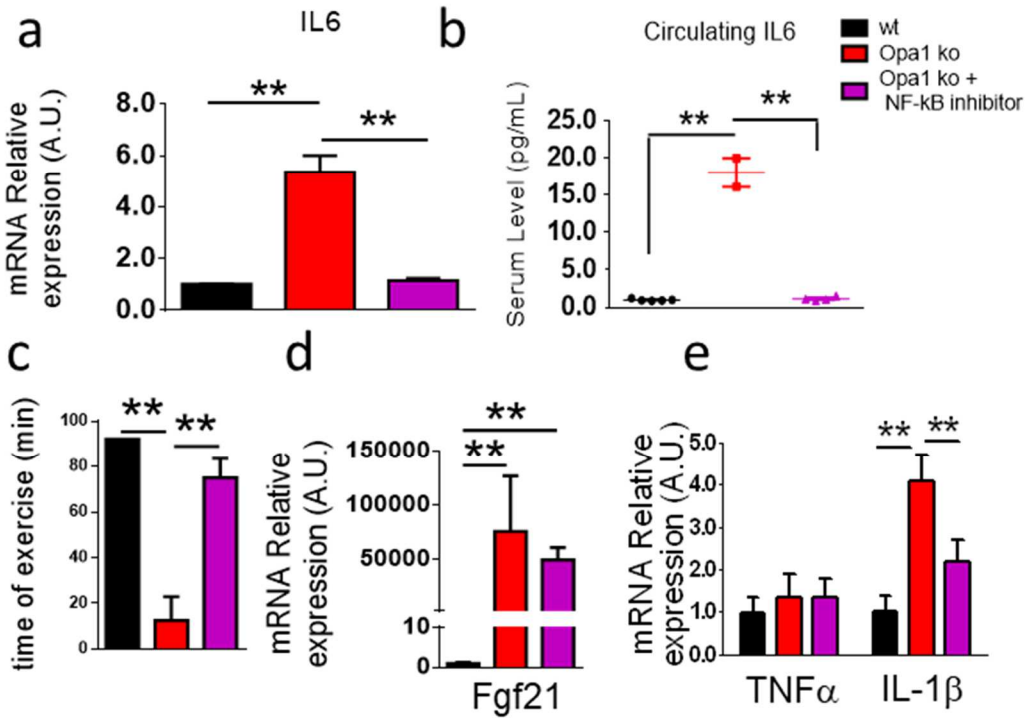

Figure 5.7. NF-KB treatment in vivo reduces IL6 and ameliorates Opa1 phenotype

a) Quantitative PCR analysis of pro-inflammatory cytokine IL6 in skeletal muscle of mice treated with NF-kB inhibitor; b) IL6 levels in serum upon NF-kB inhibition; c) time of running upon NF-kB inhibition; d) Quantitative PCR analysis of Fgf21 in skeletal muscle of mice treated with NF-kB inhibitor; e) Quantitative PCR analysis of pro-inflammatory

6. DISCUSSION

In the first part of this thesis, we have identified how OPA1 in muscles triggers a cascade of signaling that affects general metabolism and aging. We found that a functional mitochondrial network is critical for muscle-mass maintenance and healthy aging. The generation of inducible muscle-specific OPA1 and double Fgf21/Opa1 KO mice enabled us to dissect how altered mitochondrial dynamics in muscle affect the whole-body metabolism. Indeed, we have identified FGF21 as a critical link between dysfunctional mitochondria and systemic metabolic changes, organ function, and longevity.

At the moment, whether FGF21 is beneficial or detrimental is debated, primarily when related to humans (Chou et al., 2016). The FGF21 is a pleiotropic hormone that promotes a variety of physiopathological effects. Interestingly, high levels of serum FGF21 have been found in a child affected by progeria (Suomalainen et al., 2011), and circulating levels of FGF21 have been shown to increase with age in humans (Conte et al., 2018; Hanks et al., 2015). FGF21 is now recognized and used as a diagnostic marker in patients with mitochondrial myopathy (Lehtonen et al., 2016) who are no longer living.

The generation of inducible muscle-specific Drp1 (Favaro et al., 2019) and double Opa1/Drp1 ko (Romanello et al., 2019) mice, that have in common with Opa1 ko mice FGF21 induction but not the premature aging phenotype, could indicate that there are possible new synergistic candidates that can trigger the precocious senescence phenotype of OPA1 KO mice. The significant difference between Opa1 ko and the other models (Opa1/Fgf21 dko, Drp1 ko, and Opa1/Drp1 dko) is the inflammatory status. Indeed, only OPA1 ko mice display the release of pro-inflammatory cytokine into the circulation.

In the second part of this thesis, we focus our attention on the role of skeletal muscle in the promotion of inflammaging. We found that when Opa1 ko mice already display an aged phenotype, they also showed a systemic low grade of inflammation. Importantly, only the pro-inflammatory cytokines IL6 was upregulated over time in the skeletal muscle tissue and systemically. The IL6 cytokine is known to be released by either the muscle compartment (myofibers and/or satellite cells) and/or by infiltrating inflammatory cells, and its function

inside the muscle tissue is almost unknown. Potentially, it triggers and control the distinct actions of satellite cells throughout the myogenic process and during exercise, both in mice and humans. However, a clear demonstration on the source and the signaling pathways that define IL6 induction in adult skeletal muscle is still missing, and possible systemic effects of muscular IL6 are still unknown.

The natural aging process is associated with a chronic inflammatory phenotype characterized by a systemic overabundance of proinflammatory cytokines, such as IL6. This condition is associated with a chronic inflammatory phenotype so by anemia, and HSC (hematopoietic stem cells fate) alteration mainly related to IL6 activity (Pietras, 2017). IL6 and more in general inflammation, are considered key regulators of hematopoietic stem cell fate in health and disease, induced a chronic overproduction of myeloid cells and, often accompanied by loss of lymphoid output (Pietras, 2017). In our mice, hematopoietic stem cells fate is altered upon IL6 stimulation. Moreover, hepcidin transcript, a gene involved in anemia, is induced in the liver of Opa1 ko, and this is a typical

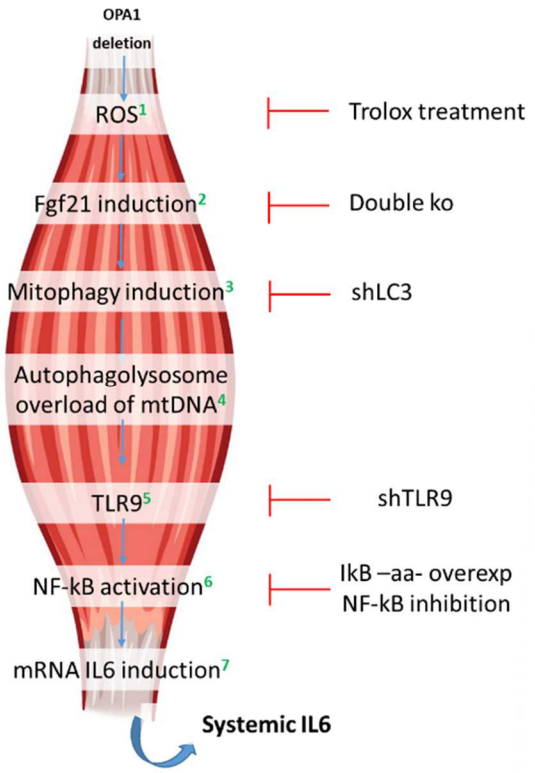

Figure 6. Signaling pathways of IL6 induction in skeletal muscle of OPA1 ko mice

response to IL6 signaling in this tissue. Our data could suggest the capacity of the muscle to control IL6 transcript but also to promote a current release of this cytokine to induce a systemic response. Thus, we aimed to identify the signaling pathways that could promote IL6 induction in OPA1 ko muscles (Figure 6).

Since Opa1 deletion in muscles leads to ROS production (Tezze et al.), we first, performed an in vivo treatment with a specific antioxidant (Figure 6 [1]), the analog of vitamin E which was sufficient to normalize IL6 expression (Figure 6 [7]) in skeletal muscle of OPA1 ko. This underlines an involvement for the ROS in the pathway that leads to the IL6 induction.

Importantly, we already published that excess of mitochondrial fragmentation present in OPA1 ko caused an increase in ROS formation. This is sufficient to induce mitochondrial stress and to cause Fgf21 induction. So next we focussed on the possible role for Fgf21in this pathway. Interesting, in the Opa1/Fgf21 ko IL6, is not induced anymore (Tezze et al., 2017a)(Figure 6[2]), suggesting its implication.

Recently, Fgf21 it has been demonstrated to controls mitophagy in skeletal muscle (Oost et al., 2019) and at the same time, we already published that in Opa1 ko mice we have an increased autophagic flux (Tezze et al., 2017b).

So we tried to find out the contribution of mitophagy in the pathways by silencing in vivo the Atg8 gene (LC3) and measuring the following normalization of IL6 transcript (Figure 6[3]). However, to confirm this result we will compare the mitophagy levels in vivo by using the pH-sensitive fluorescent reporter mt-Keima (Sun et al., 2017)in Opa1 ko and Opa1/Fgf21 ko.

The excess of autophagic flux that we measured in Opa1 ko and the strong reduction of mitochondrial mass that we observed in T2 (Tezze et al., 2017b) suggested an overload of autophagosomes (Figure 6[4]). Although, more experiments are needed. It could be useful to block the autophagic flux in vivo and inject, at the same time, the mice with EdU or BrD. These nucleosides analog to thymidine, are normally incorporated into DNA during active DNA synthesis (Lentz et al., 2010). The thymidine analogs specifically bind to mitochondrial DNA during its active DNA synthesis in non-dividing cells. Then, the co-localization by immunofluorescence can be monitored.

The innate immune system is the major contributor to acute inflammation induced by microbial infection (Takeuchi and Akira, 2010). TLR9, localized in the endolysosome senses DNA with unmethylated CpG motifs derived from bacteria and viruses. Mitochondrial DNA activates polymorphonuclear neutrophils through CpG/TLR9 interactions (Zhang et al., 2010). Under basal conditions, TLR9 is located in the endoplasmic reticulum (ER), and upon different stimulation, TLR9 translocates to the membrane of lysosomes, bind to ligands, and initiate cellular inflammation (Latz et al., 2004). We demonstrated that TLR9 is involved in IL6 induction by silencing TLR9 in vivo and looking at IL6 transcript reduction (Figure 6 [5]). We plan to perform a co-localization analysis of TLR9 and mtDNA and autophagosome to support our evidence. Interaction of TLR9 with mtDNA activates the nuclear factor kappa B (NF-kB) signaling and increases the expression of other pro-inflammatory cytokines such as tumor necrosis factor-alpha (TNFα), interleukin IL6 (Julian et al, 2013; Yu & Bennett, 2014; Zhang et al, 2014). Overexpression of NF-kB repressor, constitutively active, normalize IL6 expression as well (Figure 6 [6]). Moreover, we found out that upon NF-kB inhibition, locally and systemically, IL6 is normalized (Figure 6 [6]). Interestingly, upon pharmacological inhibition of NF-kB in mice, we normalize also IL6 circulating levels while the Fgf21 transcript is not modified. This result suggests that Fg2f1 could be upstream in the pathway of IL6 induction in skeletal muscle of Opa1 ko.

Finally, Opa1 ko upon NF-kB inhibition are less exercise intolerance. This last point is particularly interesting because IL6 could have a critical role in promoting sarcopenia, frailty, and reduced longevity altogether with FGF21.

7. BIBLIOGRAPHY

Alipoor, S.D., Mortaz, E., Garssen, J., Movassaghi, M., Mirsaeidi, M., Adcock, I.M., 2016. Exosomes and Exosomal miRNA in Respiratory Diseases. Mediators Inflamm. 2016, 5628404. https://doi.org/10.1155/2016/5628404

Amati-Bonneau, P., Valentino, M.L., Reynier, P., Gallardo, M.E., Bornstein, B., Boissière, A., Campos, Y., Rivera, H., de la Aleja, J.G., Carroccia, R., Iommarini, L., Labauge, P., Figarella-Branger, D., Marcorelles, P., Furby, A., Beauvais, K., Letournel, F., Liguori, R., La Morgia, C., Montagna, P., Liguori, M., Zanna, C., Rugolo, M., Cossarizza, A., Wissinger, B., Verny, C., Schwarzenbacher, R., Martín, M.A., Arenas, J., Ayuso, C., Garesse, R., Lenaers, G., Bonneau, D., Carelli, V., 2008. OPA1 mutations induce mitochondrial DNA instability and optic atrophy "plus" phenotypes. Brain 131, 338–351. https://doi.org/10.1093/brain/awm298

Balistreri, C.R., Candore, G., Accardi, G., Colonna-Romano, G., Lio, D., 2013. NF-κB pathway activators as potential ageing biomarkers: targets for new therapeutic strategies. Immun Ageing 10, 24. https://doi.org/10.1186/1742-4933-10-24

Belenguer, P., Pellegrini, L., 2013. The dynamin GTPase OPA1: more than mitochondria? Biochim. Biophys. Acta 1833, 176–183. https://doi.org/10.1016/j.bbamcr.2012.08.004

Bodine, S.C., Latres, E., Baumhueter, S., Lai, V.K., Nunez, L., Clarke, B.A., Poueymirou, W.T., Panaro, F.J., Na, E., Dharmarajan, K., Pan, Z.Q., Valenzuela, D.M., DeChiara, T.M., Stitt, T.N., Yancopoulos, G.D., Glass, D.J., 2001. Identification of ubiquitin ligases required for skeletal muscle atrophy. Science 294, 1704–1708. https://doi.org/10.1126/science.1065874

Bonaldo, P., Sandri, M., 2013. Cellular and molecular mechanisms of muscle atrophy. Dis Model Mech 6, 25–39. https://doi.org/10.1242/dmm.010389

Cai, D., Frantz, J.D., Tawa, N.E., Melendez, P.A., Oh, B.-C., Lidov, H.G.W., Hasselgren, P.-O., Frontera, W.R., Lee, J., Glass, D.J., Shoelson, S.E., 2004. IKKbeta/NF-kappaB activation causes severe muscle wasting in mice. Cell 119, 285–298. https://doi.org/10.1016/j.cell.2004.09.027

Chen, H., Vermulst, M., Wang, Y.E., Chomyn, A., Prolla, T.A., McCaffery, J.M., Chan, D.C., 2010. Mitochondrial fusion is required for mtDNA stability in

skeletal muscle and tolerance of mtDNA mutations. Cell 141, 280–289. https://doi.org/10.1016/j.cell.2010.02.026

Chen, Y.F., Wu, Z.M., Xie, C., Bai, S., Zhao, L.D., 2013. Expression Level of IL-6 Secreted by Bone Marrow Stromal Cells in Mice with Aplastic Anemia. ISRN Hematol 2013. https://doi.org/10.1155/2013/986219

Chou, R.-H., Huang, P.-H., Hsu, C.-Y., Chang, C.-C., Leu, H.-B., Huang, C.-C., Chen, J.-W., Lin, S.-J., 2016. Circulating Fibroblast Growth Factor 21 is Associated with Diastolic Dysfunction in Heart Failure Patients with Preserved Ejection Fraction. Sci Rep 6. https://doi.org/10.1038/srep33953

Cipolat, S., Martins de Brito, O., Dal Zilio, B., Scorrano, L., 2004. OPA1 requires mitofusin 1 to promote mitochondrial fusion. Proc. Natl. Acad. Sci. U.S.A. 101, 15927–15932. https://doi.org/10.1073/pnas.0407043101

Cogliati, S., Frezza, C., Soriano, M.E., Varanita, T., Quintana-Cabrera, R., Corrado, M., Cipolat, S., Costa, V., Casarin, A., Gomes, L.C., Perales-Clemente, E., Salviati, L., Fernandez-Silva, P., Enriquez, J.A., Scorrano, L., 2013. Mitochondrial cristae shape determines respiratory chain supercomplexes assembly and respiratory efficiency. Cell 155, 160–171. https://doi.org/10.1016/j.cell.2013.08.032

Conte, M., Ostan, R., Fabbri, C., Santoro, A., Guidarelli, G., Vitale, G., Mari, D., Sevini, F., Capri, M., Sandri, M., Monti, D., Franceschi, C., Salvioli, S., 2018. Human aging and longevity are characterized by high levels of mitokines. J. Gerontol. A Biol. Sci. Med. Sci. https://doi.org/10.1093/gerona/gly153

Delettre, C., Lenaers, G., Griffoin, J.M., Gigarel, N., Lorenzo, C., Belenguer, P., Pelloquin, L., Grosgeorge, J., Turc-Carel, C., Perret, E., Astarie-Dequeker, C., Lasquellec, L., Arnaud, B., Ducommun, B., Kaplan, J., Hamel, C.P., 2000. Nuclear gene OPA1, encoding a mitochondrial dynamin-related protein, is mutated in dominant optic atrophy. Nat. Genet. 26, 207–210. https://doi.org/10.1038/79936

Delezie, J., Handschin, C., 2018. Endocrine Crosstalk Between Skeletal Muscle and the Brain. Front Neurol 9, 698. https://doi.org/10.3389/fneur.2018.00698

Favaro, G., Romanello, V., Varanita, T., Andrea Desbats, M., Morbidoni, V., Tezze, C., Albiero, M., Canato, M., Gherardi, G., De Stefani, D., Mammucari, C., Blaauw, B., Boncompagni, S., Protasi, F., Reggiani, C., Scorrano, L., Salviati,

L., Sandri, M., 2019. DRP1-mediated mitochondrial shape controls calcium homeostasis and muscle mass. Nat Commun 10, 2576. https://doi.org/10.1038/s41467-019-10226-9

Fazeli, P.K., Lun, M., Kim, S.M., Bredella, M.A., Wright, S., Zhang, Y., Lee, H., Catana, C., Klibanski, A., Patwari, P., Steinhauser, M.L., 2015. FGF21 and the late adaptive response to starvation in humans. J. Clin. Invest. 125, 4601–4611. https://doi.org/10.1172/JCI83349

Fisher, F.M., Maratos-Flier, E., 2016. Understanding the Physiology of FGF21. Annual Review of Physiology 78, 223–241. https://doi.org/10.1146/annurev-physiol-021115-105339

Frezza, C., Cipolat, S., Martins de Brito, O., Micaroni, M., Beznoussenko, G.V., Rudka, T., Bartoli, D., Polishuck, R.S., Danial, N.N., De Strooper, B., Scorrano, L., 2006. OPA1 controls apoptotic cristae remodeling independently from mitochondrial fusion. Cell 126, 177–189. https://doi.org/10.1016/j.cell.2006.06.025

Fulop, T., Larbi, A., Dupuis, G., Le Page, A., Frost, E.H., Cohen, A.A., Witkowski, J.M., Franceschi, C., 2018. Immunosenescence and Inflamm-Aging As Two Sides of the Same Coin: Friends or Foes? Front. Immunol. 8. https://doi.org/10.3389/fimmu.2017.01960

Glass, D.J., 2005. Skeletal muscle hypertrophy and atrophy signaling pathways. Int. J. Biochem. Cell Biol. 37, 1974–1984. https://doi.org/10.1016/j.biocel.2005.04.018

Gloire, G., Legrand-Poels, S., Piette, J., 2006. NF-kappaB activation by reactive oxygen species: fifteen years later. Biochem. Pharmacol. 72, 1493–1505. https://doi.org/10.1016/j.bcp.2006.04.011

Gomes, M.D., Lecker, S.H., Jagoe, R.T., Navon, A., Goldberg, A.L., 2001. Atrogin-1, a muscle-specific F-box protein highly expressed during muscle atrophy. Proc. Natl. Acad. Sci. U.S.A. 98, 14440–14445. https://doi.org/10.1073/pnas.251541198

Hanks, L.J., Gutiérrez, O.M., Bamman, M.M., Ashraf, A., McCormick, K.L., Casazza, K., 2015. Circulating levels of fibroblast growth factor-21 increase with age independently of body composition indices among healthy

individuals. J Clin Transl Endocrinol 2, 77–82. https://doi.org/10.1016/j.jcte.2015.02.001

Hoffmann, C., Weigert, C., 2017. Skeletal Muscle as an Endocrine Organ: The Role of Myokines in Exercise Adaptations. Cold Spring Harb Perspect Med 7. https://doi.org/10.1101/cshperspect.a029793

Hunter, R.B., Stevenson, E., Koncarevic, A., Mitchell-Felton, H., Essig, D.A., Kandarian, S.C., 2002. Activation of an alternative NF-kappaB pathway in skeletal muscle during disuse atrophy. FASEB J. 16, 529–538. https://doi.org/10.1096/fj.01-0866com

Ibebunjo, C., Chick, J.M., Kendall, T., Eash, J.K., Li, C., Zhang, Y., Vickers, C., Wu, Z., Clarke, B.A., Shi, J., Cruz, J., Fournier, B., Brachat, S., Gutzwiller, S., Ma, Q., Markovits, J., Broome, M., Steinkrauss, M., Skuba, E., Galarneau, J.-R., Gygi, S.P., Glass, D.J., 2013. Genomic and proteomic profiling reveals reduced mitochondrial function and disruption of the neuromuscular junction driving rat sarcopenia. Mol. Cell. Biol. 33, 194–212. https://doi.org/10.1128/MCB.01036-12

Inagaki, T., Dutchak, P., Zhao, G., Ding, X., Gautron, L., Parameswara, V., Li, Y., Goetz, R., Mohammadi, M., Esser, V., Elmquist, J.K., Gerard, R.D., Burgess, S.C., Hammer, R.E., Mangelsdorf, D.J., Kliewer, S.A., 2007. Endocrine Regulation of the Fasting Response by PPARα-Mediated Induction of Fibroblast Growth Factor 21. Cell Metabolism 5, 415–425. https://doi.org/10.1016/j.cmet.2007.05.003

Izumiya, Y., Bina, H.A., Ouchi, N., Akasaki, Y., Kharitonenkov, A., Walsh, K., 2008. FGF21 is an Akt-regulated myokine. FEBS Lett. 582, 3805–3810. https://doi.org/10.1016/j.febslet.2008.10.021

Keipert, S., Ost, M., Johann, K., Imber, F., Jastroch, M., van Schothorst, E.M., Keijer, J., Klaus, S., 2013. Skeletal muscle mitochondrial uncoupling drives endocrine cross-talk through the induction of FGF21 as a myokine. American Journal of Physiology-Endocrinology and Metabolism 306, E469–E482. https://doi.org/10.1152/ajpendo.00330.2013

Kharitonenkov, A., Shiyanova, T.L., Koester, A., Ford, A.M., Micanovic, R., Galbreath, E.J., Sandusky, G.E., Hammond, L.J., Moyers, J.S., Owens, R.A., Gromada, J., Brozinick, J.T., Hawkins, E.D., Wroblewski, V.J., Li, D.-S.,

Mehrbod, F., Jaskunas, S.R., Shanafelt, A.B., 2005. FGF-21 as a novel metabolic regulator. J. Clin. Invest. 115, 1627–1635. https://doi.org/10.1172/JCI23606

Larsson, L., Degens, H., Li, M., Salviati, L., Lee, Y. il, Thompson, W., Kirkland, J.L., Sandri, M., 2018. Sarcopenia: Aging-Related Loss of Muscle Mass and Function. Physiological Reviews 99, 427–511. https://doi.org/10.1152/physrev.00061.2017

Latz, E., Schoenemeyer, A., Visintin, A., Fitzgerald, K.A., Monks, B.G., Knetter, C.F., Lien, E., Nilsen, N.J., Espevik, T., Golenbock, D.T., 2004. TLR9 signals after translocating from the ER to CpG DNA in the lysosome. Nat. Immunol. 5, 190–198. https://doi.org/10.1038/ni1028

Lecker, S.H., Jagoe, R.T., Gilbert, A., Gomes, M., Baracos, V., Bailey, J., Price, S.R., Mitch, W.E., Goldberg, A.L., 2004. Multiple types of skeletal muscle atrophy involve a common program of changes in gene expression. FASEB J. 18, 39–51. https://doi.org/10.1096/fj.03-0610com

Lehtonen, J.M., Forsström, S., Bottani, E., Viscomi, C., Baris, O.R., Isoniemi, H., Höckerstedt, K., Österlund, P., Hurme, M., Jylhävä, J., Leppä, S., Markkula, R., Heliö, T., Mombelli, G., Uusimaa, J., Laaksonen, R., Laaksovirta, H., Auranen, M., Zeviani, M., Smeitink, J., Wiesner, R.J., Nakada, K., Isohanni, P., Suomalainen, A., 2016. FGF21 is a biomarker for mitochondrial translation and mtDNA maintenance disorders. Neurology 87, 2290–2299. https://doi.org/10.1212/WNL.0000000000003374

Lentz, S.I., Edwards, J.L., Backus, C., McLean, L.L., Haines, K.M., Feldman, E.L., 2010. Mitochondrial DNA (mtDNA) Biogenesis: Visualization and Duel Incorporation of BrdU and EdU Into Newly Synthesized mtDNA In Vitro. J Histochem Cytochem 58, 207–218. https://doi.org/10.1369/jhc.2009.954701

Makki, K., Froguel, P., Wolowczuk, I., 2013. Adipose Tissue in Obesity-Related Inflammation and Insulin Resistance: Cells, Cytokines, and Chemokines. ISRN Inflamm 2013. https://doi.org/10.1155/2013/139239

Malicdan, M.C., Noguchi, S., Nonaka, I., Saftig, P., Nishino, I., 2008. Lysosomal myopathies: an excessive build-up in autophagosomes is too much to handle. Neuromuscul. Disord. 18, 521–529. https://doi.org/10.1016/j.nmd.2008.04.010

Mammucari, C., Milan, G., Romanello, V., Masiero, E., Rudolf, R., Del Piccolo, P., Burden, S.J., Di Lisi, R., Sandri, C., Zhao, J., Goldberg, A.L., Schiaffino, S., Sandri, M., 2007. FoxO3 controls autophagy in skeletal muscle in vivo. Cell Metab. 6, 458–471. https://doi.org/10.1016/j.cmet.2007.11.001

Mizushima, N., Komatsu, M., 2011. Autophagy: renovation of cells and tissues. Cell 147, 728–741. https://doi.org/10.1016/j.cell.2011.10.026

Mourkioti, F., Kratsios, P., Luedde, T., Song, Y.-H., Delafontaine, P., Adami, R., Parente, V., Bottinelli, R., Pasparakis, M., Rosenthal, N., 2006. Targeted ablation of IKK2 improves skeletal muscle strength, maintains mass, and promotes regeneration. J. Clin. Invest. 116, 2945–2954. https://doi.org/10.1172/JCI28721

Muñoz-Cánoves, P., Scheele, C., Pedersen, B.K., Serrano, A.L., 2013. Interleukin-6 myokine signaling in skeletal muscle: a double-edged sword? FEBS J 280, 4131–4148. https://doi.org/10.1111/febs.12338

Murgia, M., Serrano, A.L., Calabria, E., Pallafacchina, G., Lomo, T., Schiaffino, S., 2000. Ras is involved in nerve-activity-dependent regulation of muscle genes. Nat. Cell Biol. 2, 142–147. https://doi.org/10.1038/35004013

Nakahira, K., Haspel, J.A., Rathinam, V.A.K., Lee, S.-J., Dolinay, T., Lam, H.C., Englert, J.A., Rabinovitch, M., Cernadas, M., Kim, H.P., Fitzgerald, K.A., Ryter, S.W., Choi, A.M.K., 2011. Autophagy proteins regulate innate immune responses by inhibiting the release of mitochondrial DNA mediated by the NALP3 inflammasome. Nat. Immunol. 12, 222–230. https://doi.org/10.1038/ni.1980

Nishimura, T., Nakatake, Y., Konishi, M., Itoh, N., 2000. Identification of a novel FGF, FGF-21, preferentially expressed in the liver. Biochim. Biophys. Acta 1492, 203–206.

Oost, L.J., Kustermann, M., Armani, A., Blaauw, B., Romanello, V., 2019. Fibroblast growth factor 21 controls mitophagy and muscle mass. J Cachexia Sarcopenia Muscle. https://doi.org/10.1002/jcsm.12409

Otera, H., Wang, C., Cleland, M.M., Setoguchi, K., Yokota, S., Youle, R.J., Mihara, K., 2010. Mff is an essential factor for mitochondrial recruitment of Drp1 during mitochondrial fission in mammalian cells. J. Cell Biol. 191, 1141–1158. https://doi.org/10.1083/jcb.201007152

Palmer, C.S., Osellame, L.D., Laine, D., Koutsopoulos, O.S., Frazier, A.E., Ryan, M.T., 2011. MiD49 and MiD51, new components of the mitochondrial fission machinery. EMBO Rep. 12, 565–573. https://doi.org/10.1038/embor.2011.54

Pedersen, B.K., Steensberg, A., Fischer, C., Keller, C., Keller, P., Plomgaard, P., Febbraio, M., Saltin, B., 2003. Searching for the exercise factor: is IL-6 a candidate? J. Muscle Res. Cell. Motil. 24, 113–119.

Pereira, R.O., Tadinada, S.M., Zasadny, F.M., Oliveira, K.J., Pires, K.M.P., Olvera, A., Jeffers, J., Souvenir, R., Mcglauflin, R., Seei, A., Funari, T., Sesaki, H., Potthoff, M.J., Adams, C.M., Anderson, E.J., Abel, E.D., 2017. OPA1 deficiency promotes secretion of FGF21 from muscle that prevents obesity and insulin resistance. EMBO J. 36, 2126–2145. https://doi.org/10.15252/embj.201696179

Pette, D., Heilmann, C., 1979. Some characteristics of sarcoplasmic reticulum in fast- and slow-twitch muscles. Biochem. Soc. Trans. 7, 765–767. https://doi.org/10.1042/bst0070765

Pietras, E.M., 2017. Inflammation: a key regulator of hematopoietic stem cell fate in health and disease. Blood 130, 1693–1698. https://doi.org/10.1182/blood-2017-06-780882

Rai, M., Demontis, F., 2016. Systemic Nutrient and Stress Signaling via Myokines and Myometabolites. Annu. Rev. Physiol. 78, 85–107. https://doi.org/10.1146/annurev-physiol-021115-105305

Rodríguez-Nuevo, A., Díaz-Ramos, A., Noguera, E., Díaz-Sáez, F., Duran, X., Muñoz, J.P., Romero, M., Plana, N., Sebastián, D., Tezze, C., Romanello, V., Ribas, F., Seco, J., Planet, E., Doctrow, S.R., González, J., Borràs, M., Liesa, M., Palacín, M., Vendrell, J., Villarroya, F., Sandri, M., Shirihai, O., Zorzano, A., 2018. Mitochondrial DNA and TLR9 drive muscle inflammation upon Opa1 deficiency. EMBO J. 37. https://doi.org/10.15252/embj.201796553

Romanello, V., Guadagnin, E., Gomes, L., Roder, I., Sandri, C., Petersen, Y., Milan, G., Masiero, E., Del Piccolo, P., Foretz, M., Scorrano, L., Rudolf, R., Sandri, M., 2010. Mitochondrial fission and remodelling contributes to muscle atrophy. EMBO J. 29, 1774–1785. https://doi.org/10.1038/emboj.2010.60

Romanello, V., Sandri, M., 2015. Mitochondrial Quality Control and Muscle Mass Maintenance. Front Physiol 6, 422. https://doi.org/10.3389/fphys.2015.00422

Romanello, V., Scalabrin, M., Albiero, M., Blaauw, B., Scorrano, L., Sandri, M., 2019. Inhibition of the Fission Machinery Mitigates OPA1 Impairment in Adult Skeletal Muscles. Cells 8. https://doi.org/10.3390/cells8060597

Sacheck, J.M., Hyatt, J.-P.K., Raffaello, A., Jagoe, R.T., Roy, R.R., Edgerton, V.R., Lecker, S.H., Goldberg, A.L., 2007. Rapid disuse and denervation atrophy involve transcriptional changes similar to those of muscle wasting during systemic diseases. FASEB J. 21, 140–155. https://doi.org/10.1096/fj.06-6604com

Safdar, A., Tarnopolsky, M.A., 2018. Exosomes as Mediators of the Systemic Adaptations to Endurance Exercise. Cold Spring Harb Perspect Med 8. https://doi.org/10.1101/cshperspect.a029827

Sandri, M., 2008. Signaling in muscle atrophy and hypertrophy. Physiology (Bethesda) 23, 160–170. https://doi.org/10.1152/physiol.00041.2007

Sandri, M., Barberi, L., Bijlsma, A.Y., Blaauw, B., Dyar, K.A., Milan, G., Mammucari, C., Meskers, C.G.M., Pallafacchina, G., Paoli, A., Pion, D., Roceri, M., Romanello, V., Serrano, A.L., Toniolo, L., Larsson, L., Maier, A.B., Muñoz-Cánoves, P., Musarò, A., Pende, M., Reggiani, C., Rizzuto, R., Schiaffino, S., 2013. Signalling pathways regulating muscle mass in ageing skeletal muscle: the role of the IGF1-Akt-mTOR-FoxO pathway. Biogerontology 14, 303–323. https://doi.org/10.1007/s10522-013-9432-9

Sandri, M., Sandri, C., Gilbert, A., Skurk, C., Calabria, E., Picard, A., Walsh, K., Schiaffino, S., Lecker, S.H., Goldberg, A.L., 2004. Foxo transcription factors induce the atrophy-related ubiquitin ligase atrogin-1 and cause skeletal muscle atrophy. Cell 117, 399–412. https://doi.org/10.1016/s0092-8674(04)00400-3

Sartori, R., Schirwis, E., Blaauw, B., Bortolanza, S., Zhao, J., Enzo, E., Stantzou, A., Mouisel, E., Toniolo, L., Ferry, A., Stricker, S., Goldberg, A.L., Dupont, S., Piccolo, S., Amthor, H., Sandri, M., 2013. BMP signaling controls muscle mass. Nat. Genet. 45, 1309–1318. https://doi.org/10.1038/ng.2772

Schiaffino, S., Dyar, K.A., Ciciliot, S., Blaauw, B., Sandri, M., 2013. Mechanisms regulating skeletal muscle growth and atrophy. FEBS J. 280, 4294–4314. https://doi.org/10.1111/febs.12253

Schiaffino, S., Reggiani, C., 1996. Molecular diversity of myofibrillar proteins: gene regulation and functional significance. Physiol. Rev. 76, 371–423. https://doi.org/10.1152/physrev.1996.76.2.371

Schiaffino, S., Sandri, M., Murgia, M., 2007. Activity-dependent signaling pathways controlling muscle diversity and plasticity. Physiology (Bethesda) 22, 269–278. https://doi.org/10.1152/physiol.00009.2007

Scorrano, L., 2013. Keeping mitochondria in shape: a matter of life and death. Eur. J. Clin. Invest. 43, 886–893. https://doi.org/10.1111/eci.12135

Staiger, H., Keuper, M., Berti, L., Hrabe de Angelis, M., Häring, H.-U., 2017. Fibroblast Growth Factor 21-Metabolic Role in Mice and Men. Endocr. Rev. 38, 468–488. https://doi.org/10.1210/er.2017-00016

Sun, N., Malide, D., Liu, J., Rovira, I.I., Combs, C.A., Finkel, T., 2017. A fluorescence-based imaging method to measure *in vitro* and *in vivo* mitophagy using mt-Keima. Nature Protocols 12, 1576–1587. https://doi.org/10.1038/nprot.2017.060

Sun, N., Youle, R.J., Finkel, T., 2016. The Mitochondrial Basis of Aging. Mol Cell 61, 654–666. https://doi.org/10.1016/j.molcel.2016.01.028

Suomalainen, A., Elo, J.M., Pietiläinen, K.H., Hakonen, A.H., Sevastianova, K., Korpela, M., Isohanni, P., Marjavaara, S.K., Tyni, T., Kiuru-Enari, S., Pihko, H., Darin, N., Õunap, K., Kluijtmans, L.A., Paetau, A., Buzkova, J., Bindoff, L.A., Annunen-Rasila, J., Uusimaa, J., Rissanen, A., Yki-Järvinen, H., Hirano, M., Tulinius, M., Smeitink, J., Tyynismaa, H., 2011. FGF-21 as a biomarker for muscle-manifesting mitochondrial respiratory chain deficiencies: a diagnostic study. The Lancet Neurology 10, 806–818. https://doi.org/10.1016/S1474-4422(11)70155-7

Takeuchi, O., Akira, S., 2010. Pattern recognition receptors and inflammation. Cell 140, 805–820. https://doi.org/10.1016/j.cell.2010.01.022

Tezze, C., Romanello, V., Desbats, M.A., Fadini, G.P., Albiero, M., Favaro, G., Ciciliot, S., Soriano, M.E., Morbidoni, V., Cerqua, C., Loefler, S., Kern, H., Franceschi, C., Salvioli, S., Conte, M., Blaauw, B., Zampieri, S., Salviati, L., Scorrano, L., Sandri, M., 2017a. Age-Associated Loss of OPA1 in Muscle Impacts Muscle Mass, Metabolic Homeostasis, Systemic Inflammation, and

Epithelial Senescence. Cell Metabolism 25, 1374-1389.e6. https://doi.org/10.1016/j.cmet.2017.04.021

Tezze, C., Romanello, V., Desbats, M.A., Fadini, G.P., Albiero, M., Favaro, G., Ciciliot, S., Soriano, M.E., Morbidoni, V., Cerqua, C., Loefler, S., Kern, H., Franceschi, C., Salvioli, S., Conte, M., Blaauw, B., Zampieri, S., Salviati, L., Scorrano, L., Sandri, M., 2017b. Age-Associated Loss of OPA1 in Muscle Impacts Muscle Mass, Metabolic Homeostasis, Systemic Inflammation, and Epithelial Senescence. Cell Metab. 25, 1374-1389.e6. https://doi.org/10.1016/j.cmet.2017.04.021

Tezze, C., Romanello, V., Sandri, M., 2019. FGF21 as Modulator of Metabolism in Health and Disease. Front Physiol 10, 419. https://doi.org/10.3389/fphys.2019.00419

Wei, W., Dutchak, P.A., Wang, Xunde, Ding, X., Wang, Xueqian, Bookout, A.L., Goetz, R., Mohammadi, M., Gerard, R.D., Dechow, P.C., Mangelsdorf, D.J., Kliewer, S.A., Wan, Y., 2012. Fibroblast growth factor 21 promotes bone loss by potentiating the effects of peroxisome proliferator-activated receptor γ. Proc. Natl. Acad. Sci. U.S.A. 109, 3143–3148. https://doi.org/10.1073/pnas.1200797109

Whitham, M., Febbraio, M.A., 2016. The ever-expanding myokinome: discovery challenges and therapeutic implications. Nat Rev Drug Discov 15, 719–729. https://doi.org/10.1038/nrd.2016.153

Wrighting, D.M., Andrews, N.C., 2006. Interleukin-6 induces hepcidin expression through STAT3. Blood 108, 3204–3209. https://doi.org/10.1182/blood-2006-06-027631

Zhang, P., Chen, X., Fan, M., 2007. Signaling mechanisms involved in disuse muscle atrophy. Medical Hypotheses 69, 310–321. https://doi.org/10.1016/j.mehy.2006.11.043

Zhang, Q., Raoof, M., Chen, Y., Sumi, Y., Sursal, T., Junger, W., Brohi, K., Itagaki, K., Hauser, C.J., 2010. Circulating Mitochondrial DAMPs Cause Inflammatory Responses to Injury. Nature 464, 104–107. https://doi.org/10.1038/nature08780

Zhao, J., Brault, J.J., Schild, A., Cao, P., Sandri, M., Schiaffino, S., Lecker, S.H., Goldberg, A.L., 2007. FoxO3 coordinately activates protein degradation by

the autophagic/lysosomal and proteasomal pathways in atrophying muscle cells. Cell Metab. 6, 472–483. https://doi.org/10.1016/j.cmet.2007.11.004